UNIVERSIDADE DE LISBOA
FACULDADE DE CIÊNCIAS
DEPARTAMENTO DE QUÍMICA E BIOQUÍMICA

Polymorphism in Hydroxybenzoyl Compounds: Structure and Energetics

Cátia Sofia Duarte Lopes

Mestrado em Química
Especialização em Química

Dissertação orientada por:
Doutor Carlos Eduardo Sabino Bernardes
Professor Manuel Eduardo Ribeiro Minas da Piedade

2016

To my little sister
and
never giving up

Acknowledgments

First and foremost, I would like to thank Professor Dr. Manuel Eduardo Minas da Piedade, for accepting me in his group and giving me the opportunity to work with him. During this year, it was due to his knowledge and guidance that I was able to develop new essential skills to make good science. Thank you for all the valuable advice that helped me grow scientifically and personally. Also, for all the chocolates that always gave me an extra push when the work was not going so well. Dr. Carlos Eduardo Sabino Bernardes, who was always available to answer my questions and to help me whenever an obstacle appeared in the development of this work. A special thanks to both of them for all the patience, understanding and good disposition during the development of this work.

Although far away, a very special thanks to Dr. Ricardo Alexandre Gravata Simões for all his support since the very beginning of my adventure in the Molecular Energetics Group and always telling me to keep calm. Also to Dr. Abhinav Joseph for helping me understand some of my results, being available for the discussion of those with me and for saving me whenever a technical problem in the apparatus came up. Also, to all my laboratory colleagues, Rafael Bento, Miguel Rendas, and in particularly Mariana Donato, thank you for all the laughs and funny moments that passed this year. Those always helped me maintain a good mood while working.

The development of this work had several contributions from many people that without their help it would have been hardly obtained. First, I would like to say thanks to Professor Dr. Maria da Conceição from IST-UL for the HPLC analysis. Professor Dr. Hermínio Diogo from IST-UL for the differential scanning calorimetry measurements and hot stage microscopy images which assisted in identifying important results in this work. Professor Dr. Fátima Piedade from DQB-UL for the single crystal structures which without those this work would not have been completed and finally Dr. Filipe Agapito for the computational calculations which were essential to do the energetics part of this work.

Sara Realista, thank you for always inspiring me to work hard, do better and never give up, without you this journey would not have been the same and I do not know where I would be. You always made me laugh even when depressed. Paulo Martinho and Marta Saraiva, thank you both for all your wise advice and support which always helped me see things from another perspective. Also, Priscilla Ramgi, who always accompanied me in this hard journey. Thank you for all the cheering "pius". The four of you will always be in my heart and will never be forgotten! Ana Catarina Rosális, my longest friend, who has seen the ups and downs of this rollercoaster that has been this journey. Thank you for always holding my hand and keeping my head straight when my judgment got clouded.

My family, Rui Lopes, Ana Paula Lopes, Ricardo Lopes and Mafalda Lopes, for all the support they gave me to get to the top of this ladder. In particular, my mother, who is always giving me strength to go on and to never give up no matter what comes in my way. My sister, a million thanks for all the help done throughout these years, reviewing all of my works and searching for errors which always led to the most hilarious corrections and helping me with image edition. To all the Serrão family, for their amazing support throughout these years, specially Helena and Nelson Serrão, who are like second parents to me.

Last but not least, a huge thanks to Ricardo Serrão, for all your patience, all your trust, for always believing in me, never panicking and always seeing the bright side even when I did not. You are the most important person in my life and who made one of my greatest dreams possible through our combined hard work.

Thank you all for all the love, understanding and laughs throughout these years,

Resumo

O trabalho apresentado nesta tese foi realizado no Grupo de Energética Molecular (GEM), do Centro de Química e Bioquímica da Faculdade de Ciências da Universidade de Lisboa. Um dos temas principais desenvolvidos ao longo dos anos no GEM, prende-se com o estudo da relação entre a energética e a estrutura das moléculas, nomeadamente em sólidos moleculares orgânicos. A abordagem deste tema tem seguido duas linhas de investigação ligeiramente distintas. Na primeira, são estudados sistemas modelo, normalmente constituídos por pequenas moléculas (poucas dezenas de átomos), pouco dispendiosos e que podem ser facilmente manipulados. Estes estudos têm como objetivo estabelecer relações causa-efeito como, por exemplo, averiguar como uma determinada alteração na estrutura de uma molécula, implica mudanças no empacotamento em estado sólido e, consequentemente, nas propriedades físicas. Na segunda linha, os conhecimentos retirados do estudo dos sistemas modelo, são aplicados diretamente ao estudo de compostos com interesse comercial. De facto, este tipo de estudo é de extrema importância para as indústrias que usam formulações orgânicas no estado sólido, onde a indústria farmacêutica se destaca, devido à grande variedade de princípios ativos farmacêuticos que são utilizados em estado sólido.

Quando se trabalha com sólidos moleculares cristalinos por vezes, uma mesma molécula pode organizar-se com diferentes arranjos tridimensionais. A este fenómeno dá-se o nome de polimorfismo. Dado que cada forma cristalina pode apresentar diferentes propriedades físicas (e.g. cor, temperatura de fusão e solubilidade), o controlo e previsão deste fenómeno é hoje em dia crucial para a indústria. Por exemplo, para a indústria farmacêutica, se duas formas cristalinas do mesmo composto apresentarem solubilidades distintas, podem conduzir a uma biodisponibilidade diferente do medicamento no organismo do paciente. Apesar de poderem existir vários polimorfos para uma molécula em determinadas condições de pressão e temperatura, apenas uma dessas formas é termodinamicamente estável. Assim, caso não existam barreiras cinéticas, todas as formas metastáveis tendem a evoluir para a fase mais estável. Neste sentido, torna-se importante conhecer a relação energética entre as fases, a fim de evitar problemas durante, e.g. processos de armazenamento. Estes tipos de problemas podem, por esse motivo, levar a uma eventual recolha dos medicamentos baseados num dado principio ativo, e assim levar a perdas monetárias muito elevadas para a indústria.

É de realçar, no entanto, que se o polimorfismo for bem compreendido e controlado, pode levar ao desenvolvimento de novos materiais, que possuem características físicas diferentes do material de partida, que podem ser ajustadas para uma determinada aplicação sem alterar a molécula inicial. Este facto, mostra que é de todo o interesse conhecer quais os vários polimorfos existentes para cada molécula, e estudar a maneira mais adequada para os preparar e controlar.

É neste âmbito que surge o trabalho que foi desenvolvido nesta tese. Este foi realizado como continuação dos estudos iniciados no GEM para os compostos 4'-hidroxiacetofenona e 4-hidroxibenzaldeído. Ambos podem ser considerados sistemas modelo que pertencem à família de compostos do tipo 4-hidroxibenzoílos (HOC_6H_4COR). Estes revelaram-se ser compostos com a capacidade para gerar polimorfos, pois tanto para a 4'-hidroxiacetofenona ($R = CH_3$) como para o 4-hidroxibenzaldeído (R = H) já foram identificadas duas formas cristalinas diferentes. Para além destas, no caso da 4'-hidroxiacetofenona, foram também identificados três hidratos. A razão principal que leva a esta diversidade parece estar relacionada com a capacidade destas moléculas poderem formar diferentes tipos de ligações de hidrogénio como OH···O, CH···$O_{carbonilo}$ e CH···$O_{hidroxilo}$, permitindo diferentes empacotamentos cristalinos. Para além disso, do ponto de vista conformacional, nesta família de compostos, as moléculas podem ainda adotar duas conformações distintas, que diferem na orientação do átomo de hidrogénio do grupo hidroxilo

relativamente ao grupo carbonilo. Assim, um dos objetivos principais deste trabalho foi verificar de que forma um aumento do tamanho da cadeia alquilo, i.e. a introdução de um grupo apolar R progressivamente maior, influencia a formação de diferentes estruturas cristalinas. Para isto foram selecionadas quatro moléculas, em adição à 4'-hidroxiacetofenona e 4-hidroxibenzaldeído, aumentando a cadeia carbonada consecutivamente, através da adição de grupos CH_2. Neste sentido, foi realizado um estudo sistemático da energética e das estruturas cristalinas da 4'-hidroxipropiofenona (R = C_2H_5), da 4'-hidroxibutirofenona (R = C_3H_7), da 4'-hidroxivalerofenona (R = C_4H_9) e da 4'-hidroxiheptanofenona (R = C_6H_{13}).

O ponto de partida para o desenvolvimento deste trabalho, foi a caracterização energética para os compostos selecionados, dada a ausência na literatura de dados fiáveis para estes compostos. Este estudo envolveu várias etapas: *i*) a determinação das temperaturas de fusão e respetivas entalpias de fusão molares padrão (p^o = 1 bar) , $\Delta_{fus}H^o_m$, por calorimetria diferencial de varrimento; *ii*) a avaliação da entalpia de vaporização molar padrão, $\Delta_{vap}H^o_m$, da 4'-hidroxivalerofenona e 4'-hidroxiheptanofenona, e de sublimação molar padrão, $\Delta_{sub}H^o_m$, da 4'-hidroxipropiofenona e 4'-hidroxibutirofenona, por microcalorimetria Calvet; *iii*) a determinação das capacidades caloríficas molares padrão dos compostos por calorimetria diferencial de varrimento, de forma a possibilitar a correção dos valores de $\Delta_{vap}H^o_m$ e $\Delta_{sub}H^o_m$ obtidos nas condições experimentais, para entalpias de sublimação molares padrão à temperatura de referência de 298,15 K, $\Delta_{sub}H^o_m(298,15)$ *iv*) o cálculo das entalpias de formação molar padrão em estado sólido, $\Delta_f H^o_m(cr)$, a partir dos valores de $\Delta_{sub}H^o_m(298,15)$ e das entalpias de formação molar padrão em fase gasosa, $\Delta_f H^o_m$ (g), à temperatura de 298,15 K. Este trabalho foi recentemente publicado (C. S. D. Lopes, F. Agapito, C. E. S. Bernardes, M. E. Minas da Piedade *Thermochemistry of 4-HOC$_6$H$_4$COR (R = H, CH$_3$, C$_2$H$_5$, n-C$_3$H$_7$, n-C$_4$H$_9$, n-C$_5$H$_{11}$, and n-C$_6$H$_{13}$) Compounds*; *J. Chem. Thermodyn*. **2016**, DOI: 10.1016/j.jct.2016.09.026). Foi realizada uma correlação linear entre as entalpias de sublimação molares padrão a 298,15 K dos compostos com o número de átomos de carbono (R^2 = 0,986). Este resultado sugere que apesar dos diferentes empacotamentos cristalinos existentes entre as várias formas a energia de coesão é aditiva, com um aumento por cada CH_2 de 6,6±0,6 kJ·mol^{-1}.

A procura de novos polimorfos nos compostos estudados foi realizada, numa primeira etapa, pela verificação da existência de transições de fase e avaliando as temperaturas de fusão dos materiais, por calorimetria diferencial de varrimento. De uma forma geral, os ensaios realizados com os materiais de partida, não revelaram a existência de transições de fase entre a temperatura ambiente e de fusão. No caso da 4'-hidroxivalerofenona (HVP), após avaliar a fusão da amostra, esta foi ainda submetida a ciclos de aquecimento/arrefecimento. Este estudo revelou que o material que precipita a partir do líquido isotrópico da HVP, não apresenta transições de fase na gama de temperaturas estudada (153 K a 453 K). No entanto, a temperatura e entalpia de fusão são significativamente diferentes em relação à amostra inicial: enquanto o composto de partida (forma I), que é preparado por cristalização em etanol, apresenta uma temperatura de fusão de 334,2±0,7 K, e uma entalpia de fusão molar padrão de 25,75±0,26 kJ·mol^{-1}, a que precipita a partir do líquido isotrópico (forma II), funde a 324,0±0,2 K e tem uma entalpia de fusão molar padrão de 18,14±0,18 kJ·mol^{-1}. Utilizando os valores de entalpia e temperatura de fusão, foi possível concluir que a forma I é termodinamicamente mais estável que a forma II, e que estas se encontram relacionadas monotropicamente. Os resultados destes estudos termoanalíticos sobre o polimorfismo na HVP foram já submetidos para publicação estando a aguardar o resultado da avaliação (C. S. D. Lopes, C. E. S. Bernardes, M. F. M. Piedade, H. P. Diogo, M. E. Minas da Piedade; *A New Polymorph of 4'-Hydroxyvalerophenone Revealed by Thermoanalytical and X-ray Diffraction Studies*; Eur. Phys. J.). A identificação deste novo polimorfo da HVP foi ainda verificada através de estudos de difração de raios-X de cristal único, os quais permitiram determinar a organização molecular desta nova fase em estado sólido. Para além destes resultados

para a 4'-hidroxiheptanofenona (HHP), recorrendo a dados de difração de raios-X de cristal único, foram resolvidas quatro estruturas a diferentes temperaturas (150 K, 190 K, 220 K e 293 K) e identificada uma transição de fase entre 190 K e 220 K. Verificou-se que todas estas estruturas são ortorrômbicas, sendo que a transição de fase que ocorre, leva à alteração do grupo espacial, de $P2_12_12_1$ para *Pnma*, confirmando assim a existência de polimorfismo na molécula. Esta transição também foi identificada por calorimetria diferencial de varrimento. Finalmente, a partir da análise dos dados de difração de raios-X de cristal único das diferentes formas, foi possível verificar que as transições de fase sólido-sólido envolvem modificações conformacionais da cadeia alquilo nas moléculas de HHP, sem que existam alterações significativas da estrutura a nível tridimensional.

Palavras chave: entalpia de vaporização; entalpia de sublimação; entalpia de formação; polimorfismo, 4'-hidroxibenzoílos

Abstract

During the recent years, in the Molecular Energetics Group, Faculdade de Ciências da Universidade de Lisboa, an effort to systematically investigate the structure/energetic relation in molecular crystalline materials has been undertaken. One of the studies performed in this scope, involved the investigation of the 4'-hydroxybenzoyl family (HOC_6H_4CO-R), by searching for the existence of polymorphs (crystal phases with different molecular arrangements) of 4-hydroxybenzaldeheyde (R = H) and 4'-hydroxyacetophenone (R = CH_3), and relating this information with energetic data. In this work, the previous existing results were expanded for compounds with R = C_2H_5, *n*-C_3H_7, *n*-C_4H_9 and *n*-C_6H_{13}.

The thermochemistry of the compounds was investigated by determining their enthalpies of formation, fusion, vaporization and/or sublimation. These measurements were performed by Calvet-drop microcalorimetry and W1-F12 and CCSD(T)-F12 level of theory. Standard (p^o = 1 bar) molar enthalpies of formation in the solid, $\Delta_f H_m^o$ (cr), and gaseous, $\Delta_f H_m^o$ (g), states at 298.15 K were determined for the complete family of compounds studied in this work. A linear correlation was found when the $\Delta_{sub} H_m^o$ (298.15 K) values were plotted as a function of the number of carbon atoms in the alkyl side chain (n_c), with a CH_2 increment of 6.6±0.6 kJ·mol^{-1}. Despite the differences in the molecular packing between the crystalline compounds their cohesive energies are approximate additivity.

Regarding the polymorphism studies, a new phase of 4'-hydroxyvalerophenone was discovered from differential scanning calorimetry, X-ray powder diffraction and single crystal X-ray diffraction. This novel form (form II) was obtained by crystallization from the melt. It presents a fusion temperature of T_{fus} = 324.3±0.2 K and an enthalpy of fusion $\Delta_{fus} H_m^o$ = 18.14±0.18 kJ·mol^{-1}. These values are much lower than those obtained for the previously known phase (form I, T_{fus} = 334.6±0.7 K; $\Delta_{fus} H_m^o$ = 25.75±0.26 kJ·mol^{-1}), which can be prepared by crystallization from ethanol. These results suggest that form I is thermodynamically more stable than form II and both are monotropically related. Finally, for 4'-hydroxyhepatnophenone, four different structures at different temperatures (T = 150 K; 190 K; 220 K and 298 K) were solved by single crystal X-ray diffraction. A phase transition at 203 K was detected by DSC which corresponds to a new polymorph. The two forms are enantiotropicly related.

Keywords: enthalpy of vaporization; enthalpy of sublimation; enthalpy of formation, polymorphism, 4'-hydroxybenzoyls

Table of Contents

Table List

Figure List

List of Abbreviations

HBA	4-hydroxybenzaldeheyde
HAP	4'-hydroxyacetophenone
HPP	4'-hydroxypropiophenone
HBP	4'-hydroxibutyrophenone
HVP	4'-hydroxyvalerophenone
HHP	4'-hydroxyheptanophenone
HPTP	4'-hydroxyhexanophenone
HPLC-ESI/MS	High performance liquid chromatography electrospray mass spectrometry
^{1}H NMR	Proton nuclear magnetic resonance
DRIFT	Diffuse reflectance infrared fourier-transform
SCXRD	Single crystal X-ray diffraction
XRPD	X-ray powder diffraction
HSM	Hot stage microscopy
DSC	Differential scanning calorimetry
δ	Chemical deviation, ppm in ^{1}H NMR
$\tilde{v}$	Wavenumber, cm^{-1} in DRIFT
v	Stretching vibrations in DRIFT
δ	Bending vibrations in DRIFT
$\Delta_{fus}H_m^o$	Standard molar enthalpy of fusion
$\Delta_{vap}H_m^o$	Standard molar enthalpy of vaporization
$\Delta_{sub}H_m^o$	Standard molar enthalpy of sublimation
$\Delta_f H_m^o$	Standard molar enthalpy of formation
$\Delta_{fus}h^o$	Standard specific fusion enthalpy of fusion
$\Delta_{vap}h$	Specific fusion enthalpy of vaporization
$\Delta_{sub}h$	Specific fusion enthalpy of sublimation
$C_{p,m}^o$	Standard molar heat capacity
$\Delta\phi$	Heat flow
M	Molar mass
m	Sample mass
T	Temperature
T_{fus}	Fusion temperature
T_{on}	Starting temperature of a peak in a thermal event in a DSC experiment
T_{max}	Maximum temperature of a peak in a thermal event in a DSC experiment
T_i	Initial temperature
T_f	Final temperature
h k l	Miller indices
a	Unit cell vector *a* length
b	Unit cell vector *b* length
c	Unit cell vector *c* length
β	Angle between vector *a* and *c* in the unit cell
V	Volume of the unit cell
ρ_{calc}	Calculated density of the compound
Z	Number of molecules in the unit cell
Z'	Number of molecules in the asymmetric unit of the crystal unit cell

1. Introduction

Many of the organic materials prepared in industry (particularly the pharmaceutical) are obtained in the solid state (e.g. pills, capsules). Solids exist in two different forms: amorphous or crystalline. The difference between these forms is that the crystalline materials correspond to an organized state, while in the amorphous case, the molecules are in a disordered state.[1] It was in the very beginning of the 19th century that scientists became aware that crystalline solids could show more than one packing arrangement. First for inorganic compounds[2] and later for organic molecules.[3] Nowadays, it is well known that many organic molecular compounds can often exist in several crystal forms.[4-7] The ability of a given compound to present more than one crystal structure (i.e. unit cell parameters, volume and density) is known as polymorphism. [8-10] Different polymorphs should be treated as different materials, since they can exhibit dissimilar physical proprieties (e.g. color, fusion point and solubility).[8, 11-12] The study of polymorphism and related phenomena led to concepts such as conformational polymorphism (i.e different crystal packings that result from a molecular conformation change), solvatomorphism (i.e. the crystal structures that contain solvent molecules) or co-crystallization (i.e. crystal structures formed from more than one component). These classifications, however, have been subject to some debate.[10, 13]

From an industrial point of view, the fact that each polymorph corresponds to a different material allows to select the crystalline form that presents more suitable properties for a given application.[14] However, control over polymorphism is a difficult task, since new forms can appear if slight modifications are performed to the manufacturing process.[5] Thus, tight control over the production procedures is extremely important in several industries, such as explosives, dyes and pharmaceuticals.[15-18] The lack of polymorphism control, for example, in the pharmaceutical industry can cause health hazard situations, as illustrated by the well-known case of ritonavir.[19-20]

Ritonavir ($C_{37}H_{48}N_6O_5S_2$, CAS number:155213-67-5, Figure 1.1) is a protease inhibitor for the treatment of acquired immunodeficiency syndrome (AIDS), discovered in 1992. The commercial launch began in 1996 under the name 'Norvir' with two different formulations: as an oral liquid or as semi-solid capsules. Both formulations were based on ritonavir in ethanol/water solutions.[19] The International Conference on Harmonization of Technical Requirements of Registration of Pharmaceuticals for Human Use (ICH) guidelines stated that when a drug product is commercialized in solution there is no need to control the crystal form. Thus, only one crystal form was identified during the development process for the compound.[19] It was until two years later that the drug began to precipitate in the capsules, which led to an investigation that identified a new polymorph, which was much less soluble than the original form. In the following weeks this new form appeared during the formulation process and on the bulk drug.[19] Due to this fact, the manufacture of Norvir semi-solid capsules stopped. Also, the liquid Norvir formulation could not be stored at low temperature due to the risk of crystallization. This led to a serious problem on the supply of this lifesaving drug until a new formulation could be developed.[19-21]

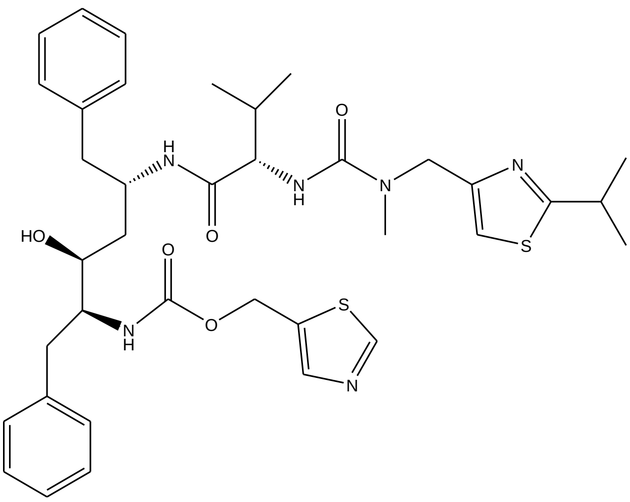

Figure 1.1. Molecular structure of ritonavir.

From an academic point of view, polymorphism can be used to investigate how intermolecular interactions, such as hydrogen bonds and Van der Waals forces can influence the different crystalline packing. The fact that this phenomenon is mainly controlled by these forces, explains why these structures can be prepared through different methods (e.g. cooling of melts, condensation of vapors).[10] Crystal engineering strategies rely on the understanding of these interactions to design molecular solids in view of specific applications. One of the most used methods in polymorphism screening is crystallization from solution under different conditions (e.g. different solvents).[10, 22] This also allows to investigate the different mechanisms of crystallization, in which the hydrogen bonds can play an important role.[22-23]

Different polymorphs can often coexist at a given temperature, but with time, they will evolve to the most stable form in the absence of kinetic factors. The relative thermodynamic stability of two different forms and the driving force for a spontaneous transformation at constant temperature and pressure is determined by the difference in Gibbs energy (ΔG) between the polymorphs as

$$\Delta G = \Delta H - T\Delta S \tag{1.1}$$

where ΔH is the enthalpy difference between the two phases, T is the temperature and ΔS is the entropy change between the two phases, that can be related, in part, to differences in disorder and lattice vibrations in the polymorphs.[10, 24] According to the ΔG value there are three possibilities: *i*) if the value is negative, the transformation will occur spontaneously unless its hindered by a kinetic barrier; *ii*) if equal to zero the system is in equilibrium because the Gibbs energy of the two phases is the same, so both phases can coexist at the same temperature and pressure conditions; *iii*) if positive the reverse transformation will tend to spontaneously occur, in the absence of kinetic barriers.[10, 24]

One way to express quantitative information about the relative stability of polymorphs is by plotting a phase diagram of the Gibbs free energy (G) as a function of temperature (T). Figure 1.2 shows typical plots for a polymorphic system composed by two polymorphs. In this figure, each intersection between two Gibbs free energy lines corresponds to a condition where two different phases can coexist in equilibrium. Hence, T_{fus} (I), T_{fus} (II) represent the temperature at which the lines of form I and form II intercept that of the liquid, respectively, so that the melting can occur. An additional interception is noted in Figure 1.2a at T_{trs} (II → I), between the curves of crystal I and II. At this point, an inversion of stability is observed between the two polymorphs and a

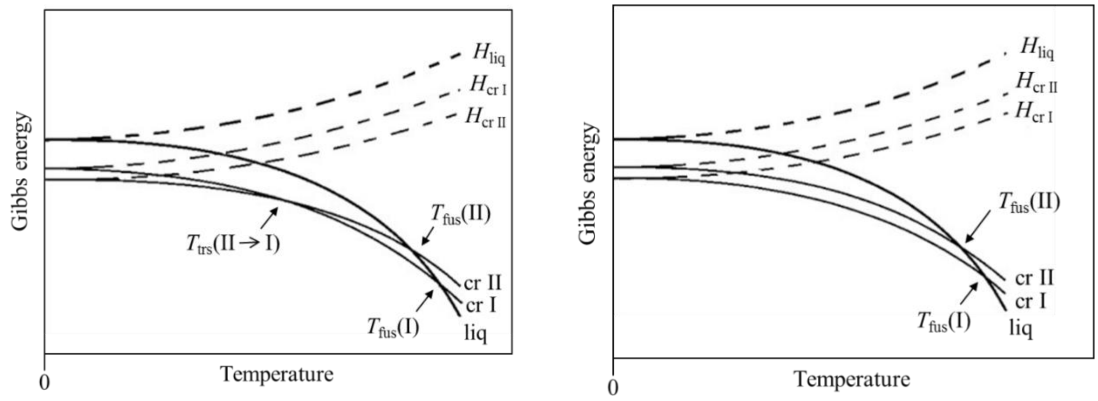

(a) (b)

Figure 1.2. Gibbs free energy variation as a function of temperature for a) a enantiotropic or b) monotropic system composed by two polymorphs (adapted from reference 15).The solid lines represent the Gibbs free energy of the two solid (cr I/ cr II) forms and the liquid state (liq). The dashed lines represent the enthalpy of the two solid ($H_{cr\ I}$/ $H_{cr\ II}$) forms and the liquid phase (H_{liq}). The T_{fus} (I) and T_{fus} (II) represent the fusion temperature of the two solid forms.

solid-solid phase transition can occur. In this particular case, because T_{trs} (II → I) is located before the melting temperature of the two phases, the system is called enantiotropic. In contrast, in Figure 1.2b, no phase transition is observed and, for this reason, form I is always more stable than form II up to melting. In this case, the system is called monotropic. Although, not related by a phase transition, it should be mentioned that, on thermodynamic grounds, if form II is prepared, it will tend to transform into form I at any temperature. This illustrates the importance of the knowledge of the thermodynamic relationship between different crystal phases, during production and storage of solid materials.[11, 15, 25]

In order to determine if a polymorphic system is either monotropic or enantiotropic, the rules recommended by Burger and Ramberger,[26] can be used. The most used rules are:

Heat of transition rule: if an endothermic phase transition between two polymorphs is observed, then the thermodynamic transition point lies at or below this temperature. In this case, the polymorphs are enantiotropically related. On the other hand, the polymorphs are monotropically related if an exothermic transition is observed at a given temperature and no phase transition occurs at a higher temperature.

Heat of fusion rule: the system is usually enantiotropic, if the polymorph with the higher temperature of fusion has the lowest enthalpy of fusion. If this does not occur, the system is monotropic. This rule can fail if the melting points of the polymorphs differ by more than 30 K.

Density rule: the most stable polymorph will show the highest density, due to the stronger intermolecular Van der Waals interactions. This rule is based on Kitaigorodskii's principle of close packing structures and for non-hydrogen bonded systems at 0 K.[27]

The investigation of polymorphic systems has been one of the main topics of research addressed at the Molecular Energetics Group of Faculdade de Ciências da Universidade de Lisboa, during the last years. The study of the structure/energetic relations that are responsible for the occurrence of polymorphism in organic crystalline materials has been one of the main goals. Good examples of this work, can be found in the investigation of the polymorphic systems of 1-(4-hydroxyphenyl)ethan-1-one (4'-hydroxyacetophenone, HAP; Figure 1.3b) and 4-hydroxybenzaldeheyde (HBA; Figure 1.3a).[28-30] Both compounds exhibit two polymorphs that are enantiotropically related and, in the case of HAP, three hydrates were identified so far.[31] Given the similarity between these molecules (an hydrogen atom in HBA is replaced in HAP for a methyl group; Figures 1.3a-b), and their identical ability to form polymorphs with several common features (packing and hydrogen motifs), it became interesting to check how the increase of the side alkyl chain (that considerably changes the Van der Waals ability of the molecules), can modify the packing features and polymorphs propensity in the 4-hydroxybenzoyl family (Figure 1.3). Thus, it became pertinent to extend the previous energetic and polymorph screenings performed to HBA and HAP, to the following compounds: 1-(4-Hydroxyphenyl)propan-1-one (4'-hydroxypropiophenone, HPP, $HOC_6H_4COC_2H_5$); 1-(4-Hydroxyphenyl)butan-1-one (4'hydroxybutirophenone, HBP, $HOC_6H_4COC_3H_7$); 1-(4-Hydroxyphenyl)pentan-1-one (4'-hydroxyvalerophenone, HVP, $HOC_6H_4COC_4H_9$) and 1-(4-Hydroxyphenyl)heptan-1-one (4'-hydroxyheptanophenone, HHP, $HOC_6H_4COC_6H_{13}$).

The work described in this thesis, presents the first steps towards the development of a comprehensive study of polymorphism in the 4-hydroxybenzoyl family. Two different topics were addressed: *i*) the use of differential scanning calorimetry (DSC), Calvet-drop microcalorimetry and theoretical methods, to evaluate enthalpies of fusion, sublimation, vaporization and formation in the gaseous and solid phases of the compounds; and *ii*) the use of single crystal X-ray diffraction and X-ray powder diffraction in combination with DSC results, as tools to identify and characterize the new polymorphic forms of these materials.

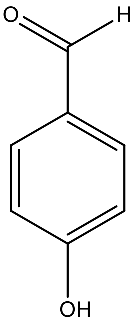

(a)

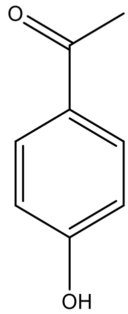

(b)

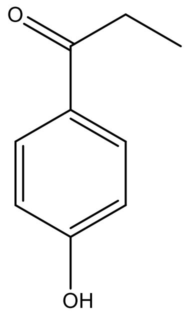

(c)

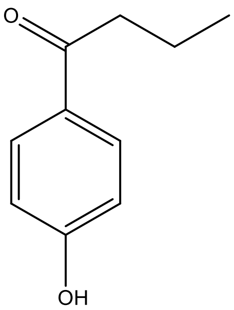

(d)

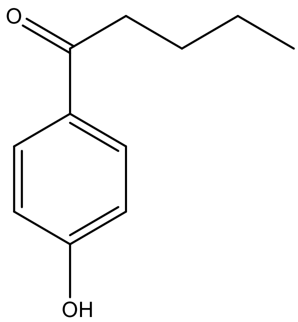

(e)

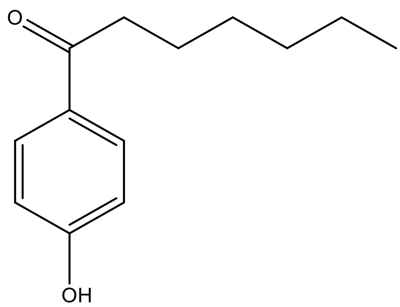

(f)

Figure 1.3. Molecules studied in this thesis: (a) 4-hydroxybenzaldeheyde; (b) 4'-hydroxyacetophenone; (c) 4'-hydroxypropiophenone; (d) 4'-hydroxybutyrophenone; (e) 4'-hydroxyvalerophenone and (f) 4'-hydroxyheptanophenone.

2. Materials and Methods

In this chapter the characterization of all materials used in this work is presented. Also described are the experimental techniques used in the characterization and in the thermodynamic measurements, with the more relevant explained in detail. Finally, a brief summary of the methodologies behind the computational calculations performed by Dr. Filipe Agapito is given.

2.1. Materials

Absolute ethanol p.a supplied by Chem-Lab and ethyl acetate (mass fraction 0.997) supplied by Fluka were used without further purification.

4-Hydroxybenzaldeheyde (HBA, CAS number: 123-08-0) supplied by Aldrich with a mass fraction of 0.98 was purified by sublimation at 350 K and 1.33 Pa. No impurities were detected by Gas Chromatography-Mass Spectrometry (GC-MS) analysis. Proton nuclear magnetic resonance (^{1}H NMR) analysis (400 MHz, $CDCl_3$): δ = 9.87 (*s*, C**H**, 1H), 7.83 (*d*, C**H**, 2H), 6.98 (*d*, C**H**, 2H), 6.15 (*s*, O**H**, 1H). Diffuse reflectance infrared Fourier-transform (DRIFT) analysis (KBr, main peaks): $\tilde{\nu}$ = 3163 ($\nu_{O\text{-}H}$); 2962 ($\nu_{C\text{-}H}$); 1660 ($\nu_{C=O}$); 1589 ($\nu_{C\text{-}C,}$ in ring). The ^{1}H NMR and DRIFT spectra are available in the Supporting Information, section A. The powder pattern recorded at 298±2 K was indexed (Table 2.1) as monoclinic, space group $P2_1/c$, a = 6.4541(20) Å, b = 13.7532(36) Å, c = 7.0286(20) Å, β = 108.19(3)º, which is in agreement with previously published results from single crystal X-ray diffraction (SCXRD)[32]: monoclinic, space group $P2_1/c$, a = 6.453(5) Å, b = 13.810(8) Å, c = 7.044(6) Å, β = 107.94(9)º. The obtained diffractograms are shown in the Supporting Information, section A.

4'-Hydroxyacetophenone (HAP, CAS number: 99-93-4) supplied by Fluka with a mass fraction of 0.98 was purified by sublimation at 368 K and 1.3 Pa. Elemental analysis for $C_8H_8O_2$: expected C 70.57%, H 5.92%; found C 70.68±0.14%, H 5.95±0.06%. No impurities were detected by high performance liquid chromatography electrospray mass spectrometry (HPLC-ESI/MS). ^{1}H NMR analysis (400 MHz, $CDCl_3$): δ = 7.92 (*d*, C**H**, 2H), 7.07 (*s*, O**H**, 1H), 6.93 (*d*, C**H**, 2H), 2.58 (*s*, C**H**$_3$, 3H). DRIFT analysis (KBr, main peaks): $\tilde{\nu}$ = 3174 ($\nu_{O\text{-}H}$); 2991 (ν_{CH_3}); 1643 ($\nu_{C=O}$); 1578 ($\nu_{C\text{-}C,}$ in ring), 1363 (δ_{CH_3}). The ^{1}H NMR and DRIFT spectra are available in the Supporting Information, section A. The powder pattern recorded at 298±2 K was indexed (see Table 2.2) as monoclinic, space group $P2_1/c$, a = 8.6153(59) Å, b = 14.9708(145) Å, c = 12.1601(178) Å, β = 92.320(249)º, which is in agreement with previous published results of SCXRD[29] obtained at the

Table 2.1. Indexation of the X-ray powder diffraction pattern for HBA form I in the range of 7° ≤ 2θ ≤ 35°.

h	*k*	*l*	2θ(obs)/º	$\Delta 2\theta$/º	*h*	*k*	*l*	2θ(obs)/º	$\Delta 2\theta$/º
-1	1	0	15.865	0.053	-1	1	2	26.920	0.031
-1	1	1	17.505	-0.010	0	1	2	27.485	0.017
0	2	1	18.495	-0.011	-2	1	1	28.675	-0.038
-1	2	0	19.410	0.030	-1	2	2	29.180	-0.003
0	3	1	23.500	-0.020	-1	4	0	29.705	-0.062
-1	3	0	24.260	0.039	1	3	1	29.790	-0.068
0	4	0	25.945	0.053	-2	2	1	30.845	-0.038
-1	0	2	26.070	-0.012	-2	2	0	31.965	0.030
0	0	2	26.685	0.007	-2	3	1	34.260	0.036

Table 2.2. Indexation of the X-ray powder diffraction pattern for HAP form I in the range of $7^0 \leq 2\theta \leq 35^0$.

h	*k*	*l*	2θ(obs)/º	$\Delta 2\theta$/º	*h*	*k*	*l*	2θ(obs)/º	$\Delta 2\theta$/º
1	0	0	11.455	-0.080	-1	2	0	23.280	0.091
0	1	1	13.335	0.065	-2	1	0	24.355	-0.004
0	0	2	15.870	0.027	-2	1	1	25.520	-0.057
1	1	1	18.105	0.008	-2	0	2	26.155	0.005
0	1	2	19.160	0.035	-1	1	3	26.925	-0.013
1	0	2	20.505	0.006	-1	2	2	27.800	-0.012
2	0	0	21.370	-0.011	0	1	4	33.760	-0.055

same temperature: monoclinic, space group $P2_1/c$, a = 7.7200(15) Å, b = 8.3600(17) Å, c = 11.280(2) Å, β = 95.02(3)º. The obtained diffractograms are shown in the Supporting Information, section A.

4'-Hydroxypropiophenone (HPP, CAS number: 70-70-2) supplied by Aldrich with a mass fraction of 0.995, was purified prior to use by sublimation at 378 K and 1.3 Pa. Elemental analysis for $C_9H_{10}O_2$: expected: C 71.98%, H 6.71%; C 71.82±0.03%, H 6.63±0.03%. No impurities were detected by HPLC-ESI/MS. ^{1}H NMR analysis (400 MHz, $CDCl_3$): δ = 7.92 (*d*, C**H**, 2H), 6.88 (*d*, C**H**, 2H), 5.55 (*s*, O**H**, 1H), 2.96 (*q*, C**H**$_2$, 2H), 1.22 (*t*, CH_3, 3H). DRIFT analysis (KBr, main peaks): $\tilde{\nu}$ = 3213 ($\nu_{O\text{-}H}$); 2970 (ν_{CH_3}); 1649 ($\nu_{C=O}$); 1572 ($\nu_{C\text{-}C,}$ in ring), 1358 ($\delta_{CH_3,\ CH_2}$). The ^{1}H NMR and DRIFT spectra are available in the Supporting Information, section A. The powder pattern recorded at 298±2 K was indexed (see Table 2.3) as monoclinic, space group $P2_1$/n, a = 8.6153(59) Å, b = 14.9708(145) Å, c = 12.1601(178) Å, β = 92.320(249)º, which is in agreement with results from SCXRD determined in this work at the same temperature (see Chapter 3, section 3.2): monoclinic, space group $P2_1/n$, a = 8.6150(19) Å, b = 14.949(4) Å, c = 12.136(2) Å, β = 92.406(13)º. The obtained diffractograms are shown in the Supporting Information, section A.

4'-Hydroxybutyrophenone (HBP, CAS number: 1009-11-6) provided by Tokyo Chemical Industry (TCI) with a mass fraction of 0.993, was previously purified by sublimation at 348 K and 3.5 Pa. Elemental analysis for $C_{10}H_{12}O_2$: expected C 73.15%, H 7.37%; found C 73.27±0.2%, H 7.45±0.1%. No impurities were detected by HPLC-ESI/MS. ^{1}H NMR analysis (400 MHz, $CDCl_3$): δ = 7.91 (*d*, C**H**, 2H), 6.89 (*d*, C**H**, 2H), 5.70 (*s*, O**H**, 1H), 2.90 (t, C**H**$_2$, 2H), 1.76 (*q*, C**H**$_2$, 2H), 1.00 (*t*, C**H**$_3$, 3H). DRIFT analysis (KBr, main peaks): $\tilde{\nu}$ = 3367 ($\nu_{O\text{-}H}$); 2962 (ν_{CH_3}); 1655 ($\nu_{C=O}$); 1579 ($\nu_{C\text{-}C,}$ in ring), 1365 ($\delta_{CH_3,\ CH_2}$). The ^{1}H NMR and DRIFT spectra are available in the Supporting Information, section A. The powder pattern recorded at 298±2 K was indexed (see Table 2.4) as monoclinic, space group $P2_1/c$, a = 8.3013(38) Å, b = 30.9332(61) Å, c = 7.9059(22) Å, β = 116.87 (2)º, which is in agreement with previously published results single crystal X-ray diffraction[33]: monoclinic, space group $P2_1$/c, a = 8.2650(17) Å, b = 30.986(6) Å,

Table 2.3. Indexation of the X-ray powder diffraction pattern for HPP in the range of $7^0 \leq 2\theta \leq 35^0$.

h	*k*	*l*	2θ(obs)/º	$\Delta 2\theta$/º	*h*	*k*	*l*	2θ(obs)/º	$\Delta 2\theta$/º
1	1	0	11.750	-0.100	0	2	2	18.810	0.013
-1	0	1	12.385	0.036	0	3	1	19.200	-0.012
-1	1	1	13.725	0.030	1	3	0	20.585	0.029
0	2	1	13.895	0.011	2	1	1	22.430	0.029
1	2	0	15.665	-0.011	-2	1	1	22.430	0.015
1	2	1	17.475	0.000	0	1	3	22.695	-0.032

Table 2.4. Indexation of the X-ray powder diffraction pattern for HBP in the range of $7^0 \leq 2\theta \leq 35^0$.

h	k	l	2θ(obs)/º	$\Delta 2\theta$/º	h	k	l	2θ(obs)/º	$\Delta 2\theta$/º
0	4	0	11.465	0.032	1	4	1	23.910	-0.009
-1	2	0	13.250	0.005	-1	4	2	25.270	-0.020
0	2	1	13.815	0.026	-1	8	1	26.400	-0.006
-1	4	1	17.240	0.024	0	4	2	27.795	0.012
0	6	1	21.315	-0.016	-2	4	2	28.320	-0.001
0	8	0	22.980	-0.002	1	8	1	31.280	-0.006

c = 7.9200(16) Å, β = 116.94(3)º. The obtained diffractograms are shown in the Supporting Information, section A.

4'-Hydroxyvalerophenone (HVP, CAS number: 2589-71-1) provided by TCI with a mass fraction of 0.993 was previously purified by crystallization. A solution of 25 cm^3 of ethanol was saturated with HVP at 328 K. With the solution still warm, it was filtered into an Erlenmeyer flask, using Whatman Grade 1 qualitative filter paper. Subsequently the solution was stored in a cooler and kept at 255 K. Well-formed crystals were obtained in approximately 4 days. Through vacuum filtration using a sintered glass funnel, the crystals were separated from the initial solution and dried in air at 293±2 K. Elemental analysis for $C_{11}H_{14}O_2$: expected C 74.13%, H 7.92%; found C 74.33±0.05%, H 7.45±0.1%. No impurities were detected by HPLC-ESI/MS. ^{1}H NMR analysis (400 MHz, $CDCl_3$): δ = 7.92 (*d*, C**H**, 2H), 6.91 (*d*, C**H**, 2H), 6.55 (*s*, O**H**, 1H), 2.93 (*t*, C**H**$_2$, 2H), 1.71 (*m*, C**H**$_2$, 2H), 1.40 (*m*, C**H**$_2$, 2H), 0.94 (*t*, C**H**$_3$, 3H). DRIFT analysis (KBr, main peaks): $\tilde{\nu}$ = 3221 ($\nu_{O\text{-}H}$); 2933 (ν_{CH_3}); 1645 ($\nu_{C=O}$); 1587 ($\nu_{C\text{-}C,}$ in ring), 1344 ($\delta_{CH_3,\ CH_2}$). The ^{1}H NMR and DRIFT spectra are available in the Supporting Information, section A. The powder pattern recorded at 298±2 K was indexed (see Table 2.5) as monoclinic, space group $P2_1/c$, a = 9.9881(45) Å, b = 10.4446(40) Å, c = 9.8792(45) Å, β = 107.52 (4)^0, which is in agreement with prior published results obtained by SCXRD[34] at the same temperature: monoclinic, space group $P2_1$/c, a = 9.990(2) Å, b = 10.454(2) Å, c = 9.882(2) Å, β = 107.46(3)^0. The obtained diffractograms are shown in the Supporting Information, section A.

4'-Hydroxyheptanophenone (HHP, CAS number: 14392-72-4) provided by TCI with a mass fraction of 0.999, was used as received. Elemental analysis for $C_{13}H_{18}O_2$: expected: C 75.69%, H 8.80%; found C 75.79±0.05%, H 8.94±0.07%. No impurities were detected by HPLC-ESI/MS. ^{1}H NMR analysis (400 MHz, $CDCl_3$): δ = 7.91 (*d*, C**H**, 2H), 6.89 (*d*, C**H**, 2H), 5.70 (*s*, O**H**, 1H), 2.90 (t, C**H**$_2$, 2H), 1.76 (*q*, C**H**$_2$, 2H), 1.00 (*t*, C**H**$_3$, 3H). DRIFT analysis (KBr, main peaks): $\tilde{\nu}$ = 3305 ($\nu_{O\text{-}H}$); 2922 (ν_{CH_3}); 1662 ($\nu_{C=O}$); 1585 ($\nu_{C\text{-}C,}$ in ring), 1345 ($\delta_{CH_3,\ CH_2}$). The ^{1}H NMR and DRIFT spectra are available in the Supporting Information. The powder pattern recorded at 298±2 K was indexed (see Table 2.6) as orthorhombic, space group P_{nma}, a = 14.1372(32) Å, b = 7.2079(14) Å, c = 11.7393(15)º, which is in agreement with results from SCXRD determined in this work at the same temperature (see Chapter 3, section 3.2): orthorhombic, space group P_{nma}, a = 14.158(3) Å, b = 7.2246(17) Å, c = 11.762(3)º. The obtained diffractograms are shown in the Supporting Information, section A.

Table 2.5. Indexation of the X-ray powder diffraction pattern for HVP in the range of $7^{o} \leq 2\theta \leq 35^{o}$.

h	*k*	*l*	2θ(obs)/°	$\Delta 2\theta$/°	*h*	*k*	*l*	2θ(obs)/°	$\Delta 2\theta$/°
1	0	0	9.300	0.023	-2	2	1	25.020	0.075
0	1	1	12.655	0.012	-2	2	0	25.315	0.026
0	2	0	16.945	-0.019	0	3	1	27.220	-0.067
1	1	1	17.380	0.070	-2	2	2	27.995	-0.057
-1	0	2	18.295	-0.017	-3	1	0	29.355	-0.024
0	0	2	18.940	0.117	0	1	3	29.675	-0.007
0	2	1	19.410	-0.008	-2	1	3	30.235	0.030
-1	1	2	20.275	0.073	-2	3	1	31.595	0.060
-2	1	0	20.525	0.046	-1	2	3	31.925	-0.193
-2	0	2	22.220	0.045	-3	2	0	32.845	-0.145
1	2	1	22.840	0.071	-2	2	3	33.725	-0.012
-2	1	2	23.745	-0.027	-2	3	2	34.185	0.092

Table 2.6. Indexation of the X-ray powder diffraction pattern for HHP in the range of $7^{0} \leq 2\theta \leq 35^{0}$.

h	*k*	*l*	2θ(obs)/°	$\Delta 2\theta$/°	*h*	*k*	*l*	2θ(obs)/°	$\Delta 2\theta$/°
1	0	1	9.860	0.075	0	2	0	24.710	0.027
2	0	0	12.510	-0.002	0	1	3	25.84	-0.047
0	1	1	14.455	0.047	1	1	3	26.615	-0.041
0	0	2	15.130	0.048	4	1	0	28.075	-0.022
1	1	1	15.715	-0.002	2	1	3	28.820	-0.028
1	0	2	16.380	0.042	1	2	2	29.760	0.016
2	1	0	17.555	-0.004	0	0	4	30.425	-0.008
2	1	1	19.130	0.003	3	1	3	32.190	-0.007
2	0	2	19.675	0.032	1	1	4	33.545	-0.001
1	1	2	20.500	0.017	1	2	3	34.350	0.042
1	0	3	23.600	0.028	0	2	0	24.710	0.027
3	0	2	24.210	0.009	0	1	3	25.84	-0.047

2.2.General Methods

Elemental analyses (C, H) were performed by Laboratório de Análises of Instituto Superior Técnico (LAIST) of Universidade de Lisboa (UL), using a Fisons Intruments EA1108 apparatus. The analyses were made in duplicate, so that the reported values correspond to their average, and the uncertainties are twice the mean deviation.

High performance liquid chromatography electrospray mass spectrometry (HPLC-ESI/MS) was performed at Centro de Química Estrutural, Instituto Superior Técnico (CQE-IST), UL, using a HPLC Dionex Ultimate 3000, consisting of a binary pump HPG3200, an autosampler WPS300, a diode array UV absorbance detector (DAD 3000) set to 254 nm and a column oven TCC3000. This apparatus was coupled in line to a LCQ Fleet ion trap mass spectrometer equipped with an ESI ion source (Thermo Scientific). Methanolic solutions of the compounds were injected into a Phenomenex Luna C18 (2) column (150 mm × 2 mm, 3 μm) at 308 K, by a Rheodyne injector with a 0.02 cm^3 loop. Separation was performed at a flow rate of 3.33×10^{-3} $cm^{-3} \cdot s^{-1}$, with a 300 s linear gradient from 50 to 80% (v/v) of acetonitrile in 0.1% of formic acid in water followed by a 600 s linear gradient until a 100% of acetonitrile. Afterwards, the column was re-equilibrated with 50% acetonitrile in 0.1% (v/v) of formic acid in water for a period of 600 s. The mass spectrometer was operated in the ESI (+/-) ion modes, with optimized parameters: ion spray voltage, ±4.5 kV; capillary voltage, 16/-18 V; tube lens offset, -63/58 V, sheath gas (N_2), 80 arbitrary units; auxiliary gas, 5 arbitrary units; capillary temperature, 573 K. The mass spectra correspond to an average of 20 to 35 scans, recorded in the range between 50 to 500 Da. The data acquisition and processing were carried out using the Xcalibur software.

Proton nuclear magnetic resonance spectra (^{1}H NMR) were obtained at room temperature in a Bruker Ultrashield 400 MHz instrument. The solvent used was deuterated chloroform ($CDCl_3$; Aldrich, 99.8 atom % D) with 1% (v/v) TMS. It was stored over molecular sieves (Aldrich, 4 Å, 8-12 mesh), which were activated prior to use at approximately 0.1 Pa and 493 K during at least 6 h.

Diffuse reflectance infrared Fourier-transform (DRIFT) spectroscopy was performed in a Nicolet 6700 spectrometer (Thermo Electron Corp., Madison, WI) equipped with a deuterated triglycine sulfate (DTGS) detector (4000 – 400 cm^{-1}) and a Smart Diffuse Reflectance (SDR) kit (Thermo Electron Corp.). The spectra were collected with a resolution of 2 cm^{-1}, using 528 scans for the sample and background experiments. The background spectra were recorded with pure KBr (Aldrich, FTIR grade) and the samples were prepared by mixing KBr with the compound in appropriate weight proportions to obtain spectral absorbance in the range of applicability of the Kubelka-Munk transformation.[35]

Single crystal X-ray diffraction (SCXRD) was performed at Laboratório de Cristalografia, CQE-IST-UL. The experiments were done at 167±2 K and 293 K, using a Bruker AXS-KAPPA APEX II and a D8 Quest area detectors diffractometers. The crystals were coated with Paratone-N oil and mounted on a Kaptan loop. A graphite-monochromated Mo Kα (λ = 0.71073 Å) radiation source running at 50 kV and 30 mA was used. An empirical absorption correction was enforced using Bruker SADABS[36] and data reduction was done with Bruker SAINT[37] program. The structures were solved by direct methods with Bruker SHELXS[38] and refined by full-matrix-least-squares on F^2 using SHELXL[38] programs within WINGX-Version 2014.1.[39] Non-hydrogen atoms were refined with anisotropic thermal parameters. Hydrogen atoms were located in the density map and isotropic displacement parameters, U_{iso}(H), refined freely. Structural representations were made using Mercury 3.8[40], and PLATON was used for the hydrogen bond interactions.[41]

X-ray powder diffraction (XRPD) patterns were obtained on Philips X'Pert PRO apparatus equipped with an X'Celerator detector with automatic data acquisition (X'Pert Data Collector, v2.0b, software). The apparatus had a vertical goniometer (PW 3050/60). A Cu Kα radiation source was used. The tube amperage was 30 mA and the tube voltage 40 kV. The diffractograms were recorded at ~293 K in the range 7º < 2θ < 35º. Data was collected in the continuous mode, with a step size of 0.017º (2θ) and scan step times of 20 s. The samples were mounted on an aluminum sample holder. The indexation of the powder patterns was performed using the program Checkcell.[42]

Hot stage polarized optical microscopy (HSM) studies for HVP and HHP were carried out with an Olympus BX51 microscope equipped with a Linkam LTS360 liquid nitrogen-cooled cryostage and a Linkam TMS94 programmable temperature controller. The microstructure of the sample was monitored by taking microphotographs with an Olympus C5060 wide zoom camera. Images were recorded at selected temperatures with 250× or 500× magnification. The sample was placed between two microscope slides and inserted into the hot stage. It was then subjected to a temperature program analogous to that used in the DSC experiments, in the range 173 K to 393 K, using heating/cooling rates of 10 K·min^{-1}.

2.3. Differential Scanning Calorimetry

Differential scanning calorimetry (DSC) was used to assess the purity and evaluate the existence of polymorphism in the studied compounds. For this purpose, the samples were investigated for the occurrence of solid-solid phase transitions and the enthalpies and temperature of fusion determined. Three calorimeters were used (see Figure 2.1): *a*) a DSC 7 from Perkin-Elmer, which was operated above room temperature to determine enthalpies and temperatures of fusion; *b*) a the DSC 204 F1 Phoenix from Netzch, that was used to determine the heat capacities and to evaluate the existence of polymorphism in the temperature range 213 K to 475 K; and *c*) a temperature-modulated TA Instruments 2920 MTDSC apparatus, operated as a conventional DSC, that was used to perform additional polymorphism studies starting at 150 K.

The Perkin-Elmer DSC 7 is controlled by a TAC 7/DX thermal analysis unit, that is connected to a computer and operated with the Pyris V. 7.0 Software from Perkin-Elmer. This calorimeter is a power compensation DSC[43-44] (see Figure 2.2.), where the cell (**1**) has two separated furnaces, the reference furnace (**2**) and the sample furnace (**3**), in which the reference crucible (**4**) and the sample crucible (**5**) are placed, respectively. Each of these furnaces is equipped with a heat source (**6**) and a temperature sensor (**7**). The furnaces are controlled by two separated temperature systems, one for average temperature control and another for differential temperature control. The first system ensures that both the sample and the reference temperatures are increased at a programmed rate, β. When the sample experiences an endothermic (e.g. fusion) or exothermic (e.g. crystallization) transformation or a heat capacity change (e.g. glass transition), a temperature difference (ΔT) develops between the two furnaces. At this point, the differential temperature control system adjusts the power supplied to each of the furnaces to maintain ΔT as small as possible during the course of the experiment. Finally, the difference of the power supplied to the sample and the reference are converted to the heat flow rate, $\Delta\phi$.

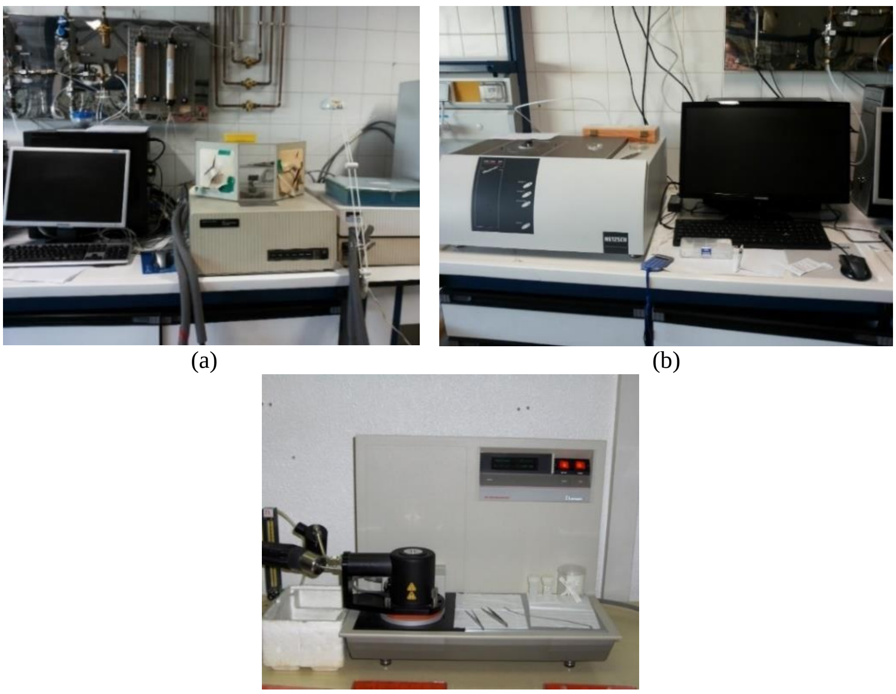

(a) (b)

(c)

Figure 2.1. DSC apparatus used in this work: (a) DSC 7 from Perkin-Elmer, (b) DSC 204 F1 Phoenix from Netzch and (c) TA Instruments 2920 MTDSC.

The Netzch DSC 204 F1 Phoenix and TA Instruments 2920 MTDSC apparatus are disc type heat flux differential scanning calorimeters. As represented in Figure 2.3, these instruments only have one block furnace (**1**) where the temperature is controlled by a computer. Inside this block, both the reference (**2**) and sample crucibles (**3**), are placed over two temperature sensors (**4**) on the supporting disk. During the experiment, if a thermal event occurs, it is identified by a difference in the temperature that develops between the two crucibles. This difference is then recorded and converted to a heat flow rate difference between the sample and the reference.

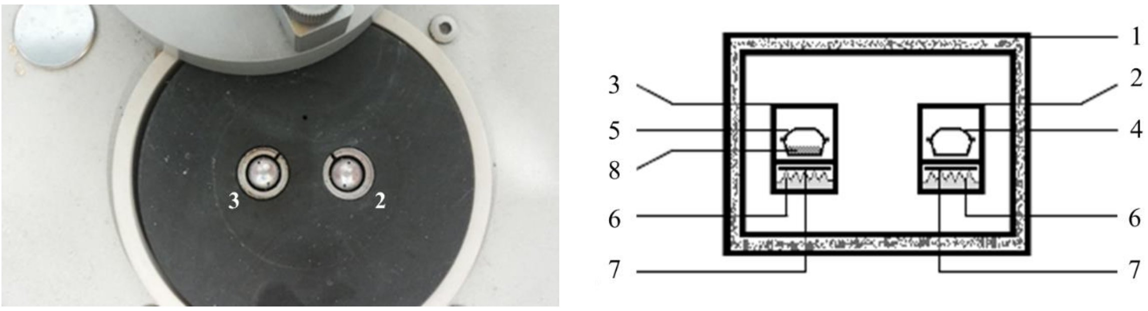

(a) (b)

Figure 2.2. (a) Detail of the two separated furnaces in DSC 7 from Perkin-Elmer and (b) scheme of the power compensation apparatus (adapted from reference 43): **1**, cell; **2**, reference furnace; **3**, sample furnace; **4**, reference crucible; **5**, sample crucible; **6**, heat source **7**, temperature sensor; and **8**, sample.

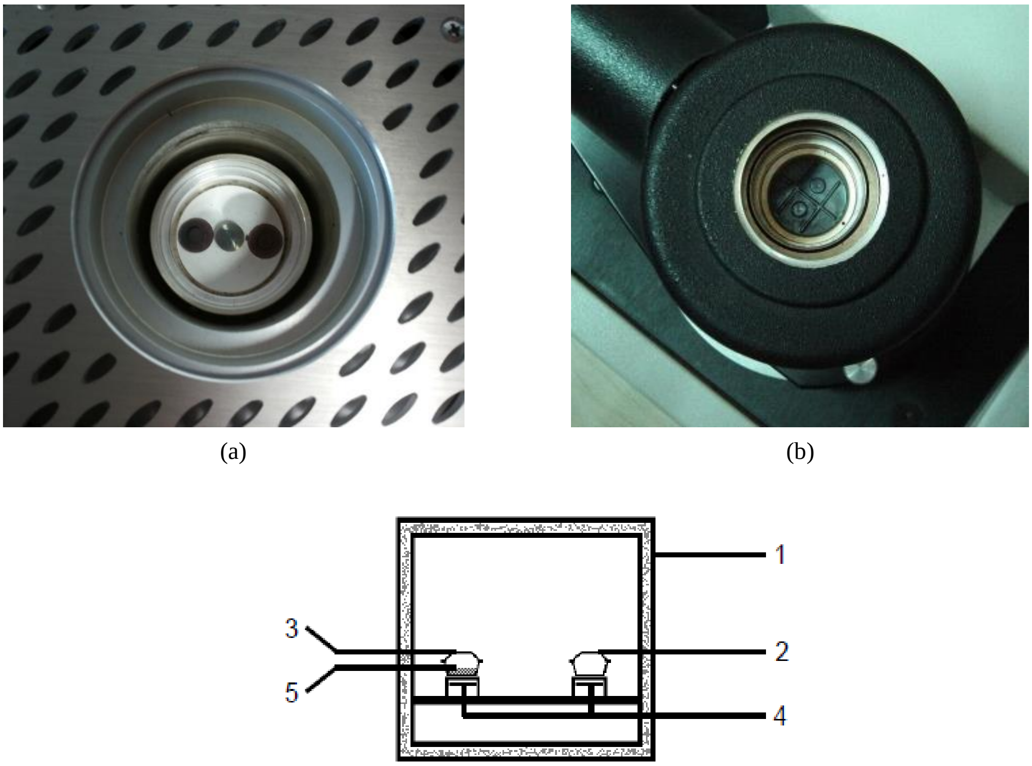

(c)

Figure 2.3. (a) Image of Netzch DSC 204 F1 Phoenix furnace and (b) the TA Instruments 2920 MTDSC furnace. (c) Schematic of a disk type heat flux apparatus (adapted from reference 43): **1**, block furnace; **2**, reference crucible; **3**, sample crucible; **4**, temperature sensors; and **5**, sample.

The temperature and energy scales of the calorimeters were calibrated, based on the fusion of standard substances (temperature and enthalpies of fusion). In the case of the Perkin-Elmer DSC 7, the calibration was performed using indium (Perkin-Elmer; mass fraction 0.99999, T_{fus} = 429.75 K), lead (Goodfellow, mass fraction 0.99995, T_{fus} = 600.61 K) and zinc (Perkin-Elmer; mass fraction 0.99999, T_{fus} = 692.65 K). The calibration of the Netzch DSC 204 F1 Phoenix apparatus was carried out using a calibration kit (6.239.2-91.3.00) containing samples of adamantane (T_{trs} = 208.65 K), indium (T_{fus} = 429.75 K,), tin (T_{fus} = 505.05 K), bismuth (T_{fus} = 544.55 K), zinc (T_{fus} = 692.65 K) and cesium chloride (T_{fus} = 749.15 K). The TA Instruments 2920 MTDSC was calibrated using *n*-decane (Fluka, mass fraction > 0.998, T_{fus} = 243.75 K), *n*-octadecane (Fluka, mass fraction 0.999, T_{fus} = 301.77 K), hexatriacontane (Fluka, mass fraction >0.995, T_{fus} = 347.30 K), indium (TA Instruments, DSC standard, T_{fus} = 430.61 K) and tin (TA Instruments, DSC standard, T_{fus} = 506.03 K). For all apparatus the calibration was periodically verified by measuring the temperature and enthalpy of fusion of indium.

In a typical DSC experiment, the sample was sealed inside an aluminum crucible and weighted with a precision of ±0.1 μg, on a Mettler XP2U or a Mettler UMT2 ultra-micro balance. The crucibles (sample and reference) were placed on the disks (disk type heat flux DSC) or inside the furnaces (power compensated DSC). Each experiment involves the increase or decrease of the furnace(s) temperature at a constant rate, while recording the output signal of the calorimeter as a function of the temperature and time (Figure 2.4). It was assigned that positive heat flow rates correspond to endothermic effects while negative heat flow rates correspond to exothermic events. By using the apparatuses software, for each thermal event in the thermogram, the onset temperature, T_{on}, the peak temperature, T_{max}, and the standard specific enthalpy, Δh^{o}, were computed. When the process corresponded to the fusion of the compound, T_{on} was assigned as its fusion temperature, T_{fus}.

The standard specific enthalpy was calculated from the area (A) of the curve corresponding to the thermal event and the standard molar enthalpy, ΔH^{o}_{m}, of the process was determined by equation 2.1:

$$\Delta H^{o} = \Delta h^{o} \times M \qquad (2.1)$$

in which M corresponds to the molar mass of the sample.

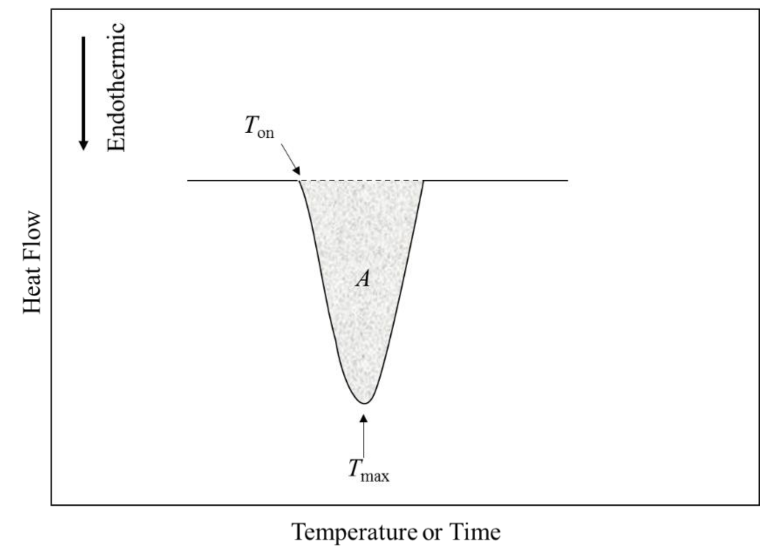

Figure 2.4. Thermogram of an endothermic event where T_{on}, corresponds to the onset temperature, T_{max}, the peak temperature and A to the area of the curve, that is proportional to the standard specific enthalpy of the process.

The determination of the enthalpies and temperatures of fusion were performed using the procedure described above on DSC 7 from Perkin-Elmer and performed under nitrogen (Air liquid N45) flow, at a rate of 30 $cm^3 \cdot min^{-1}$. All the experiments were done with a heating rate of 5 $K \cdot min^{-1}$. The temperature and heat flow were calibrated at the same heating rate as indium. The sample masses used for these determinations were: HPP 1 to 4 mg; HBP 1 to 2 mg; HVP 3 to 7 mg; and for HHP 2 to 5 mg (see Supporting Information, section B).

The heat capacity measurements on HPP, HBP, HVP and HHP, as mentioned above, were carried out on the Netzch DSC 204 F1 Phoenix, using the dynamic mode.[43] The experiments were performed in a single temperature range and involved three different stages (Figure 2.5, gray curve): a fore period, where the system was maintained at the initial temperature, T_i, during 20 minutes; the main period, where the temperature was increased at a constant rate; and the after period, where the system was kept for 20 minutes at the final temperature, T_f.

A typical heat capacity determination involves three consecutive measurements using the same temperature program and the same set of crucibles (Figure 2.5): *i*) a blank experiment performed with two empty crucibles (zero line), *ii*) a run using a reference sapphire disk (Netzsch, ref. 6.239.2-91.5), placed in the sample crucible, and *iii*) a run performed with the sample. In all experiments, the reference crucible was left untouched. The crucibles were chosen so that, the difference in the mass between them when empty was less than 0.01 mg. During the described procedure the heating rates used were 5 $K \cdot min^{-1}$ for HPP and HBP, and 2 $K \cdot min^{-1}$ for HVP and HHP. All runs were performed under a nitrogen stream (Air liquid N45), with a flow rate of 20 $cm^3 \cdot min^{-1}$. The sample masses were: HPP 8 to 16 mg; HBP 3 to 6 mg; HVP 4 to 13 mg; and for HHP 6 to 14 mg (see Supporting Information, section C). Sapphire (Netzch, ref.6.239.2-91.5; ~12mg), was used as the reference material This procedure was previously tested with benzoic acid in the range of 215 K to 345 K.[45] The accuracies obtained at heating rates of 2 $K \cdot min^{-1}$ and 10 $K \cdot min^{-1}$ were 2% and 3%, respectively, taking as benchmark the adiabatic calorimetry data previously reported by Furukawa *et. al.*.[46]

In this work, the heat capacity values were computed with the Netzch Proteus Analysis Software V.6.1.0, using the option ‘C*p* ratio method’. Through this method the molar heat capacity of the sample (S) at a given temperature is given by:[43]

$$C^{o}_{p,\mathrm{m}}\,(\mathrm{S}) = k\frac{M}{m\beta}\Delta\phi \qquad (2.2)$$

where m is the mass of the sample, $\Delta\phi$ is the difference in the heat flow rate between the blank, $\Delta\phi_0$, and the sample, $\Delta\phi_S$, and k is a calibration factor obtained at the same temperature as:

$$k = \frac{C^{o}_{p,\mathrm{m}}\,(\alpha\text{-}\mathrm{Al_2O_3})_\mathrm{L}}{C^{o}_{p,\mathrm{m}}\,(\alpha\text{-}\mathrm{Al_2O_3})_\mathrm{R}} \qquad (2.3)$$

where $C^{o}_{p,\mathrm{m}}(\alpha\text{-}\mathrm{Al_2O_3})_\mathrm{L}$ corresponds to the heat capacity of sapphire reported in literature by Archer[47] and $C^{o}_{p,\mathrm{m}}(\alpha\text{-}\mathrm{Al_2O_3})_\mathrm{R}$ is the molar heat capacity of sapphire obtained experimentally using equation 2.2, assuming $k = 1$ and $\Delta\phi = \Delta\phi_R - \Delta\phi_0$ with $\Delta\phi_R$ representing the heat flow recorded with the sapphire reference.

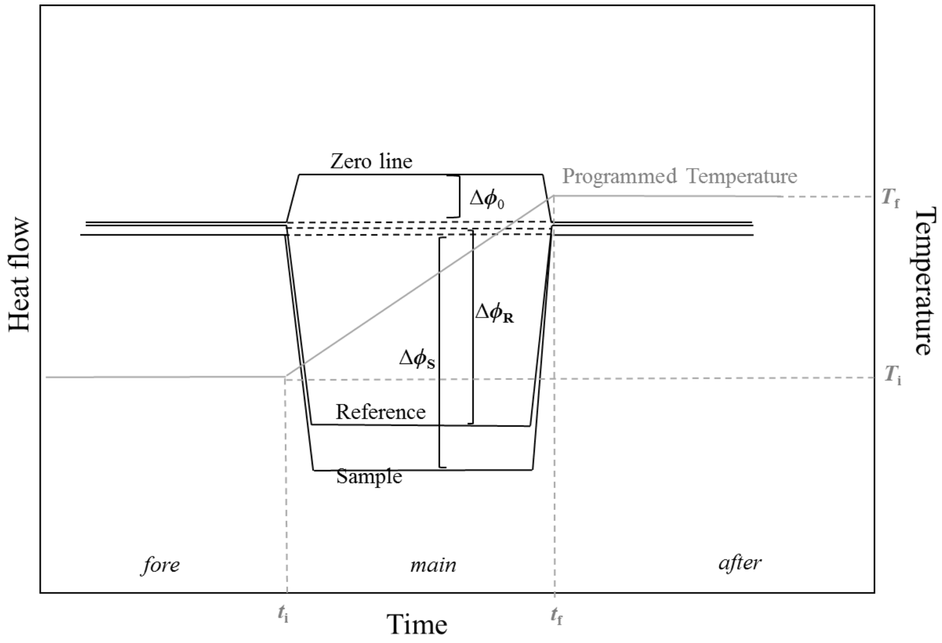

Figure 2.5. Schematic representation of the experimental procedure required to determine heat capacity by DSC using the dynamic mode. The gray curve indicates the temperature program used in the three independent runs (black curves): *i*) blank experiments (zero line) performed using two empty crucibles; *ii*) run performed using a reference compound; and *iii*) experiment with a compound sample. $\Delta\phi_0$, $\Delta\phi_R$, $\Delta\phi_S$ corresponds to the heat flow rate difference of the zero line, reference and sample, respectively.

2.4. Calvet Microcalorimetry

Calvet microcalorimetry was used to determine the enthalpy of sublimation of HPP and HBP and the enthalpy of vaporization of HVP and HHP. The apparatus, is shown in Figures 2.6 and 2.7, is based on a DAM Calvet microcalorimeter.[48-49]

(a) (b)

Figure 2.6. (a) Picture of the Calvet microcalorimeter used in this work, with (b) a close up of the wells.

This apparatus can be used from room temperature up to 473 K and is composed by four wells (**1**, **1'** and **2**, **2'**) operating in pairs (only one pair of wells was used in this work), each one containing a microcalorimetric element (**3**). These are surrounded by a large furnace (**4**), whose temperature was controlled with a precision of ±0.1 K with a Eurotherm 2404 PID unit. In turn, the calorimeter temperature was measured with a precision of ±0.1 K by a Tecnisis 100 Ω platinum resistance thermometer, inserted into one of the microcalorimeter elements not used in the experiments. A Hewlett-Packard 34420A nanovoltmeter was used to measure the differential heat flow through the thermocouples (**5**) of the microcalorimetric elements. Two identical cells, (**6**; 9 mm external diameter by 800 mm height) are inserted in one of the wells pairs, so that the bottom is completely surrounded by the measuring element. One of these cells is used to insert the sample, while the other acts as reference. Each cell consists of a brass cylinder closed at the bottom (**7**; 17 mm external diameter by 100 mm height), and screwed at the top, to a Teflon tube (**8**; 17 mm external diameter by 600 mm height). A glass cell (**9**; 10 mm external diameter by 800 mm height), is placed inside the Teflon tube and brass cylinder. The space between the glass cell and brass element is filled with silicon paste (Sidevan) to improve the thermal contact between them. This glass cell rests over a brass piece (**10**) containing a Manganin wire resistance of 200 Ω (**11**). This resistance is used for the calibration of the apparatus by Joule effect. Above one of the glass cells, there is a small furnace (**12**), where the sample contained in a capillary (**13**) is initially inserted. This well is closed at the bottom by a movable pin (**14**), and, at the top, a miniature platinum resistance sensor (**15**; Labfacility, 1/10), is inserted close to the sample to measure its temperature. By pulling the pin, the sample is dropped into the glass cell, guided by a funnel (**16**). During the experiments, the glass cell is closed by a glass lid and, if necessary, evacuated through the inlet (**17**) which is connected to a vacuum/inert gas (N_2) line.

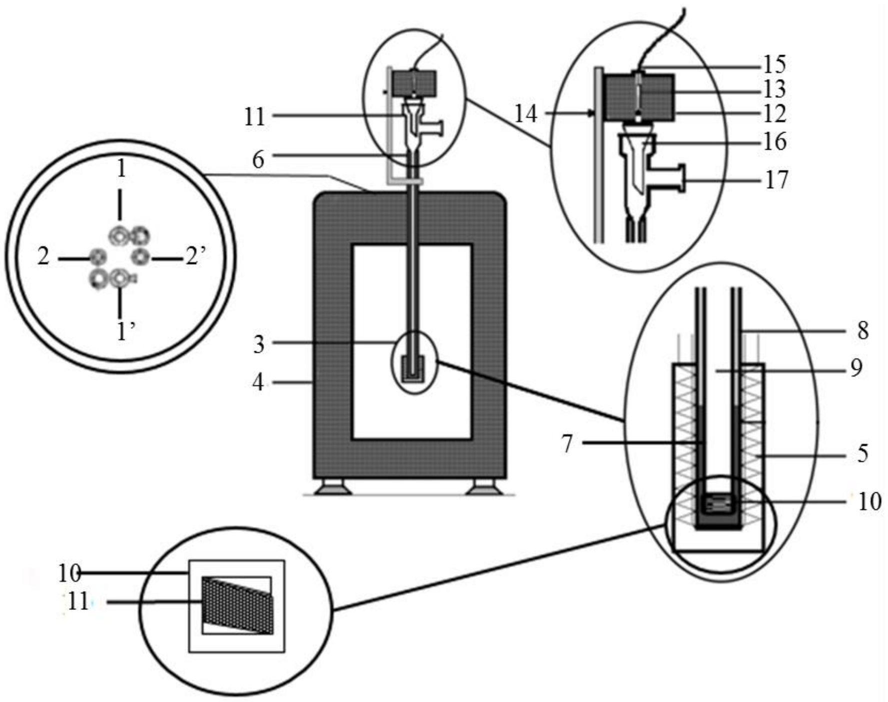

Figure 2.7. Schematic of the Calvet microcalorimeter (adapted from references 48 and 49): **1**, **1'**, **2** and **2'**, wells, **3**, microcalorimetric element, **4,** furnace, **5**, thermocouples, **6**¸measuring cell, **7**, brass cylinder, **8**, Teflon tube, **9**, glass cell, **10**, brass piece, **11**, Manganin wire resistance, **12**, drop furnace, **13**, sample, **14**, movable pin, **15**, lid with platinum resistance sensor, **16**, funnel, **17**, inlet connected to a vacuum/inert gas system.

The pumping system includes an Edwards E02 oil diffusion pump with a liquid nitrogen trap and an Alcatel Adixen Pascal series 2005SD rotary pump. A second liquid nitrogen trap keeps the vacuum system apart from the measuring cell. Only the rotary pump, which can reach an ultimate pressure of approximately 0.13 Pa, was used in this work.

The sensors used to measure the temperature of the calorimetric cell and of the sample inside the small furnace are connected in a four-wire configuration to a Hewlett Packard 34401A multimeter. The calibration of the two sensors was performed against a standard platinum resistance thermometer, which had been previously calibrated at an accredited facility according to the International Temperature Scale ITS-90.

Both the data acquisition and the electrical calibration are computer controlled by the CBCAL 1.0 program.[50] The output of a thermal event is displayed as a plot, in which the heat flow rate $\Delta\phi$, between the reference and the sample calorimetric cells is plotted as a function of time. A typical output from a Calvet drop experiment is represented in Figure 2.8. Initially, N_2 is inserted in the system (*i* in Figure 2.8). At the same time, the sample inside a small glass capillary is weighted on a Mettler XP2U ultra-micro balance with a precision of ±0.1μg. The sample masses used were: HPP 3 to 7 mg; HBP 1 to 6 mg; HVP 2 to 4 mg; and HHP 1 to 11 mg. (see Supplementary Information, Section D).

The sample is positioned inside the drop furnace and equilibrated for about 10 min at 298.15 K. After acquiring a suitable baseline, the furnace pin (**14** in Figure 2.7) is pulled, allowing the sample to fall into the calorimetric cell. An endothermic peak (*ii* in Figure 2.8) is observed as a result of heating the sample from T_{i} (the temperature of the furnace **12** in Figure 2.7) to T_{f} (the Calvet temperature). The calorimetric cell was set at T_{f} = 381.12±0.01 K for HPP and HHP, T_{f} = 351.22±0.01 K for HBP, and T_{f} = 341.73±0.01 K for HVP (the indicated T_{f} correspond to the average of the measurements made and the uncertainties to twice the standard error of the mean from those determinations, see Supplementary Information, Section D). When the curve returned to the baseline the cells were evacuated to approximately 0.13 Pa. The obtained curve (*iii* in Figure 2.8) represents the sublimation/vaporization process of the sample.

The specific enthalpy of sublimation or vaporization, $\Delta_{\mathrm{vap/sub}}h_{\mathrm{m}}$, of the compounds studied in this work, at a given temperature, T, was calculated by

$$\Delta_{\mathrm{vap/sub}}h_{\mathrm{m}}\,(T) = \frac{(A_{\mathrm{iii}} - A_b)}{m\,\varepsilon} \tag{2.4}$$

where m corresponds to the mass of sample, A_{iii} and A_{b}, are the areas of the sublimation or vaporization process (Figure 2.8) and the pumping of N_2 contribution to the process (Figure 2.9), respectively, and ε is the energy equivalent of the calorimeter (calibration constant) given by the following equation

$$\varepsilon = \frac{A_{\mathrm{c}}}{VIt} \tag{2.5}$$

where A_{c} (Figure 2.9), corresponds to the area of the calibration measuring curve, V and I are the current voltage and intensity, respectively, applied to the Manganin wire resistance, during a period of time t. The electrical calibrations were performed at the same temperatures of the main experiments. The following values were obtained: 63.713±0.067 $\mathrm{mV{\cdot}J^{-1}{\cdot}s}$ for HPP and HHP; 64.111±0.037 $\mathrm{mV{\cdot}J^{-1}{\cdot}s}$ for HBP, and 63.929±0.103 $\mathrm{mV{\cdot}J^{-1}{\cdot}s}$ for HVP (the indicated ε values correspond to the average of the measurements made and the uncertainties to twice the standard error of the mean from those determinations, see Supplementary Information, Section D).

The standard molar enthalpy of sublimation or vaporization at the working temperature, $\Delta_{vap/sub}H^{o}_{m}(T)$, was obtained through

$$\Delta_{vap/sub}H^{o}_{m} = \Delta_{vap/sub}h_{m} \times M \quad (2.6)$$

in which, $\Delta_{vap/sub}h_{m}$, corresponds to the average of all the measurements and M is the molar mass of the compound.

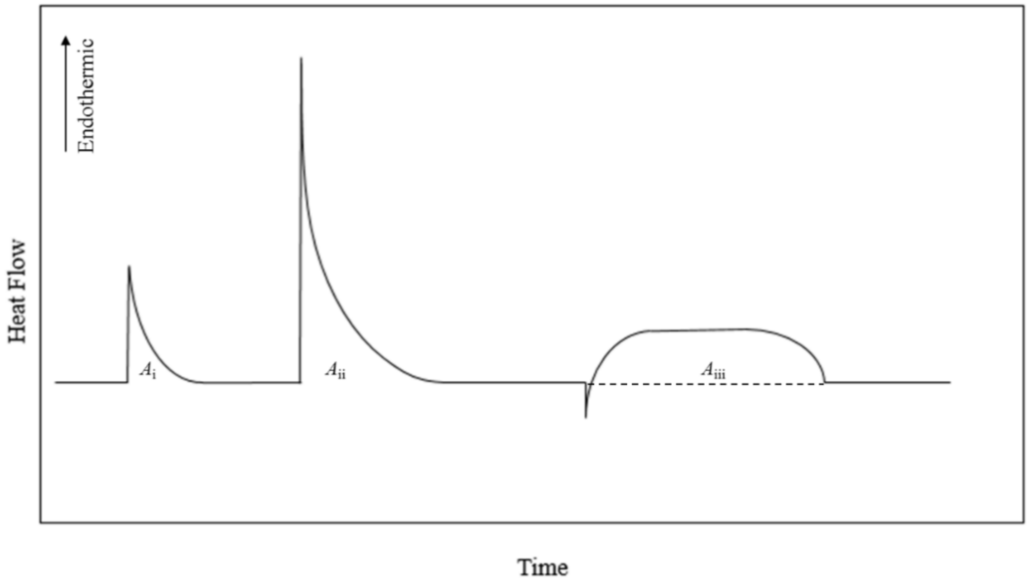

Figure 2.8. Scheme of a Calvet drop experiment: A_i, N_2 introduction, A_{ii}, sample drop, A_{iii}, sublimation/vaporization experiment.

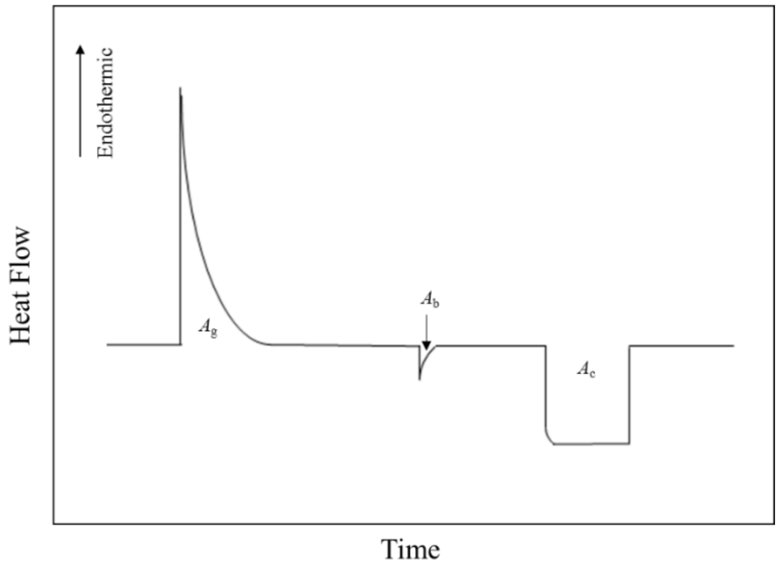

Figure 2.9. Schematic representation of the auxiliary measuring curves required for the computation of the molar enthalpies of sublimation or vaporization of the compounds: A_g, represents the area associated to the energy necessary to heat the glass from 298.15 K to the sublimation/vaporization temperature; A_b, is the area of the thermal effect associated with pumping of the N_2 atmosphere in the cells; and A_c represents the area associated with the determination of the energy equivalent of the calorimeter.

For HPP and HBP, the correction of the enthalpy of sublimation, $\Delta_{\text{sub}}H^{\text{o}}_{\text{m}}(T)$, to 298.15 K relied in the equation:

$$\Delta_{\text{sub}}H^{\text{o}}_{\text{m}}(298.15\text{ K}) = \Delta_{\text{sub}}H^{\text{o}}_{\text{m}}(T) + \int_{T}^{298.15\text{ K}} \left[C^{\text{o}}_{p,\text{ m}}(\text{g}) - C^{\text{o}}_{p,\text{ m}}(\text{cr})\right]\text{d}T \quad (2.7)$$

while the calculation of the enthalpies of sublimation of HVP and HHP at 298.15 K from the corresponding $\Delta_{\text{vap}}H^{\text{o}}_{\text{m}}(T)$ values, was performed using:

$$\Delta_{\text{sub}}H^{\text{o}}_{\text{m}}(298.15\text{ K}) = \Delta_{\text{vap}}H^{\text{o}}_{\text{m}}(T) + \int_{T}^{298.15\text{ K}} C^{\text{o}}_{p,\text{ m}}(\text{g})\,\text{d}T - [H^{\text{o}}_{\text{m}}(\text{cr, 298.15 K}) - H^{\text{o}}_{\text{m}}(1,T)] \quad (2.8)$$

In equations (2.7) and (2.8) $C^{\text{o}}_{p,\text{ m}}(\text{cr})$ and $C^{\text{o}}_{p,\text{ m}}(\text{g})$ correspond to the standard molar heat capacities of the compounds in the solid and gaseous states, respectively. The temperature dependence of $C^{\text{o}}_{p,\text{ m}}(\text{cr})$ was determine by DSC, while the analogous dependence of $C^{\text{o}}_{p,\text{ m}}(\text{g})$ was obtained by Statistical Mechanics[51] (more details in section 2.5). The term $\left[H^{\text{o}}_{\text{m}}(\text{cr, 298.15 K}) - H^{\text{o}}_{\text{m}}(1,T)\right]$ is the difference between the standard molar enthalpy of the solid at 298.15 K and the liquid at the experimental vaporization temperature, *T*. This value was determined from numeric integration of the heat capacity values found in the DSC experiments and by direct measure with the Calvet microcalorimeter, using the equation:

$$[H^{\text{o}}_{\text{m}}(\text{cr, 298.15 K}) - H^{\text{o}}_{\text{m}}(1,T)] = \frac{M(A_{\text{ii}} - A_{\text{g}})}{m\,\varepsilon} \quad (2.9)$$

where A_{ii} is the area of the measuring curve associated with dropping the glass capillary containing the compound into the calorimeter (Figure 2.8), and A_{g} is the area required to heat the same mass of glass, as the one used in the experiments, from 298.15 K to the temperature *T* (Figure 2.9). These experiments used samples with the mass range from 3 to 9 mg for HVP and 5 to 7 mg for HHP.

To obtain A_{g}, an empty glass tube, weighted on a Mettler XP2U ultra-micro balance with a precision of ±0.1µg, was inserted inside the drop furnace and left to equilibrate for ~10 minutes. The capillary was then dropped into the cell and the corresponding curve recorded. The contribution of the glass was finally obtained from a linear correlation between the capillary mass (m_{c}) and the area of the measured curve.

At the end of each set of experiments the capillaries and the calorimetric cell were checked for residues. No residues were found in the capillaries and calorimetric cell after the experiments, indicating that the measured processes correspond to clean vaporizations or sublimations.

2.5. Computational Details

All theoretical calculations used in this thesis were carried out by Dr. Filipe Agapito (CQB FCUL). B3LYP-D3 dispersion corrected[52] hybrid density functional[53-54] calculations using the cc-pVTZ basis set were performed to optimize the structures of the compounds studied in this work. The relative energies of *E* and *Z* conformers were analyzed, showing that *E* conformers had lower energy. Therefore, the structures of the *E* conformers were used in all subsequent theoretical calculations. The vibrational frequencies, scaled by 0.9889,[55] obtained at the same level of theory, were used to determine gas-phase heat capacity at constant pressure ($C^{\circ}_{p,\mathrm{m}}$(g)) for all the molecules used in this work with temperature ranging from 200 to 400 K with increments of 1 K.

3. Results and Discussion

The main goal of this thesis, as previously mentioned, is the study of polymorphism on the selected compounds for this work by two different approaches: the energetic and structural. Due to the lack of reliable data in literature for these compounds, the energetic studies can be separated into several different stages: *i*) determination of both fusion temperatures and standard (p^o = 1 bar) molar enthalpies of fusion, $\Delta_{fus}H^o_m$, by differential scanning calorimetry (DSC); *ii*) determination of the standard molar enthalpy of vaporization, $\Delta_{vap}H^o_m$, for 4'-hydroxyvalerophenone (HVP) and 4'-hydroxyheptanophenone (HHP) and the standard molar enthalpy of sublimation, $\Delta_{sub}H^o_m$, for 4'-hydropropiophenone (HPP) and 4'-hydroxybutirophenone (HBP) by Calvet drop microcalorimetry; *iii*) heat capacity measurements of the compounds to allow the suitable correction of the $\Delta_{vap}H^o_m$ and $\Delta_{sub}H^o_m$ to T = 298.15 K and; *iv*) finally, the standard molar enthalpies of formation both in the solid state, $\Delta_f H^o_m$ (cr), as in the gaseous state, $\Delta_f H^o_m$ (g), at T = 298.15 K. These last values were only possible to obtain through the computational calculations done by Filipe Agapito.

After obtaining all the energetics data, the structural approach to study possible polymorphs began. At an initial stage, DSC measurements were made to assess if changing the temperature would show evidence of new polymorphs on the molecules studied. The main discoveries done by this technique were then ascertained by single crystal X-ray diffraction (SCXRD), X-ray powder diffraction (XRPD) and hot stage microscopy (HSM).

This chapter presents the results obtained for all this data, as well as a discussion of those results. All the molar quantities were based on molar masses, *M*, calculated from atomic weights accordingly to the IUPAC Commission in 2013[56]. The values reported throughout this work correspond to the average of five measurements and the uncertainties indicated correspond to twice the standard deviation of the mean of those measurements (unless otherwise stated), which is given by the following equation:

$$\sigma_m = \left[\frac{\sum_{i=1}^{n}(\Delta_r H_i - \langle\Delta_r H\rangle)^2}{n(n-1)}\right]^{1/2} \qquad (3.1)$$

where $\langle\Delta_r H\rangle$ and $\Delta_r H_i$ corresponds to the mean of the determinations and the values of the individual experiments, respectively.[43]

The energetic line of the work developed within this thesis has already been approved for publishing on *The Journal of Chemical Themodynamics* under the title *Thermochemistry of* HOC_6H_4COR *(R = H,* CH_3, C_2H_5, *n-* C_3H_7, *n-* C_4H_9, *n-* C_5H_{11} *and n-* C_6H_{13}*) compounds* with the DOI 10.1016/j.jct.2016.09.026. The polymorphism studies done for 4'-hydroxyvalerophenone have also been accepted for publication on *The European Physical Journal* under the title *A New Polymorph of 4'-Hydroxyvalerophenone Revealed by Thermoanalytical and X-ray Diffraction Studies*.

3.1. Energetics

No phase transitions other than fusion were observed for the starting materials used in this work, in the temperature ranges selected for each compound as can be seen in Figure 3.1. This fact indicates that from room temperature until the fusion no other crystalline structures are present on the compounds. The onset (T_{on}) and maximum (T_{max}) temperatures of the peak fusion obtained through DSC measurements for all the compounds are presented in Table 3.1. It was assigned that the fusion temperature, T_{fus}, corresponds to the value of T_{on}. The corresponding molar enthalpy of fusion ($\Delta_{fus}H^{o}_{m}$) obtained for the compounds is also listed in Table 3.1 (see Supporting Information, section B).

The standard (p^{0} = 1 bar) molar heat capacities of the compounds studied in this work were determined by DSC, as described elsewhere (Chapter 2, section 2.3). The heat capacity measurements for 4'-hydroxypropiophenone (HPP), 4'-hydroxybutyrophenone (HBP), 4'-hydroxyvalerophenone (HVP) and 4'-hydroxyheptanophenone (HHP) were determined in the following temperature ranges: 283.15 K to 384.15 K for HPP; 283.15 K to 351.15 K for HBP; 283.15 K to 352.15 K for HVP and 283.15 K to 387.15 K for HHP. In the case of HPP and HBP the results obtained only correspond to the solid state while for HVP and HHP the results refer to both the solid and liquid states. All this data is presented in Supporting Information, section C and illustrated in Figure 3.2. The $C^{o}_{p,m}$ values reported are the average determinations of all the

Table 3.1. Results obtained by DSC for, T_{fus}, T_{max}, and $\Delta_{fus}H^{o}_{m}$ of the studied molecules.

Compound	T_{fus} / K	T_{max} / K	$\Delta_{fus}H^{o}_{m}$ / kJ·mol^{-1}
HPP	421.6±0.4	423.4±0.4	31.64±0.38
HBP	364.7±0.2	366.1±0.3	23.99±0.04
HVP	334.6±0.7	336.9±0.2	25.75±0.26
HHP	364.7±0.3	366.5±0.6	31.49±0.10

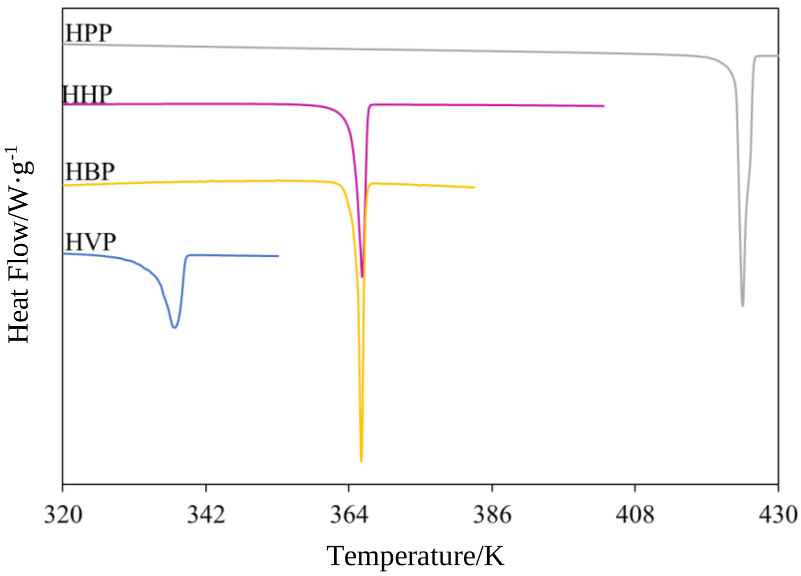

Figure 3.1. Typical DSC measuring curves obtained for HPP, HBP, HVP and HHP. All the curves were previously normalized with the mass of the respective sample.

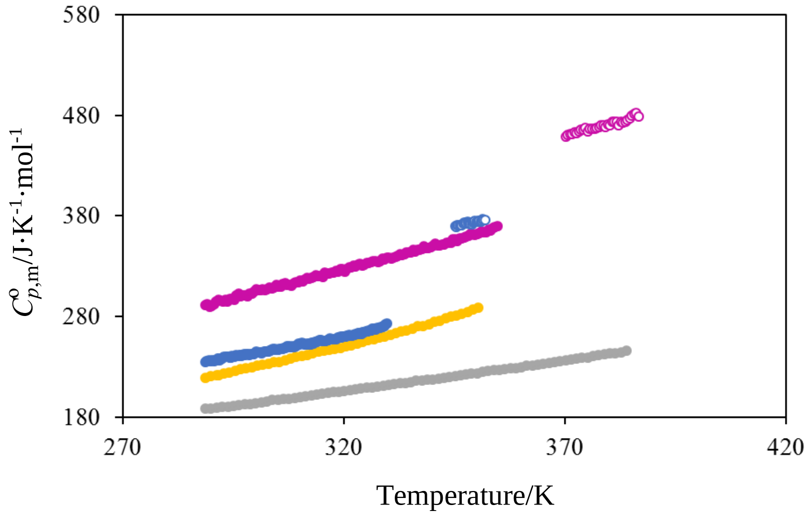

Figure 3.2. Heat capacities determinations for solid state, $C^{o}_{p,m}$ (cr) which are illustrated as full round markers while the heat capacities determinations for liquid state, $C^{o}_{p,m}$ (liq) are represented as empty round markers. The grey markers correspond to HPP, the yellow markers to HBP, the blue markers to HVP and the purple markers for HHP.

performed runs (three to eight measurements) and the uncertainties correspond to twice the standard deviation of the mean for those experiments. The standard molar heat capacities of the gaseous state in the range of 200 K to 400 K, were determined with Statistical Mecahnics[51] using harmonic vibration frequencies obtained by the B3LYP-D3/cc-pVTZ method and scaled by 0.9889.[55] The obtained $C^{o}_{p,m}$ values of the solid, liquid and the gaseous state were fitted according to the following equation:

$$C^{o}_{p,m}/\text{J}\cdot\text{K}^{-1}\text{mol}^{-1} = a\,(T/\text{K})^2 + b\,(T/\text{K}) + c \qquad (3.2)$$

using the MS Excel LINEST function. The obtained *a*, *b* and *c* coefficients are summarized in Table 3.2, as well as their application range.

Table 3.2. Coefficients of the heat capacity obtained by equation (3.2) for the solid, liquid and gaseous states.

		T/K	a	b	c	R^2
HPP	(cr)	288.7 - 350.5		0.6032±0.0018	13.03±0.59	0.9994
	(g)	200 - 400	–(1.0343±0.0391)·10^{-4}	0.5596±0.0024	14.48±0.34	0.99997
HBP	(cr)	288.7 - 350.5		1.0932±0.0111	–(98.13±3.55)	0.995
	(g)	200 - 400	–(5.9887±0.4994)·10^{-5}	0.5979±0.0030	19.77±0.44	0.99996
HVP	(cr)	288.7 - 329.2		0.8266±0.0060	–(4.12±1.87)	0.991
	(l)	346.2 - 351.9		0.7967±0.0981	95.49±34.23	0.94
	(g)	200 - 400	–(1.2263±0.6005)·10^{-5}	0.6317±0.0036	25.98±0.53	0.99995
HHP	(cr)	288.7 - 354.7		1.1550±0.0052	–(42.61±1.69)	0.997
	(l)	370.2 - 386.7		1.1893±0.0565	19.47±21.39	0.93
	(g)	200 - 400	(8.0565±0.8048)·10^{-5}	0.7021±0.0048	37.79±0.71	0.99994

The Calvet-drop microcalorimetry measurements led to following specific enthalpies of sublimation or vaporization that were calculated from equation (2.4): $\Delta_{sub}h$ (HPP) = 748.74±1.98 J·g^{-1} and $\Delta_{vap}h$ (HHP) = 490.99±3.34 J·g^{-1} at T_f = 381.12±0.01 K, $\Delta_{sub}h$ (HBP) = 695.05±3.79 J·g^{-1} at T_f = 351.22±0.01 K, $\Delta_{vap}h$ (HVP) = 539.05±1.36 J·g^{-1} at T_f = 341.73±0.01 K. The values reported are the average of the number of measurements (five to seven experiments) performed for each compound. All the values are presented in the Supporting Information, section D.

The standard molar enthalpies of sublimation and vaporization were obtained using equation (2.6): $\Delta_{sub}H^o_m$(HPP) = 112.44±0.64 kJ·mol^{-1}, $\Delta_{sub}H^o_m$(HBP) = 114.13±1.25 kJ·mol^{-1}, $\Delta_{vap}H^o_m$(HVP) = 96.08±0.57 kJ·mol^{-1} and $\Delta_{vap}H^o_m$(HHP) = 101.28±1.39 kJ·mol^{-1}. The corrections of $\Delta_{sub}H^o_m$(HPP) and $\Delta_{sub}H^o_m$(HBP) form the Calvet temperature, T, to 298.15 K relied on equation (2.7) while the enthalpies of sublimation of HVP and HHP at 298.15 K were obtained from the corresponding $\Delta_{vap}H^o_m(T)$ relied on equation (2.8).

As mentioned in the previous chapter in section 2.4, the value for the $[H^o_m(\text{cr, 298.15 K}) - H^o_m(1,T)]$ was obtained by two different methods. This was done only for HVP and HHP by direct measurement of the process obtained by Calvet-drop calorimetry and numerical integration of the appropriate heat capacity determined by DSC (see Supplementary Information, section C). For HVP, the first method led to $[H^o_m(\text{cr, 298.15 K}) - H^o_m(\text{l, 341.73 K})]$ = –(39.79±0.12) kJ·mol^{-1} while the second give $[H^o_m(\text{cr, 298.15 K}) - H^o_m(\text{l, 341.73 K})]$ = –39.56 kJ·mol^{-1}. The average value of both determinations $[H^o_m(\text{cr, 298.15 K}) - H^o_m(\text{1, 341.73 K})]$ = –(39.68±0.12) kJ·mol^{-1}, was taken in this work. The uncertainty reported corresponds to the mean deviation of the two results. In turn, the results for HHP were: $[H^o_m(\text{cr, 298.15 K}) - H^o_m(\text{1, 381.12 K})]$= –(61.51±0.25) kJ·mol^{-1} (Calvet microcalorimetry) and $[H^o_m(\text{cr, 298.15 K}) - H^o_m(\text{1, 381.12 K})]$ = –61.92 kJ·mol^{-1} (DSC), giving a mean value $[H^o_m(\text{cr, 298.15 K}) - H^o_m(\text{1, 381.12 K})]$ = –(61.72±0.20) kJ·mol^{-1}. The obtained values by the two different approaches reveals a good internal consist and accuracy of the $[H^o_m(\text{cr, 298.15 K}) - H^o_m(1, T)]$ values. In Table 3.3, a summary of the obtained $\Delta_{sub}H^o_m$ values at 298.15 K, along with previously reported data for HBA and HAP is shown.

Figure 3.3 demonstrates an approximately linear relationship which was obtained by plotting $\Delta_{sub}H^o_m$ values obtained within the molecular energetics group (99.7±0.4 kJ·mol^{-1} for HBA cr I; 100.2±2.8 kJ·mol^{-1} for HBA cr II; 103.2±0.8 kJ·mol^{-1} for HAP cr I; 104.3±0.4 kJ·mol^{-1} for HAP cr II; 114.5±0.6 for HPP kJ·mol^{-1}; 116.7±1.3 kJ·mol^{-1} for HBP; 125.9±0.6 kJ·mol^{-1} for HVP; 139.3±1.4 kJ·mol^{-1} for HHP) against the number of carbon atoms in the alkyl side chain, n_c. A least squares fit to the data was performed and led to

$$\Delta_{sub}H^o_m/\text{kJ·mol}^{-1} = (6.65\pm0.65)\ n_c + (98.84\pm1.88) \quad (3.3)$$

for 95% probability, with a regression coefficient of R^2 = 0.986. Equation (3.3) reproduces the data set in which it was based with a maximum deviation of 2.4 kJ·mol^{-1} and a standard deviation of 2.0 kJ·mol^{-1} This slope is similar to those obtained from linear least squares fits to $\Delta_{sub}H^o_m$ vs. T data for series of 4-n-akylbenzoic acids (5.50±0.29)[57] and 4-n-alkyloxybenzoic acids (5.75±1.07)[58]. Also through equation (3.3) it is possible to estimate the value of $\Delta_{sub}H^o_m$ for 1-(4-hydroxyphenyl)-1-pentanone (HPTP, R = C_5H_{11}) presented in table 3.3, where the assigned uncertainty corresponds to the maximum deviation mentioned above. Additionally, this figure also suggests a good internal consistency between the enthalpies of sublimation obtained in this work and those previously determined for HBA[28, 30] and HAP[29].

Table 3.3. Thermochemical data for 4-HOC_6H_4COR compounds (R = H, CH_3, C_2H_5, n-C_3H_7, n-C_4H_9, n-C_5H_{11} and n-C_6H_{13}), at T = 298.15 K and p^o = 1 bar.[a]

Compound	R	$-\Delta_f H_m^o(cr)$ /(kJ·mol^{-1})	$\Delta_{sub} H_m^o$ /(kJ·mol^{-1})	$-\Delta_f H_m^o(g)$ /(kJ·mol^{-1})
HBA	H			215.0±4.0[b]
(cr I)		320.0±2.0[d]	99.7±0.4[d]	220.3±2.0[d]
		320.3±1.3[e]	102.5±0.5[e]	217.8±2.4[h]
			92.0±1.5[f]	
			99.0±3.4[g]	
(cr II)		320.5±2.0[h]	100.2±2.8[h]	
HAP	CH_3			259.7±4.0[b]
(cr I)		368.9±1.9[i]	103.2±0.8[i]	265.7±2.1[i]
(cr II)		369.4±1.9[i]	104.3±0.4[i]	
HPP	C_2H_5	397.3±4.0[k]	114.5±0.6[j]	282.8±4.0[b]
HBP	C_3H_7	420.8±4.2 [k]	116.7±1.3[j]	304.1±4.0[c]
HVP	C_4H_9	451.6±4.0[k]	125.9±0.6[j]	325.7±4.0[c]
HPTP	C_5H_{11}	479.4±4.7[l]	132.1±2.4[l]	347.3±4.0[c]
HHP	C_6H_{13}	508.4±4.2[k]	139.3±1.4[j]	369.1±4.0[c]

[a]Expanded uncertainties, $U = 2u_c$. [b]W1-F12 calculations; uncertainties were estimated based on a previous accuracy assessment of the theoretical methodology 59. [c]CCSD(T)-F12/cc-pVDZ-F12 calculations; uncertainties were estimated based on a previous accuracy assessment of the theoretical methodology 59 [d]Reference 28. [e]Reference 60. [f]Reference 28, 61. [g]References 28, 62. [h]Reference 30. [i]Reference 29. [j]This work, Calvet-drop vaporization microcalorimetry. [k]Calculated as $\Delta_f H_m^o(cr) = \Delta_f H_m^o(cr) - \Delta_{sub} H_m^o$ by using the theoretically computed $\Delta_f H_m^o(g)$ values and experimentally determined or estimated results obtained in this work. [l]Estimated from equation (3.3).

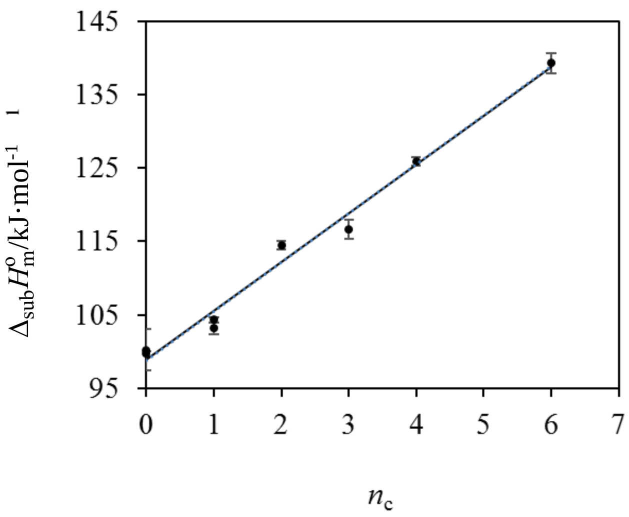

Figure 3.3. Standard molar enthalpies of sublimation for the compounds studied at 298.15 K, as function of the number of carbon (n_c) atoms in the alkyl side chain.

The standard molar enthalpies of formation in the gas phase of the compounds studied in this work were determined by theoretical calculations and are also listed in Table 3.3. Additionally, the reported experimental $\Delta_f H_m^o(g)$ values for R = (H, CH_3), and the enthalpies of formation in the crystalline state, $\Delta_f H_m^o$ (cr) obtained through the computed $\Delta_f H_m^o(g)$ values with the experimentally determined $\Delta_{sub} H_m^o$ data. An uncertainty of 4 kJ·mol^{-1} was attributed to the calculated $\Delta_f H_m^o(g)$ results, based on a previous assessment of the theoretical methodology carried out using n-alkanes and alkylimidazoles.[59] As shown in Table 3.3, where comparison is possible, the theoretically computed and experimental $\Delta_f H_m^o(g)$ values are in good agreement within their combined uncertainties. This suggests that the effect of conformers and tautomers in the thermochemistry of these molecules should be within the assigned experimental errors.

3.2. Polymorphism Studies

An easy, quick and affordable way to conduct a preliminary polymorphism study is through differential scanning calorimetry (DSC). All the molecules were initially studied using a DSC 204 F1 Phoenix from Netzch or a TA Instruments 2920 MTDSC. Additionally, single crystal X-ray diffraction (SCXRD) and X-ray powder diffraction (XRPD) were performed to complete these studies. The DSC results presented are those obtained from the TA instruments 2920 MTDSC which was able to reach lower temperatures than the DSC 204 F1 Phoenix from Netzch. The results shown correspond to 4'-hydroxyvalerophenone (HVP) and 4'-hydroxyheptanophenone (HHP). For the other compounds the phase transitions detected were not reproducible on both apparatuses and therefore their results were not presented. The experiments are composed by successive cycles of heating and cooling of the compounds. The SCXRD allowed to obtain structures for the first time, for 4'-hydroxypropiophenone (HPP) and 4'-hydroxyheptanophenone (HHP). Also it was possible to access the already known structure of 4'-hydroxyvalerophenone (HVP). While investigating this family no suitable crystals were obtained for 4'-hydroxybutyrophenone (HBP).

Although the results from DSC did not show any evidence of polymorphism HPP structures were determined at two different temperatures (150±2 K and 293±2 K) to investigate if any structural changes occurred. The crystal data and refinement parameters obtained for both structures are listed in Table 3.4. The results show that the crystal system, space group and Z/*Z'* did not change with different temperatures. An expansion took place on *a* and *c* axis, as well as in the volume of the unit cell. Furthermore, a decrease of *b* and *β* was reported. Also, a decrease on the densities of the molecule from the low temperature to high temperature took place (see Table 3.4). The only differences detected were on the cell parameters which were expected to change as the temperature changed. In Figure 3.4 it is possible to see the relative orientation of the -CO and -OH groups in the molecule and the packing motifs found in this compound. The two equivalent molecules of HPP exhibit an *E* conformation (Figure 3.4a), which according to the computational calculations is more stable than the *Z* conformer. In the crystalline packing of this compound, each equivalent molecule is arranged alternatively via OH···O hydrogen bonds forming planar one-dimensional chains of the $C^1_1(8)$ type. These chains are characterized by having eight atoms between one donor and one acceptor of the hydrogen bond (Figure 3.4b). These chains grow almost with an angle of 90º and the packing is done parallel to the initial chains. One of the chains grows along the *b* axis, while the other grows along the bisection between the *a* and *c* axis (Figure 3.5). The hydrogen bond is of the type "head-to-tail" OH···O ($d_{OH\cdots O}$) between the hydroxyl group ("head", hydrogen donor) of one molecule and the carbonyl group ("tail", acceptor) of an adjacent molecule. In-between chains the hydrogen bonds have different distances. In the *b* chain $d_{OH\cdots O}$ = 1.766 Å, while on the other chain $d_{OH\cdots O}$ = 1.793 Å. These chains are reinforced by $CH_{ring}\cdots O_{carbonyl}$ interactions ($d_{CH\cdots O}$ = 2.566 Å for the *b* chain and $d_{CH\cdots O}$ = 2.604 Å for the *ac* bisect chain) involving a ring CH bond and a carbonyl oxygen from an adjacent molecule. In addition, the packing is also reinforced with $CH_{ring}\cdots O_{hydroxyl}$ since the chains grow with the "head" in the opposite way of the "tail" ($d_{CH\cdots O}$ = 2.599 Å for the *b* chain and $d_{CH\cdots O}$ = 2.623 Å for the *ac* bisect chain).

Table 3.4. Crystal data and structure refinement parameters for 4'-hydroxypropiophenone at 150 and 293 K.

	4'-Hydroxypropiophenone	
Empirical Formula	$C_9H_{10}O_2$	$C_9H_{10}O_2$
Formula Weight	150.17	150.17
Temperature	150(2)	293(2)
Wavelength (Å)	0.71073	0.71073
Crystal size (mm^{-3})	0.400 × 0.300 × 0.150	0.400 × 0.300 × 0.150
Crystal system	Monoclinic	Monoclinic
Space Group	$P2_1/n$	$P2_1/n$
a (Å)	8.4860(16)	8.6150(19)
b (Å)	14.976(3)	14.949(4)
c (Å)	12.045(2)	12.136(2)
β (deg)	93.434(7)	92.406(13)
V ($Å^{-3}$)	1528.0(5)	1561.6(6)
Z	4	4
Z'	2	2
ρ_{calc} ($g{\cdot}cm^{-3}$)	1.306	1.277
μ (mm^{-1})	0.091	0.090
F (000)	640	640
θ limits (deg)	2.763- 26.467	2.163 – 26.085
Limiting indices	$-9 \leq h \leq 10$	$-10 \leq h \leq 10$
	$-11 \leq k \leq 10$	$-17 \leq k \leq 13$
	$-15 \leq l \leq 14$	$-14 \leq l \leq 14$
No. of reflns collected/unique	6180 / 2687 [*R*(int) = 0.0321]	7060 / 2690 [*R*(int) = 0.0551]
Completeness to *θ* (0%)	85.5	87.3
Refinement Method	Full-matrix least-squares on F^2	Full-matrix least-squares on F^2
Data/restraints/params	2687 / 0 / 279	2687 / 0 / 279
GOF on F^2	0.930	0.967
Final *R* indices [$l > 2\sigma(l)$]	$R_1 = 0.0471$, w $R_2 = 0.0994$	$R_1 = 0.0492$, w $R_2 = 0.1061$
R índices (all data)	$R_1 = 0.1018$, w $R_2 = 0.1146$	$R_1 = 0.1318$, w $R_2 = 0.1413$
Largest diff peak and hole (e $Å^{-3}$)	0.169 and -0.200	0.144 and -0.137

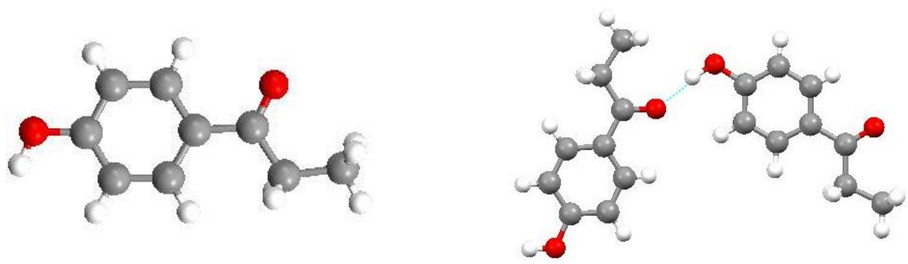

(a) (b)

Figure 3.4. Structure obtained for 4'-hydroxypropiophenone using the software Mercury[40] (a) geometry of the conformer and (b) the hydrogen bonding displayed by the molecule. These images apply for both structures determined at different temperatures.

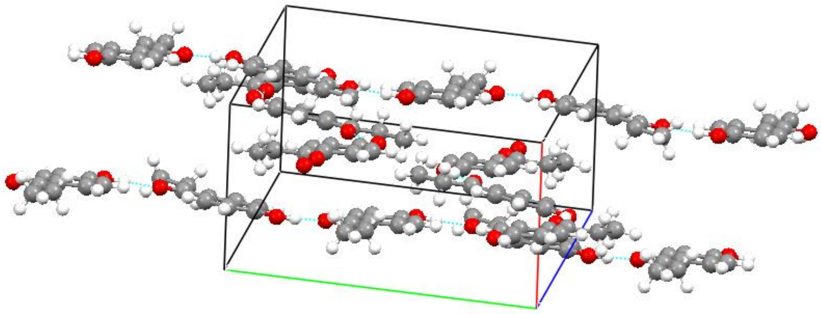

Figure 3.5. Crystal packing of 4'-hydroxypropiophenone obtained using the software Mercury.[40]

The distance between the stacking is 2.704 Å and occurs between the $OH_{hydroxyl}$ and a H from the alkyl chain of the compound. All distances reported correspond to the structure determined at room temperature. While observing the structure determined at low temperature, it is expected that a decrease occurs in the distances, since low temperatures lead to a contraction of the structure. The distance of the hydrogen bond on the *b* chain changes to $d_{OH\cdots O}$ = 1.736 Å, while the other chain passes to $d_{OH\cdots O}$ = 1.766 Å. The $CH_{ring}\cdots O_{carbonyl}$ interactions for the *b* chain also decreased ($d_{CH\cdots O}$ = 2.547Å), however, the same behavior is not seen on the *ac* bisect chain ($d_{CH\cdots O}$ = 2.624 Å) where the value is maintained. For both chains the $CH_{ring}\cdots O_{hydroxyl}$ distance decreased ($d_{CH\cdots O}$ = 2.546 Å for the *b* chain and $d_{CH\cdots O}$ = 2.523 Å for the *ac* bisect chain). Additional, the distance between the stacking is also diminished (*d* = 2.626 Å). This behavior is expected since they refer to a structure obtained at a lower temperature.

Initially for 4'-hydroxyvalerophenone DSC experiments were performed in the temperature range of 153 K to 453 K (Figure 3.6) with the previous characterized sample obtained by crystallization from ethanol. The sample was cooled from 296 K to 153 K and then heated at a rate of 10 $K\cdot min^{-1}$. No transitions were detected other than fusion within the cooling and heating experiments. An endothermic peak corresponding to the fusion process was detected at T_{fus} = 335.6±0.7 K and T_{max} = 337.9±0.4 K. The standard molar enthalpy associated to this peak was $\Delta_{fus}H^{o}_{m}$ = 26.67±0.04 $kJ\cdot mol^{-1}$. Note that these results are in good agreement with the previous fusion temperature and enthalpy of fusion for the same compound determined by DSC 7 from Perkin Elmer (T_{fus} = 334.6±1.5 K, T_{max} = 336.9±0.2 K and $\Delta_{fus}H^{o}_{m}$ = 25.75±0.26 $kJ\cdot mol^{-1}$). When the isotropic liquid was cooled to 212 K at the same rate as before and an exothermic peak was obtainedwith T_{crys} = 308.8±1.6 K, T_{max} = 303.9±3.0 K and $\Delta_{crys}H^{o}_{m}$ = −(16.68±0.84) $kJ\cdot mol^{-1}$. Further cooling of the crystalized sample showed no additional thermal events. Subsequent heating of the crystallized sample from 212 K to 353 K at 10 $K\cdot min^{-1}$ revealed an endothermic peak T_{fus} = 324.3±0.2 K, T_{max} = 327.6±0.6 K and $\Delta_{fus}H^{o}_{m}$ = 18.14±0.18 $kJ\cdot mol^{-1}$. The detailed values of the measurements obtained for each complete cycle are presented in the Supporting Information, section B.

The difference in the values reported for T_{fus} and $\Delta_{fus}H^{o}_{m}$, between the starting material obtained from ethanol crystallization (first run) and the material crystallized from melt (second run), corresponds to 11.2 K and 8.5 $kJ\cdot mol^{-1}$, respectively. The large difference between these values suggests that the material crystallized from melt corresponds to a new form of HVP (form II). After the cycles were performed the crucibles were opened to evaluate if any decomposition of the sample occurred. No decomposition was noted.

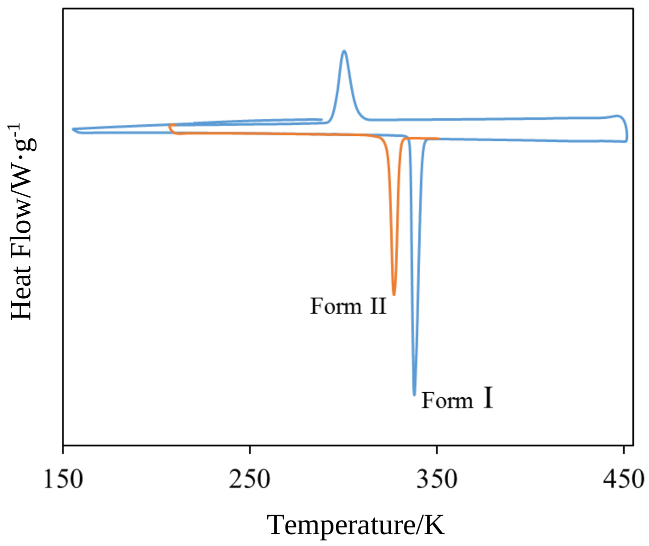

Figure 3.6. Results of the DSC experiments for HVP performed in the temperature range 153 K to 453 K using TA Instruments 2920 MTDSC. The blue line corresponds to the initial form I sample and to the first cooling/heat cycle. The orange curve, corresponds to HVP form II obtained after crystallization from melt.

To support the results found by DSC, cross polarized hot stage microscopy (HSM) was performed. The HSM images in Figure 3.7a to 3.7c show the crystallization of the isotropic liquid, between 303 K and 298 K. These results are in good agreement with those previously obtained by DSC, in which the exothermic peak corresponds to this process (Figure 3.6). Figures 3.7d and 3.7e confirm that between 323 K and 329 K the fusion of the new form takes place, which is in agreement with the endothermic peak obtained at 324.3±0.2 K. These results suggest that a new polymorph for HVP was discovered. Since form I (starting material) has a higher fusion temperature and enthalpy than form II (crystallized from melt) the relationship between them, based on Burger and Ramberger's *heat of fusion* rule (see Chapter 1), is monotropic. This relationship can be illustrated by a qualitative Gibbs energy and enthalpy vs. temperature phase diagram which is shown in Figure 3.8. To obtain a quantitative type diagram, there is still not enough data available.

The diagram in Figure 3.8 relies on several considerations: *i*) the heat capacity difference between the two polymorphs is approximately constant; *ii*) at 0 K $G = H - TS = H$; *iii*) at the fusion temperatures of both phases (form I = 335.6±0.7 K, form II = 324.3±0.2 K) the Gibbs energy of the liquid phase equals the solid form considered; *iv*) under the same conditions, the enthalpy differences between the liquidus and solid lines for both forms are given by the corresponding enthalpies of fusion (form I $\Delta_{fus}H^{o}_{m}$ = 26.67±0.04 kJ·mol^{-1}, form II $\Delta_{fus}H^{o}_{m}$ = 18.14±0.18 kJ·mol^{-1}). The diagram lines for the different forms (form I corresponds to the orange line, while form II corresponds to the yellow line) do not cross before fusion which is a characteristic of a monotropic relationship, where one polymorph is always thermodynamically more stable than the other along the full solid state domain. This data supports the existence of a new polymorph. To corroborate this finding, SCXRD and XRPD were performed on HVP crystalized from ethanol (form I) and HVP crystalized after melt (form II). As mentioned in Chapter 2 the starting material was indexed with good agreement with the published structure. A summary of the more relevant results from the published data is presented in Table 3.5 which will help to discuss some structural differences between the two forms. The crystal data and refinement parameters obtained for HVP form II are listed in Table 3.6.

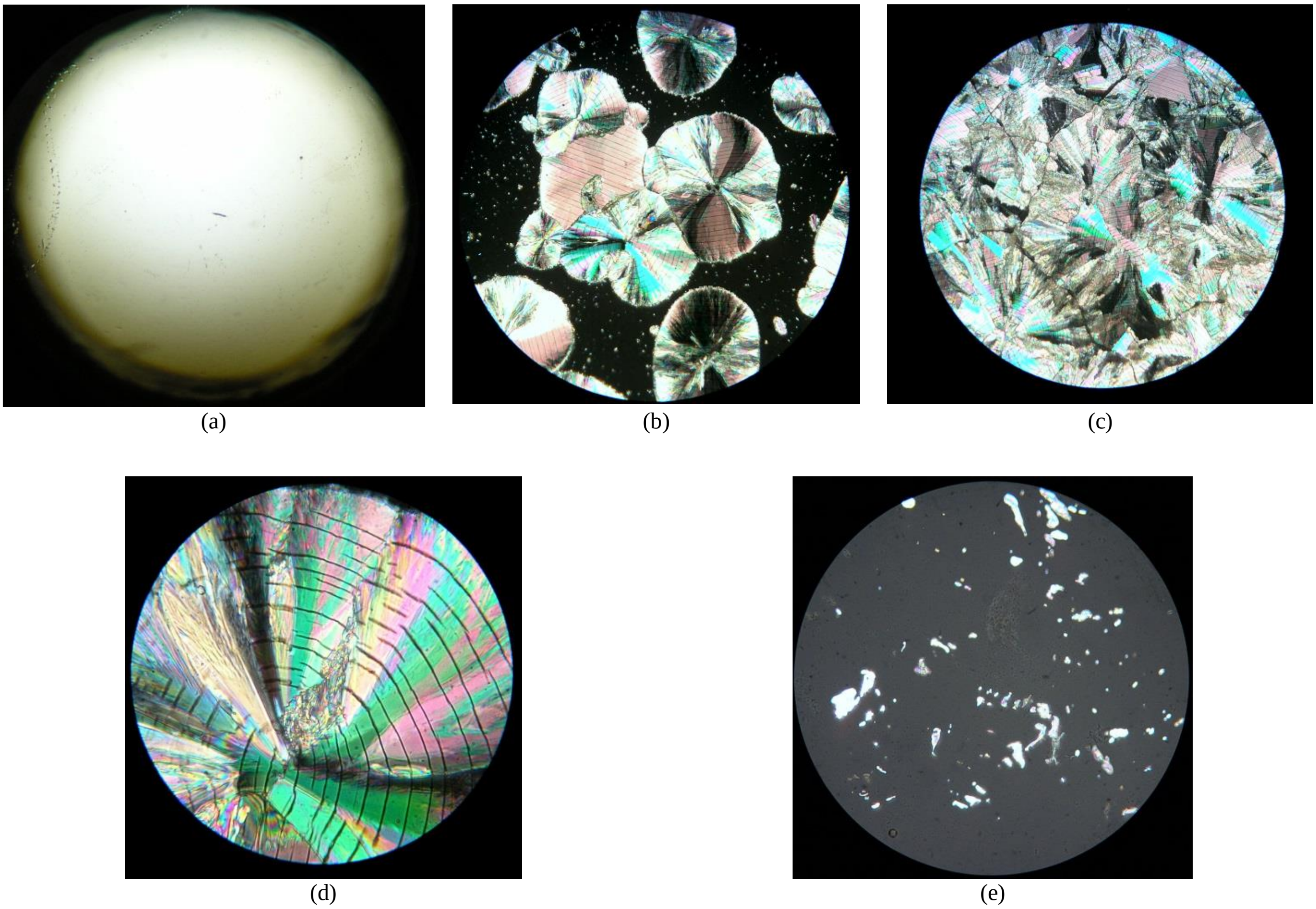

Figure 3.7. Hot stage polarized optical microscopy images showing the crystallization of the new HVP polymorph (form II) from melt and its subsequent fusion: (a) isotropic liquid at 353 K (250×); (b) initial stages of crystallization at 298 K (250×); (c) the material at 283 K, after complete crystallization (250×); (d) form II further cooled to 263 K (500×); (e) form II undergoing melting at ~328 K, after being heated from 263 K (500×).

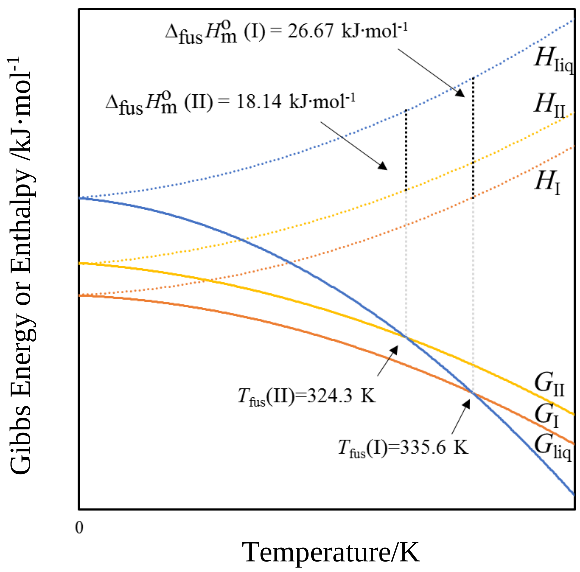

Figure 3.8. Schematic representation of the Gibbs energy and enthalpy versus temperature phase diagram highlighting the monotropic relationship of the HVP polymorphic system.

Table 3.5. Crystal data for form I of 4'-hydroxyvalerophenone obtained by single crystal X-ray available on literature.[34]

4'-Hydroxyvalerophenone (Form I)			
Empirical Formula	$C_{11}H_{14}O_2$	*a* (Å)	9.990(2)
Formula Weight	178.22	*b* (Å)	10.454(2)
Temperature	298(2)	*c* (Å)	9.882(2)
Wavelength (Å)	0.71073	*β* (º)	107.46(3)
Crystal size (mm^{-3})	0.300 × 0.200 × 0.200	V ($Å^{-3}$)	984.5(4)
Crystal Color	Colorless	Z / Z'	4 / 1
Crystal system	Monoclinic	ρ_{calc} ($g\cdot cm^{-3}$)	1.202
Space Group	$P2_1/c$	μ (mm^{-1})	0.08

Table 3.6. Crystal data and structure refinement parameters for 4'-hydroxyvalerophenone form II determined by single crystal X-ray diffraction at 296 K.

4'-Hydroxyvalerophenone (Form II)	
Empirical Formula	$C_{11}H_{14}O_2$
Formula Weight	178.22
Temperature	296(2)
Wavelength (Å)	0.71073
Crystal size (mm^{-3})	0.800 × 0.400 × 0.100
Crystal Color	Colorless
Crystal system	Monoclinic
Space Group	$C2/c$
a (Å)	8.4860(16)
b (Å)	14.976(3)
c (Å)	12.045(2)
β (deg)	111.054(13)
V ($Å^{-3}$)	2068.2(10)
Z	8
Z'	1
ρ_{calc} ($g\cdot cm^{-3}$)	1.145
μ (mm^{-1})	0.090
F (000)	768
θ limits (deg)	2.733 – 25.979
Limiting indices	$-23 \leq h \leq 23$
	$-9 \leq k \leq 8$
	$-17 \leq l \leq 14$
No. of refns collected/ unique	76645/1949 [*R*(int) = 0.0510]
Completeness to θ (0%)	98.3
Refinement Method	Full-matrix least-squares on F^2
Data/restraints/params	149 / 1 /159
GOF on F^2	0.850
Final *R* indices [$l > 2\sigma(l)$]	$R_1 = 0.0537$, w $R_2 = 0.1287$
R indices (all data)	$R_1 = 0.1696$, w $R_2 = 0.1669$
Largest diff peak and hole (e $Å^{-3}$)	0.172 and -0.144

When comparing the data presented in both Tables 3.5 and 3.6 the most important information to start this discussion is the change in the space group. This change is normally associated with polymorphism. The starting material had a space group $P2_1/c$ while the new form structure has a $C2/c$ space group. In Figure 3.9 the two different conformations are shown. It is possible to confirm that indeed this is a case of conformational polymorphism where the molecule changes from a *Z* conformation to a *E* conformation. The computational calculations showed that the *E* conformer had the lowest energy. This fact suggests that the initial structure after melting tends to crystallize at the lowest energy structure, which is expected due to the thermodynamical process. The different conformation of form I and form II causes several differences on the cell parameters. Only the *a* length suffers a decrease while *b*, *c* and *β* are increased. An expansion on the volume of the unit cell was detected as well as an increment in *Z* (form I, *Z*/*Z'*: 4/1; form II, *Z*/*Z'*: 8/1). The density of the molecule also decreases, which is in good agreement with the information obtained by the Gibbs free energy vs. temperature diagram that indicates that the relation between these polymorphs is monotropic and the thermodynamics *density rule*.[26]

Form I presents a "herringbone" type structure with the main chains growing in the direction of the *b* axis (Figure 3.10) and are $C^1_1(8)$ type. These chains are non-planar and have approximately a 90º angle between them. The "head-to-tail" OH···O ($d_{OH\cdots O}$) hydrogen bond between the hydroxyl group of one molecule and the carbonyl group of an adjacent molecule is what sustains this type of structure ($d_{OH\cdots O}$ = 1.898 Å). Also hydrogen bonding of the type $CH_{ring}\cdots O_{hydroxyl}$ gives a contribution for the structure stability ($d_{CH\cdots O}$ = 2.546 Å). The π-π stacking ($d_{\pi\text{-}\pi}$ = 3.163 Å and $d_{\pi\text{-}\pi}$ = 3.640 Å) and the $OH_{hydroxyl}\cdots O$ are both responsible for the infinite propagation of the crystalline structure. As mentioned above the new form of HVP has a different space group, however it also presents $C^1_1(8)$ chains as form I, also growing in the direction of the *b* axis for all the chains (Figure 3.11a). In form II, $C^1_1(8)$ motifs are also propagated infinitely by the $OH_{hydroxyl}\cdots O$ bond ($d_{OH\cdots O}$ = 1.898 Å), but in this polymorph the chains are planar (Figure 3.11a). In this case the chains are formed by molecules that are all parallel to each other compelling the hydrogen bond OH···O from the hydroxyl group with the carbonyl group to increase. Although in the case of polymorph I the chains are formed by molecules that are perpendicular to each other allowing a closer interaction between molecules (Figure 3.10) this occurrence leads to a large increase of the volume of the crystal lattice in polymorph II. The 3D packing is formed by stacking antiparallel $C^1_1(8)$ chains (Figure 3.11b).

To support the information obtained by SCXRD additional studies using X-ray diffraction powder (XRDP) were performed. Figure 3.12 shows a comparison of the XRPD patterns obtained for HVP where: (a) corresponds to the simulated single crystal data for form I[34]; (b) to the starting material and (c) for the obtained material crystallized from melt. As it is possible to see, the first two patterns are equivalent, but a clear difference is noted on the last pattern, proving that HVP has indeed a new form (II).

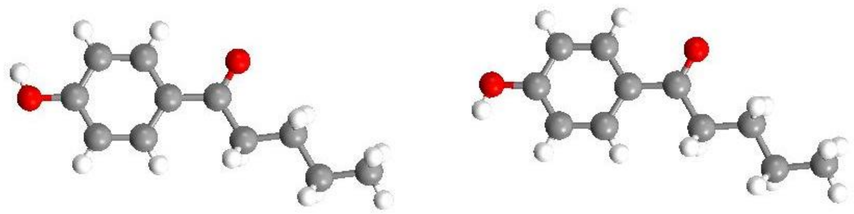

(a) (b)

Figure 3.9. Structures obtained for 4'-hydroxyvalerophenone at room temperature using the software Mercury[40]: (a) geometry obtained for form I presenting a *Z* conformation and (b) obtained for form II showing a *E* conformation.

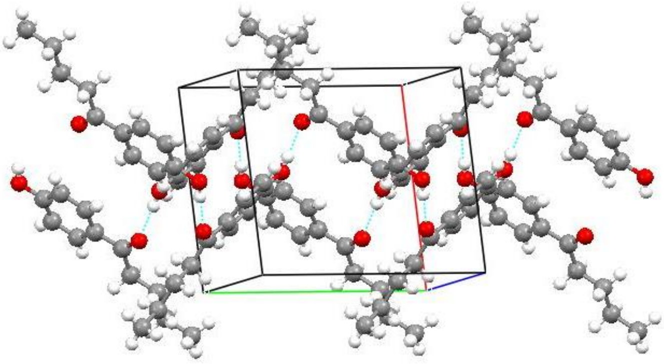

Figure 3.10. Crystal packing of 4'-hydroxyvalerophenone form I obtained from available literature[34] using the Mercury software.[40]

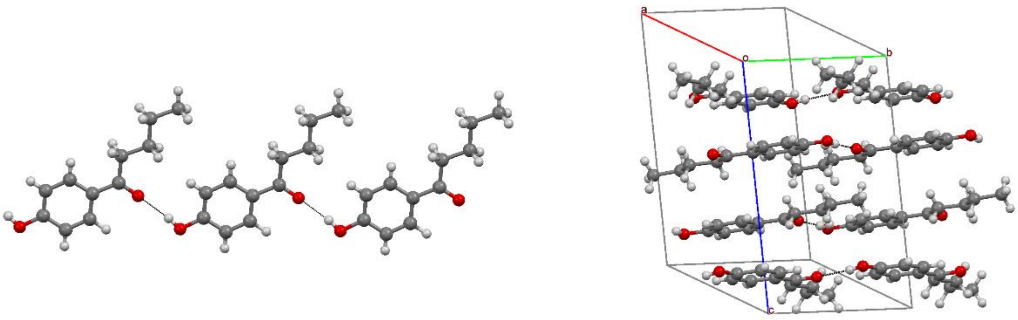

(a) (b)

Figure 3.11. Crystal structure of 4'-hydroxyvalerophenone form II using the Mercury software.[40] (a) $C^{1}_{1}(8)$ chains with the molecules all parallel to each other; (b) crystal packing with stacking of antiparallel chains.

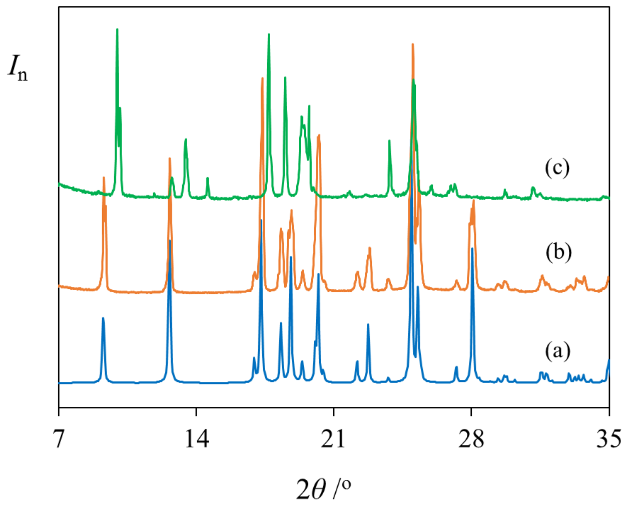

Figure 3.12. Comparison of the X-ray powder diffraction (XRPD) patterns of HVP: (a) simulated from single crystal X-ray diffraction data previously reported (form I)[34] (b) obtained for the starting material of the DSC and HSM experiments (form I); (c) recorded for the material crystallized from the melt (form II).

Finally, the same procedure was done for 4'-hydroxyheptanophenone (HHP). The DSC experiments were carried out in the temperature range 165 K to 453 K using the material as received (crystal system orthorhombic, space group *Pnma*). Figure 3.13 shows that, when the sample was cooled from 286 K to 165 K with a heating rate of 10 K·min^{-1}, a small exothermic peak is detected with onset T_{trs} = 202.8 K, maximum at T_{max} = 202.0 K, and standard molar enthalpy of transition $\Delta_{trs}H^{o}_{m}$ = −0.29 kJ·mol^{-1}. After this process, the sample was heated at the same rate from 165 K to 453 K. Two endothermic peaks were detected. The first peak corresponds to a phase transition (T_{trs} = 201.5 K, T_{max} = 203.15 K and $\Delta_{trs}H^{o}_{m}$ = 0.24 kJ·mol^{-1}), while the second is associated to the fusion of the starting material at T_{fus} = 365.3 K, T_{max} = 367.9 K and $\Delta_{fus}H^{o}_{m}$ = 29.07 kJ·mol^{-1}. Note that the results obtained for the fusion of the sample are in agreement with the data obtained using the DSC 7 from Perkin Elmer (T_{fus} = 365.0±0.2 K, T_{max} = 367.0±0.2 K and $\Delta_{fus}H^{o}_{m}$ = 31.40±0.12 kJ·mol^{-1}). Cooling the isotropic liquid from 453 K to 165 K, reveals the crystallization of the compound at T_{crys} = 341.5 K, T_{max} = 341.0 K with $\Delta_{crys}H^{o}_{m}$ = −26.78 kJ·mol^{-1} and, the phase transition observed in the first cooling run at T_{trs} = 201.5 K is observed. This indicates that, below T_{trs}, a new phase of HHP is reversibly prepared. Based on Burger and Ramberger's *Heat of transition* rule, the relationship between them is enantiotropic. To confirm this information, cross polarized HSM was performed. The HSM images in Figure 3.14a and 3.14b show the crystallized material above and below the transition temperature and reveal no evidence of a phase transition. In contrasts, Figures 3.14c and 3.14d, obtained on heating the sample, from 323 K to 368 K, exhibit the melting of the material around 368 K, in good agreement with the DSC observation.

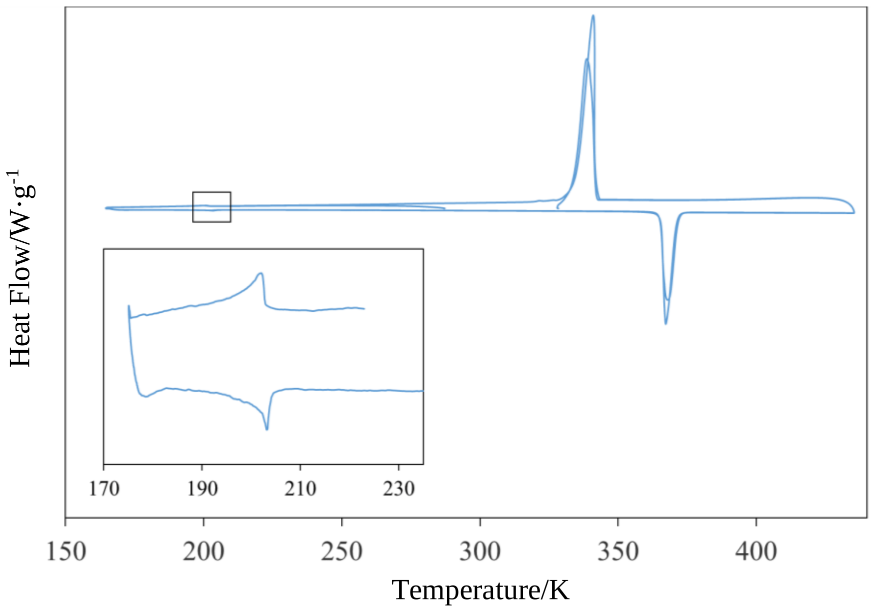

Figure 3.13. Results of the DSC experiments for HHP performed on the temperature range 165 K to 453 K using TA Instruments 2920 MTDSC. A close up of the identified phase transition is also displayed.

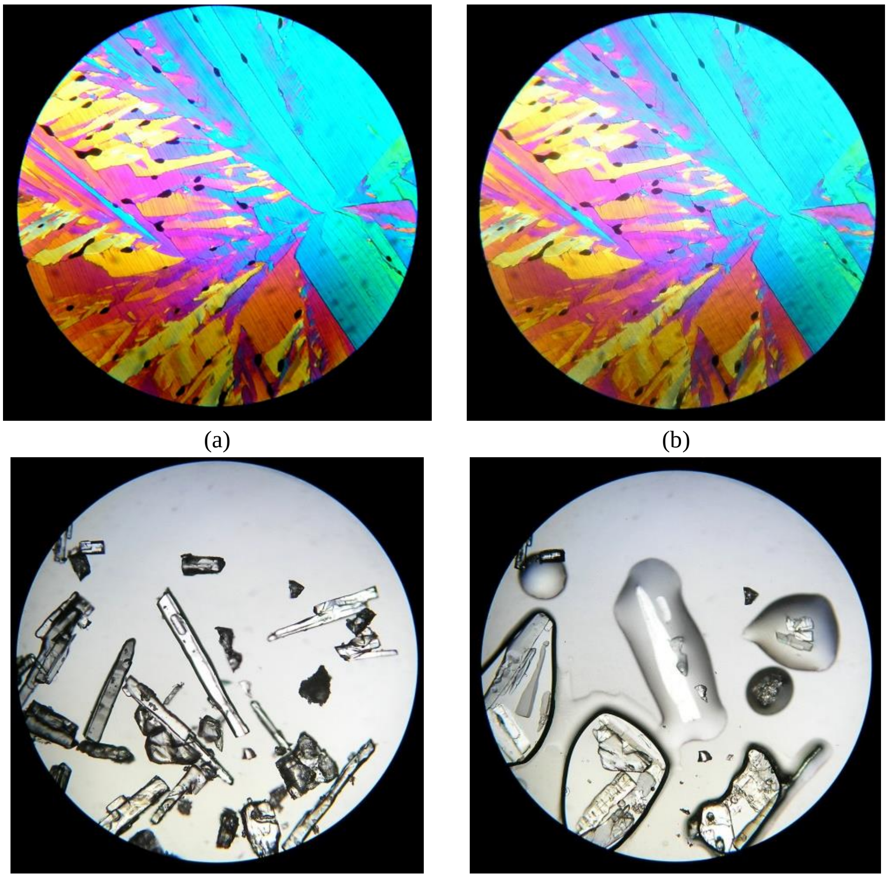

(a) (b) (c) (d)

Figure 3.14. Hot stage polarized optical microscopy images showing the cooling where the phase transition was not detected and subsequent heating of HHP until the fusion process starts: (a) crystalline sample at 213 K (250×); (b) crystalline material after the phase transition at 183 K (250×); (c) crystalline material at 323 K (250×); (d) crystalline material starting to melt at 368 K.

To confirm this findings, SCXRD studies were performed starting at low temperature until room temperature to assess if this transition does indeed occur. The results obtained by this technique confirmed the phase transition. Four structures were solved at different temperatures (150, 190, 220 and 293 K). The crystal data and refinement parameters obtained for these are listed in Table 3.7. Starting with the low temperature structures solved at 150±2 K and 190±2 K for HHP, the results obtained show that the crystal system, space group and Z/*Z'* were the same, and a small increase in the cell parameters was detected (see Table 3.7). The relative orientation -CO and -OH groups in the molecule corresponds to an *Z* conformer for both structures at the two temperatures, and the only molecular difference between the two are the torsion angles in the alkyl tail of the molecules (72.9º, -179.23º at 150K and 71.55º, -179.81º at 190K) (Figure 3.15). The crystal lattice is composed by planar chains of the $C^1_1(8)$ type, and that grow in a "herringbone" structure due to the angle formed by the "head to tail" hydrogen bonding (α = 109.01º). The infinite growth of the chains is supported by the hydrogen bond, OH···O ($d_{OH\cdots O}$ = 1.857 Å), between the hydroxyl and the carbonyl group along the *b* axis (Figure 3.16). Also $CH_{ring}\cdots O_{carbonyl}$ interactions ($d_{CH\cdots O}$ = 2.616 Å) are relevant for the structure. All the distances reported to this point are for the structure obtained at 150 K. The structure determined at 190±2 K has also the same type of chains described above although with some small differences (Figure 3.17). The angle formed by the "head to tail" hydrogen bonding OH···O corresponds to 109.25º and $d_{OH\cdots O}$ = 1.880 Å. In addition to presenting the $CH_{ring}\cdots O_{carbonyl}$ interaction ($d_{CH\cdots O}$ = 2.620 Å), it also has $CH_{alkyl}\cdots\pi$ interactions ($d_{CH\cdots\pi}$ = 2.732 Å). These values are very close to those found for the first structure, thus suggesting that the reason for the differences reported is the increasing temperature.

Table 3.7. Crystal data and structure refinement parameters for 4'-hydroxyheptanophenone determined by single crystal X-ray diffraction.

	4'-Hydroxyheptanophenone			
Empirical Formula	$C_{13}H_{18}O_2$	$C_{13}H_{18}O_2$	$C_{13}H_{18}O_2$	$C_{13}H_{18}O_2$
Formula Weight	206.27	206.27	206.27	206.27
Temperature	150(2)	190(2)	220(2)	293(2)
Wavelength (Å)	0.71073	0.71073	0.71073	0.71073
Crystal size (mm^{-3})	0.40×0.20×0.15	-	-	0.60×0.30×0.25
Crystal system	Orthorhombic	Orthorhombic	Orthorhombic	Orthorhombic
Space Group	$P2_12_12_1$	$P2_12_12_1$	*Pnma*	*Pnma*
a (Å)	11.6090(4)	11.6581(4)	14.1173(7)	14.158(3)
b (Å)	14.1158(5)	14.1228(5)	7.189(4)	7.2246(17)
c (Å)	7.0590(2)	7.0949(3)	11.6857(6)	11.762(3)
V ($Å^{-3}$)	1156.76(7)	1168.14(8)	1174.41(11)	1203.0(5)
Z	4	4	4	4
Z'	1	1	1	1
ρ_{calc} ($g \cdot cm^{-3}$)	1.184	1.173	1.189	1.238
μ (mm^{-1})	0.078	0.077	0.084	0.081
F (000)	448	448	456	472
θ limits (deg)	2.271 - 27.165	2.885 – 30.873	2.866 – 31.236	2.878 – 26.398
Limiting indices	$-14 \leq h \leq 12$ $-18 \leq k \leq 18$ $-8 \leq l \leq 9$	$-15 \leq h \leq 15$ $-20 \leq k \leq 19$ $-10 \leq l \leq 7$	$-20 \leq h \leq 20$ $-8 \leq k \leq 10$ $-16 \leq l \leq 16$	$-17 \leq h \leq 17$ $-9 \leq k \leq 5$ $-14 \leq l \leq 14$
No. of refns collected/ unique	14173/2553 [*R*(int) = 0.0209]	5429/3182 [*R*(int) = 0.0201]	20954/2021 [*R*(int) = 0.0287]	9489/1321 [*R*(int) = 0.0497]
Completeness to θ (%)	99.9	99.0	98.0	99.0
Refinement Method	Full-matrix least-squares on F^2			
Data/restraints/params	2553/0/208	3182/0/183	2021/4/98	1321/9/132
GOF on F^2	0.930	1.031	2.684	1.339
Final *R* indices [$l > 2\sigma(l)$]	$R_1 = 0.0323$, $wR_2 = 0.0889$	$R_1 = 0.0659$, $wR_2 = 0.1797$	$R_1 = 0.1669$, $w R_2 = 0.5259$	$R_1 = 0.1195$, $w R_2 = 0.3069$
R índices (all data)	$R_1 = 0.0385$, $wR_2 = 0.0921$	$R_1 = 0.0789$, $wR_2 = 0.1905$	$R_1 = 0.1857$, $w R_2 = 0.5551$	$R_1 = 0.1478$, $w R_2 = 0.3402$
Largest diff peak and hole (e $Å^{-3}$)	0.222 and -0.166	0.754 and -0.518	2.115 and -1.547	0.623 and -0.533

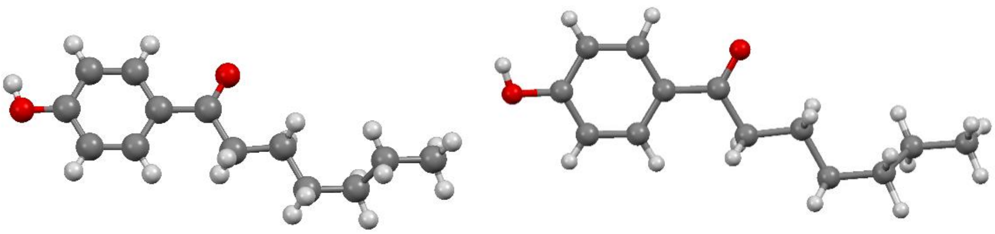

(a) (b)

Figure 3.15. Structure obtained for 4'-hydroxyheptanophenone using the Mercury software[40] where it is possible to see that the molecule has a *Z* conformation, at 150K(a) and 190K(b).

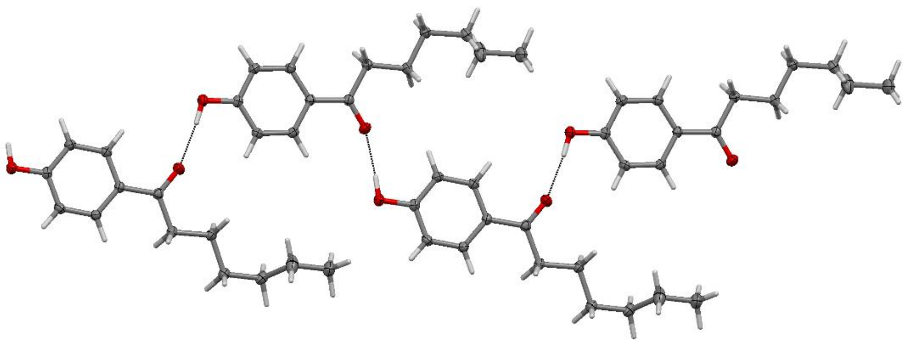

Figure 3.16. Packing motif $C^1_1(8)$ growing in a herringbone form of 4'-hydroxyheptanophenone obtained through single crystal X-ray diffraction at 150 K using the Mercury software.[40]

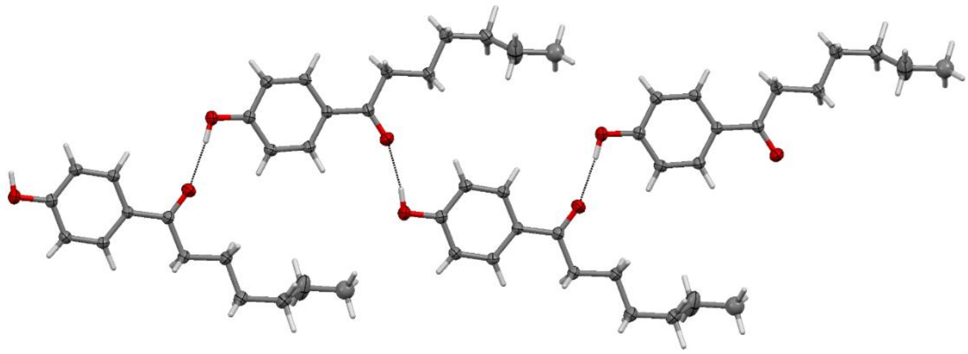

Figure 3.17. Crystal packing chain of 4'-hydroxyheptanophenone obtained through single crystal X-ray diffraction at 190 K using the Mercury software.[40]

The structure obtained at 220±2 K is different from the previously described. One difference immediately observed was the change in the space group of the molecule to *Pnma*. This is an indication that this transition corresponds to a new polymorph. All the cell parameters (e.g. *a*, *c*, *V* and *ρ*) with the exception for the *b* length had increased. The increase of the density also suggests that the relationship between them is enantiotropic based on the thermodynamics *density rule* (see Chapter 1). Although the space group changes, when observing the relative orientation -CO and -OH groups in the molecule it still has a *Z* conformation.

The alkyl chain of the molecule has a very different conformation at this temperature being planar and presenting torsion angles 0º and 180º (figure 3.18a). The crystal lattice is composed by four main chains of the $C^1_1(8)$ type. These chains are planar between them and their growth is characterized by the same "herringbone" structure as the previous structures (α = 109.46º). The infinite growth of the chains is supported by the $OH \cdots O_{carbonyl}$ which grows along the *a* axis ($d_{CH \cdots O}$ = 1.873 Å) (Figure 3.18b). To reinforce this structure there are also $CH_{ring} \cdots O_{carbonyl}$

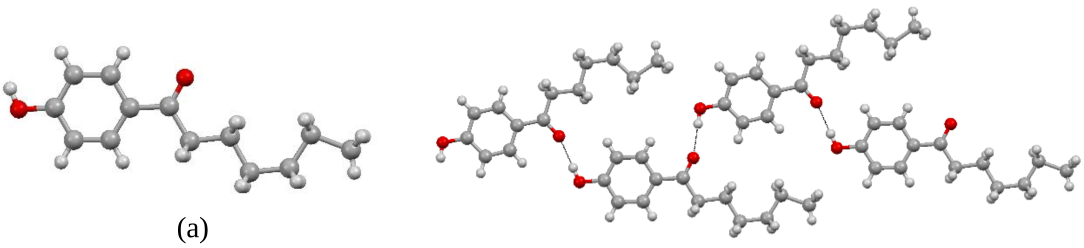

(a)

(b)

Figure 3.18. Molecular structure of 4'-hydroxyheptanophenone (a) and $C^1_1(8)$ chain in herringbone form in crystal packing obtained through single crystal X-ray diffraction at 220 K using the Mercury software.[40]

interactions ($d_{CH\cdots O}$ = 2.649 Å) in similarity to the low temperature structures. All the values obtained for the common interactions had a small increase which is in agreement with the fact that the volume of the unit cell is increasing with temperature.

The last structure was obtained at 293±2 K. The space group and *Z*/*Z'* remained unaltered. All the cell parameters suffered an increase (e.g. *a*, *b*, *c*, *V* and *ρ*). The same *Z* conformation is still adopted by the molecule. The alkyl chain also suffers a hindered rotation that is shown by the values of the torsion angles (69.21º and 156.72º) (figure 3.19a). The crystal lattice has the same number of $C^1_1(8)$ type chains which are planar between them and the same "herringbone" motif (α = 110.29º) as the other structures caused by the infinite propagation of $OH\cdots O_{carbonyl}$ interactions ($d_{CH\cdots O}$ = 1.917 Å) on the *a* axis (Figure 3.19b). To reinforce the structure several interactions need to be taken into account: $CH_{ring}\cdots O_{carbonyl}$ interactions ($d_{CH\cdots O}$ = 2.669 Å), $CH_{alkyl}\cdots O_{hydroxyl}$ interactions ($d_{CH\cdots O}$ = 2.654 Å). The same tendency as described in all the other structures of an increase in the distance of the interactions is also verified here which is due to the highest temperature studied for this molecule. Although it was possible to identify the phase transition by DSC and SCXRD, only a small difference in the crystal packing, is observed (see Figure 3.20). This is due to the phase transition resulting from a modification only in the alkyl chain of the molecule, as can be seen in Figure 3.21. This subtle change may be the reason why no evidence of a phase transition is observed in the hot stage microscopy (HSM) experiments.

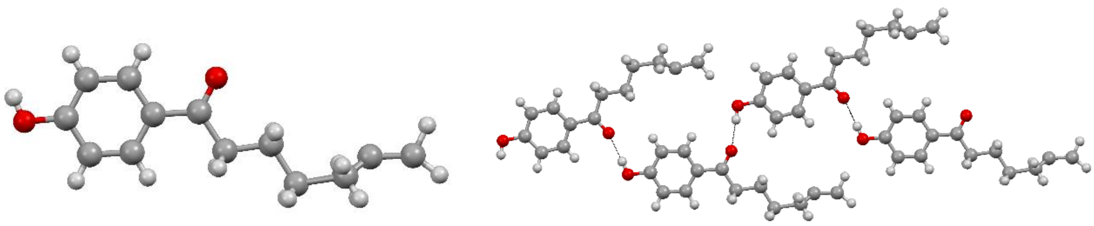

(a) (b)

Figure 3.19. Molecular (a) and **c**rystal packing motif (b)of 4'-hydroxyheptanophenone obtained through single crystal X-ray diffraction at 293 K using the Mercury software.[40]

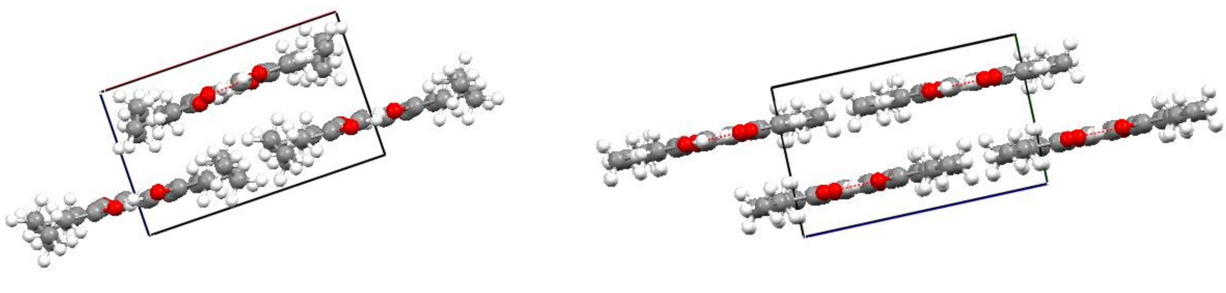

(a) (b)

Figure 3.20. Crystal stacking of the parallel chains of 4'-hydroxyheptanophenone (a) at 190 K and (b) 220 K.

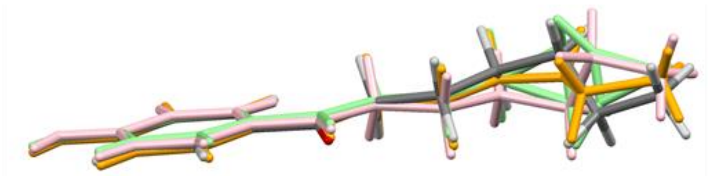

Figure 3.21. Overlay of the molecular structures obtained for 4'-hydroxyheptanophenone at 150 K (gray), 190 K (orange), 220 K (pink) and 293 K (green).

Some final remarks still need to be done considering all the complete family of compounds studied in this work. For completeness reasons, additional crystallographic data and crystal packing motifs for the other compounds of the hydroxybenzoil family studied are given in Table 3.8 and Figure 3.22. All the systems studied are based on $C^1_1(8)$ molecular chains, that have no preferential orientation and conformation. These chains are created by the $OH\cdots O_{carbonyl}$ hydrogen bonding, which involves the hydroxyl group of the molecule and the carbonyl group in an adjacent molecule. In addition to this main interaction several other molecular interactions were identified (e.g $CH_{ring}\cdots O_{carbonyl}$, $CH_{alkyl}\cdots O_{hydroxyl}$, π-π stacking) which are dependent of the chains orientations. For 4-hydroxybenzaldeheyde (HBA)[30], 4'-hydroxyacetophenone (HAP)[29, 31], 4'-hydroxyvalerophenone (HVP) and 4'-hydroxyheptanophenone (HHP) there are two polymorphs for each of these molecules and three additional hydrates in the case of HAP.

Table 3.8. Crystal Data for HBA, HAP, HVP at 298 K and HBP at 293 K.

	HBA		HAP		HBP
Empirical Formula	$C_7H_6O_2$		$C_8H_8O_2$		$C_{10}H_{12}O_2$
Form	I	II	I	II	-
Crystal System	Monoclinic	Monoclinic	Monoclinic	Orthorhombic	Monoclinic
Space group	$P2_{1/c}$	$P2_{1/c}$	$P2_{1/c}$	$P2_1\,2_1\,2_1$	$P2_{1/c}$
a (Å)	6.4473(25)	6.6992(8)	7.7200(15)	6.1097(11)	8.2650(17)
b (Å)	13.7652(17)	13.5550(12)	8.3600(17)	9.5293(14)	30.986(6)
c (Å)	7.0402(23)	7.1441(11)	11.280(2)	24.313(4)	7.9200(16)
β (º)	108.00(3)	107.94(9)	95.02(3)		116.94(3)
V (Å^3)	597.2	597.7	725.2(3)	1415.5(4)	1808.2(6)
Z	4	4	4	8	8
Z'	1	1	1	2	2
ρ_{calcd} (g·cm^{-3})	1.358	1.357	1.247	1.278	1.206

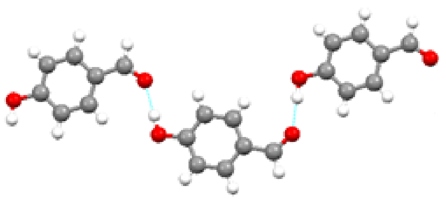

(a)

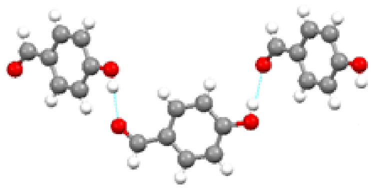

(b)

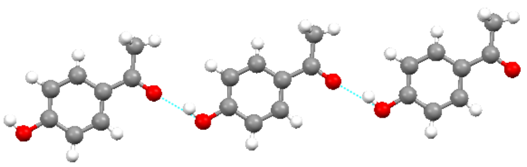

(c)

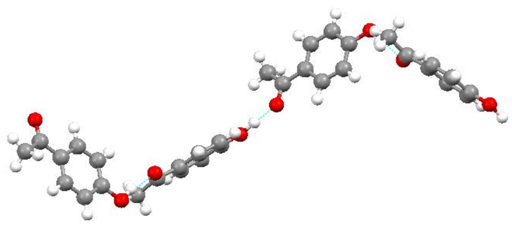

(d)

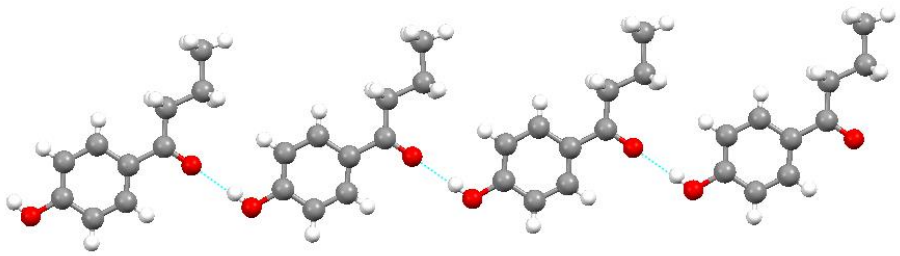

(e)

Figure 3.22. Crystal packing motif for 4-hydroxybenzaldeheyde (a) form I, (b) form II, 4'-hydroxyacetophenone (a) form I, (b) form II and 4'-hydroxybutyrophenone.

4. Conclusion

This work main goal was the study of polymorphism on compounds of the hydroxybenzoyl family (HOC_6H_4COR, R = H, CH_3, C_2H_5, n-C_3H_7, n-C_4H_9, n-C_5H_{11} and n-C_6H_{13}). Special attention was given to the energetics and structure of these molecules.

From a structural point of view, the results show that for 4'-hydroxyvalerophenone (HVP) two distant forms were prepared. HVP form I (highest T_{fus} = 335.6±0.7 K) was obtained by crystallization with ethanol, while HVP form II (lowest T_{fus} = 324.3±0.2 K) was prepared from melt of the initial sample. To ascertain if a new polymorph of HVP was obtained, several techniques were used, such as differential scanning calorimetry (DSC), hot stage microscopy (HSM), single crystal X-ray diffraction (SCXRD) and X-ray powder diffraction (XRPD). The results collected from these experiments confirmed that a new form was obtained. The polymorphs are monotropically related, which indicates that form I is always more stable that the newly identified phase. Both structures are monoclinic but have different space groups (form I $P2_1/c$, form II $C2/c$) and the relative orientation of the -CO and -OH groups changes: form I has *Z* conformation while form II has an *E* conformation.

In turn, 4'-hydroxyheptanophenone results show a phase transition at T_{trs} = 203 K. To verify if this event corresponds to a phase transition to a new polymorph a DSC and SCXRD study was also employed. The obtained results, revealed that, before the transition temperature, the crystalline material was orthorhombic with the space group $P2_12_12_1$, and afterwards, the space group changes to *Pnma*. It was found however, that below and above T_{trs} structural modifications could be observed, that are related with changes in mobility of the alkyl chain, without space group and unit cell parameters with significant changes.

In addition to these main findings, the same type of studies were performed for all remaining molecules of the hydroxybenzoyl family investigated in this work, where it was possible to obtain for the first time a single crystal structure for 4'-hydroxypropiophenone. Although no polymorphs for the other compounds were possible to identify, some conclusions from the study of the determined single crystal structures of the materials can be highlighted: *i*) all the structures present $C^1_1(8)$ molecular chains; *ii*) no preferential orientation and/or conformation is observed; *iii*) the hydrogen bonding that is always responsible for the growth of these chains is OH···O, involving the hydroxyl and carbonyl groups of adjacent molecules.

The energetics path allowed to determine the standard molar enthalpy of fusion at 298.15 K and the standard molar enthalpy of formation for both solid and gas phase for all the compounds studied in this work. A linear relationship was found between the $\Delta_{sub}H^o_m$ and the alkyl chain growth of the molecules. Although the crystalline structures solved do not present a regular pattern for both configuration and morphology of the molecules, approximate additivity of their cohesive energies with the growth of the alkyl chain is observed with a CH_2 increment in resemblance with similar results obtained for both 4-*n*-alkylbenzoic acids and 4-*n*-alkyloxybenzoic acids. As a final remark this work confirms that, indeed, this type of family is extremely rich in solid state.

This work, leaves several open question that may be addressed in future works. These includes: *i*) a refinement of the structures obtained for HHP at 293 K; *ii*) extend the polymorph screenings using, for example, crystallizations from different solvents; *iii*) the determinations of the solubilities, between several others.

5. References

1. J. W. Mullin, *Crystallization*. 4 ed.; Butterworth-Heinemann: Oxford, 2001.
2. E. Mitscherlich, *Ann. Chim et Phys.* **1821,** *19*, 350.
3. F. Whoehler; J. Liebig, *J. Am. Pharm.* **1832,** *3*, 249.
4. M. R. Caira, *Cur. Chem.* **1998,** *198*, 163-208.
5. A. Llinàs; J. M. Goodman, *Drug Discov. Tod.* **2008,** *13* (5/6), 198-210.
6. S. L. Price, *Chem. Soc. Rev* **2014,** *43*, 2098-2111.
7. C. E. S. Bernardes; M. L. S. Matos Lopes; J. R. Ascenso; M. E. Minas da Piedade, *Cryst. Growth Des.* **2014,** *14*, 5436-5441.
8. H. G. Brittain, *Polymorphism in Pharmaceutical Solids*. 2 ed.; Informa Healthcare USA: New York, 2009; Vol. 192.
9. J. Haleblian; W. McCrone, *J. Pharm. Sciences* **1969,** *58* (8), 911-929.
10. B. Rodríguez-Spong; C. P. Price; A. Jayasankara; A. J. Matzgerb; N. Rodríguez-Hornedoa, *Adv. Drug Deliv. Rev.* **2004,** *56* (3), 241-274.
11. J. Bernstein; R. J. Davey; J. O. Henck, *Angew. Chem. Int. Ed.* **1999,** *38*, 3340-3461.
12. E. S. Ferrarii; R. J. Davey; W. I. Cross; A. L. Gillon; C. S. Towler, *Cryst. Growth Des.* **2003,** *3* (1), 53-60.
13. T. L. Threlfall, *Analyst.* **1995,** *120*, 2435-2460.
14. B. C. Hancock; M. Parks, *Pharm. Res.* **2000,** *17* (4), 397-404.
15. J. Bernstein, *Polymorphism in Molecular Crystals*. 14 ed.; Oxford University Press: Oxford, 2002.
16. J. Li; T. B. Brill, *Propell. Explos. Pyrot.* **2007,** *32* (4), 329-330.
17. N. Panin; F. J. J. Leusen; F. F. B. J. Janssen; P. Verwer; H. Meekes; E. Vliega; G. Derooverd, *J. Appl. Cryst.* **2007,** *40*, 105–114.
18. P. Vishweshwar; J. A. McMahon; M. Oliveira; M. L. Peterson; M. J. Zaworotko, *J. Am. Chem. Soc.* **2005,** *127*, 16802-16803.
19. J. Bauer; S. Spanton; R. Henry; J. Quick; W. Dziki; W. Porter; J. Morris, *Pharm. Res.* **2001,** *18* (6), 859-866.
20. S. R. Chemburkar; J. Bauer; K. Deming; H. Spiwek; K. Patel; J. Morris; R. Henry; S. Spanton; W. Dziki; W. Porter; J. Quick; P. Bauer; J. Donaubauer; B. A. Narayanan; M. Soldani; D. Riley; K. McFarland, *Org. Process Res. Dev.* **2000**, 413-417.
21. D. A. Snider; W. Addicks; W. Owens, *Adv. Drug Deliv. Rev.* **2004,** *56*, 391-395.
22. G. R. Desiraju, *J. Chem. Sci* **2010,** *122* (5), 667-675.
23. G. R. Desiraju, *Acc. Chem. Res* **2002,** *35*, 565-573.
24. P. W. Atkins; J. de Paula, *Physical Chemistry*. 9 ed.; Oxford University Press: New York, 2010.
25. D. Giron, *J. Therm. Anal. Cal.* **2001,** *64*, 37-60.
26. A. Burger; R. Ramberger, *Micro. Chem. Act.* **1979,** *72* (3), 259-271.
27. A. I. Kitajgorodskij, *Acta Cryst.* **1965,** *18*, 585-590.
28. C. E. S. Bernardes; M. E. Minas da Piedade, *J. Phys. Chem. A* **2008,** *112*, 10029-10039.
29. C. E. S. Bernardes; M. F. M. Piedade; M. E. Minas da Piedade, *Cryst. Growth Des.* **2008,** *8* (7), 2419-2430.
30. R. G. Simões; C. E. S. Bernardes; M. E. Minas da Piedade, *Cryst. Growth Des.* **2013,** *13*, 2803-2814.
31. C. E. S. Bernardes; M.E. Minas da Piedade, *Cryst. Growth Des.* **2012,** *12*, 2932-2941.
32. F. Iwasaki, *Acta Cryst.* **1977,** *B33*, 1646-1648.
33. B. Xu; Z. Q. Feng; J. T. Wang; L. G. Hu; J. Huang, *Acta Cryst.* **2006,** *E62*, o2603-o2605.
34. Z.H. Luo; H. J. Zhu; S. Liu, *Acta Cryst.* **2006,** *E62*, o5054-o5055.
35. P. Kubelka; F. Munk, *Z. Tech Phys* **1931,** *12*, 593-601.
36. *SABADS, Area-detector Absorption Correction*, Bruker AXS Inc.: Madinson, WI, 2004.
37. *SAINT, Area-detector Integration Software (Version7.23)*, Bruker AXS Inc.: Madinson, WI, 2004.
38. G. M. Sheldrick, *Acta Crystallographica Section A* **2008,** *64*, 112-122.
39. L. J. Farrugia,. *J. Appl. Crystallogr.* **2012,** *45*, 849-854.

40. C. F. Macrae, P. R. Edgington, P. Mccabe, E. Pidcock, G. P Shields, R. Taylor, M. Towler, J. v. d. Streek, *J. Appl. Crystallogr.* **2006,** *39*, 453-457.
41. A. L. Spek, *J. Act. Cryst. D* **2009,** *65*, 148-155.
42. J. Laugier, B. Bouchu,. *Checkcell*.
43. J. A. M. Simões, M. E. Minas da Piedade, *Molecular Energetics: Condensed-Phase Thermochemical Techniques*. Oxford University Press: New York, 2008.
44. M. E. Brown, *Handbook of Thermal Analysis and Calorimetry: principles and pratice*. Elsevier science B.V.: Amesterdam, 1998; Vol. 1.
45. A. Joseph; C. E. S. Bernardes; M. E. Minas da Piedade, Unpublished Results. 2016.
46. G. T. Furukawa; R. E. Mccoskey; G. J. King, *J. Res. Natl. Bur. Stand.* **1951,** *47*, 256-261.
47. D. G. Archer, *J. Phyl Chem. Ref. Data* **1993,** *22* (6), 1441-1453.
48. C. E. S. Bernardes; M. E. Minas da Piedade, *Meas. Sci. Techonol.* **2006,** *17*, 1405-1408.
49. T. Kiyobayashi; M. E. Minas da Piedade, *J. Chem. Thermodyn.* **2001,** *33*, 11-21.
50. C. E. S. Bernardes, *CBCAL 1.0: A program for calorimeter control and data aquisition*, FCUL: Lisboa, 2008.
51. K. K. Irikura; D.J. Frurip, Computacional Thermochemistry. Prediction and Estimation of Molcular Thermodynamics. ACS symposium Series: Washington, 1998.
52. S. Grimme; J. Antony; S. Ehrlich; H. Krieg, *J. Chem. Phys.* **2010,** *132*, 154104-19.
53. A. D. Becke, *J. Chem. Phys.* **1993,** *98* (7), 5648-5652.
54. P. J. Stephens; F. J. Devlin; C. F. Chabalowski; M. J. Frisch, *J. Chem. Phys.* **1994,** *98* (45), 11623-11627.
55. M. K. Kesharwani; B. Brauer; J. M. L. Martin, *J. Phys. Chem. A* **2015,** *119*, 1701-1714.
56. J. Meija; T, B. C.; R. D. Loss; T. Walczyk; T. Prohaska, *Pure Appl. Chem* **2016,** *88*, 265-291.
57. M. J. S. Monte, A. R. R. P. Almeida, M. A. V. Ribeiro da Silva, *J. Chem. Thermodyn.* **2004,** *36* (5), 385-392.
58. J. M. S. Fonseca, L. M. N. B. F. Santos, M. J. S. Monte, *J. Chem. Eng. Data* **2010,** *55* (6), 2238-2245.
59. J. Vitorino, F. Agapito, C. E. S. Bernardes, M. E. Minas da Piedade, *J Chem Thermodyn* **2015,** *80*, 59-64.
60. M. D. M. C. Ribeiro da Silva; M. V. Goncalves; M. J. S. Monte, *J. Chem. Thermodyn.* **2010,** *42*, 472-477.
61. A. Aihara, *Bull. Chem. Soc. Jpn.* **1960,** *33*, 194-200.
62. G. H. Parsons; C. H. Rochester; C. E. C. Wood, *J. Chem. Soc. B* **1971**, 533-536.

Supporting Information

A) Characterization of Starting Materials

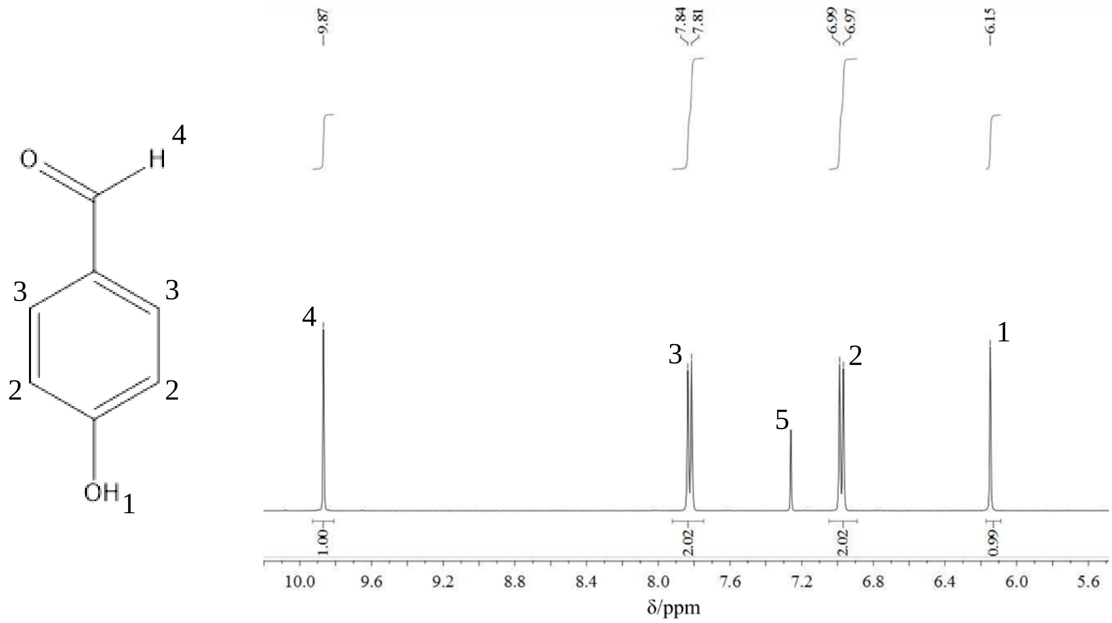

Figure SA.1. Proton nuclear magnetic resonance ([1]H NMR) spectra of 4-hydroxybenzaldeheyde (HBA) after purification. Peaks marked as 5, correspond to the solvent peak and to impurities present in the solvent.

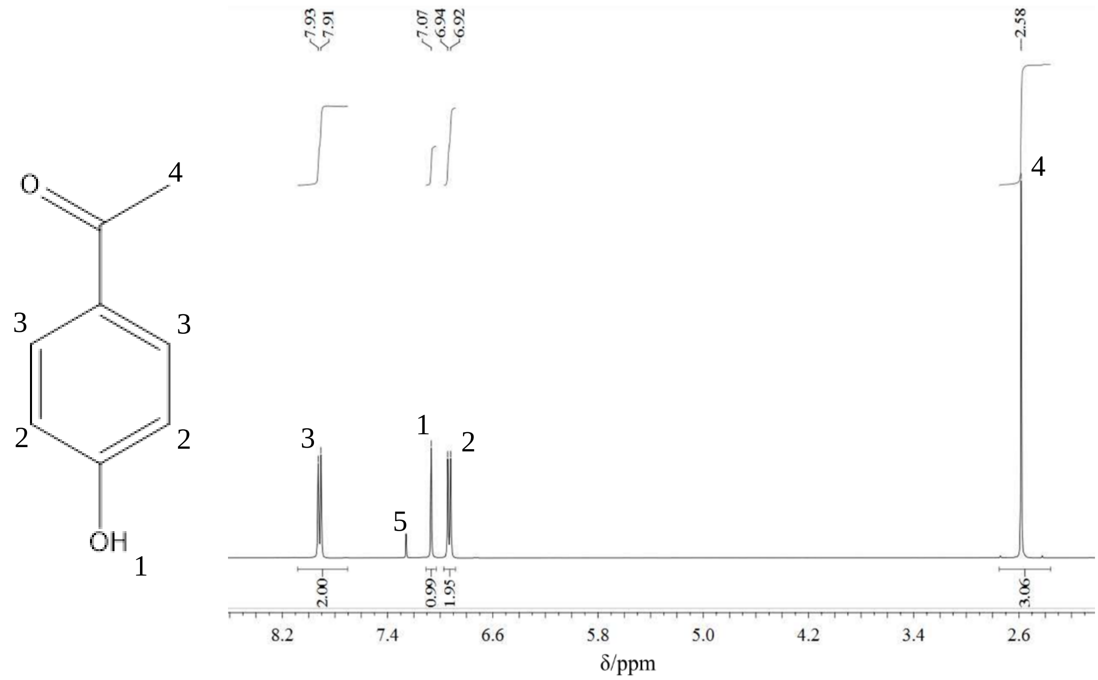

Figure SA.2. [1]H NMR spectra of 4'-hydroxyacetophenone (HAP) after purification. Peaks marked as 5, correspond to the solvent peak and to impurities present in the solvent.

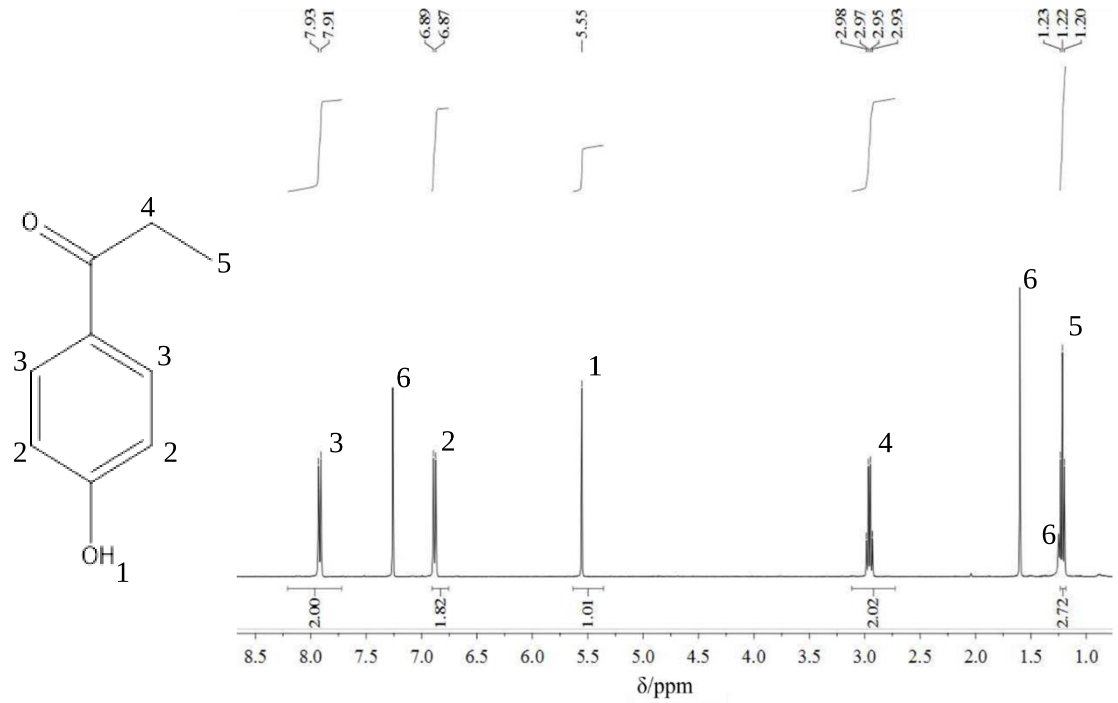

Figure SA.3. ^{1}H NMR spectra of 4'-hydroxypropiophenone (HPP) after purification. Peaks marked as 6, correspond to the solvent peak and to impurities present in the solvent.

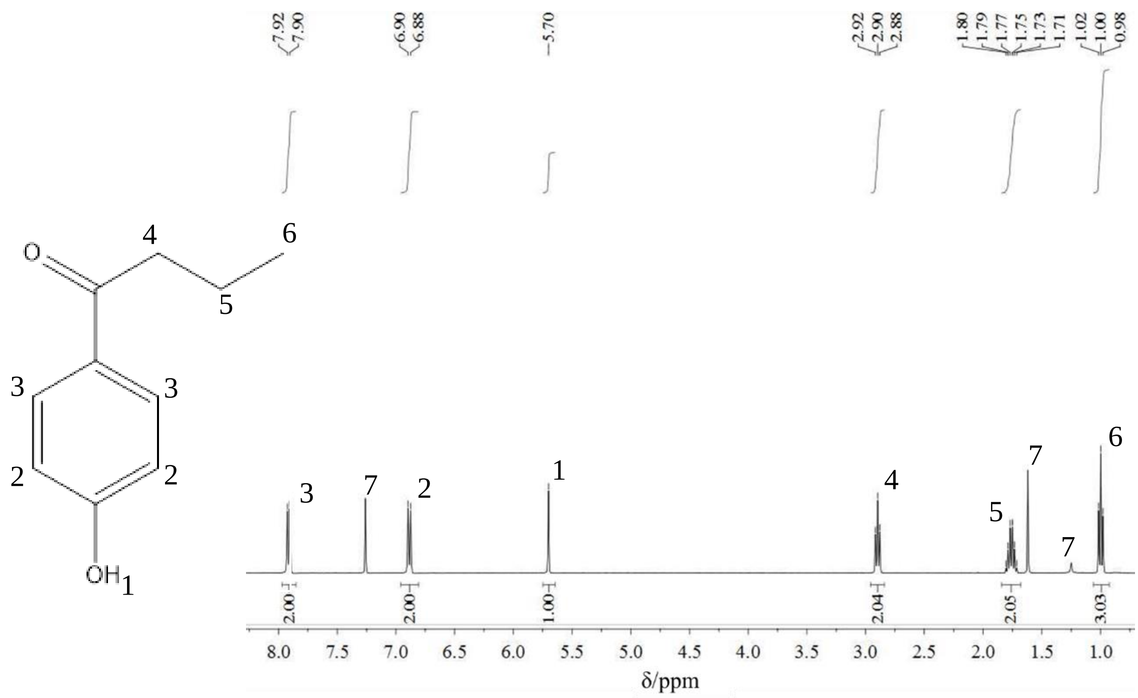

Figure SA.4. ^{1}H NMR spectra of 4'-hydroxybutirophenone (HBP) after purification. Peaks marked as 7, correspond to the solvent peak and to impurities present in the solvent.

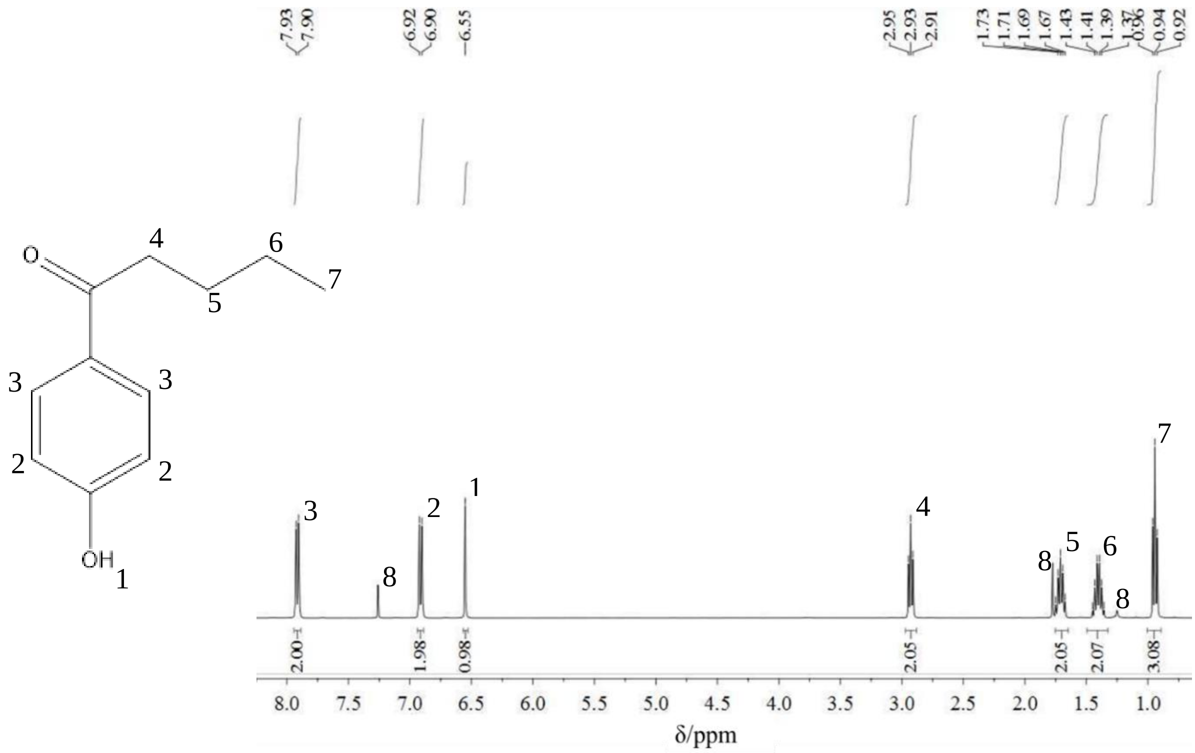

Figure SA.5. ^{1}H NMR spectra of 4’-hydroxyvalerophenone (HVP) after purification. Peaks marked as 8, correspond to the solvent peak and to impurities present in the solvent

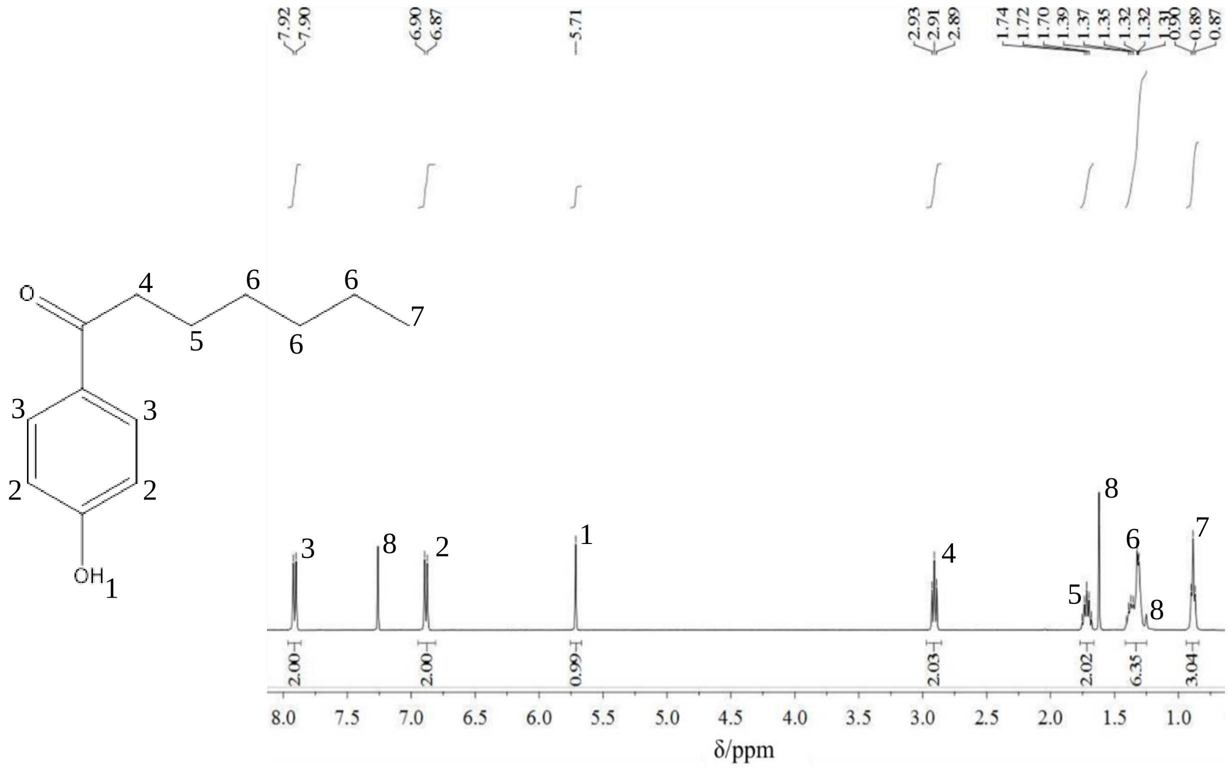

Figure SA.6. ^{1}H NMR spectra of 4’-hydroxyheptanophenone (HHP) after purification. Peaks marked as 8, correspond to the solvent peak and to impurities present in the solvent.

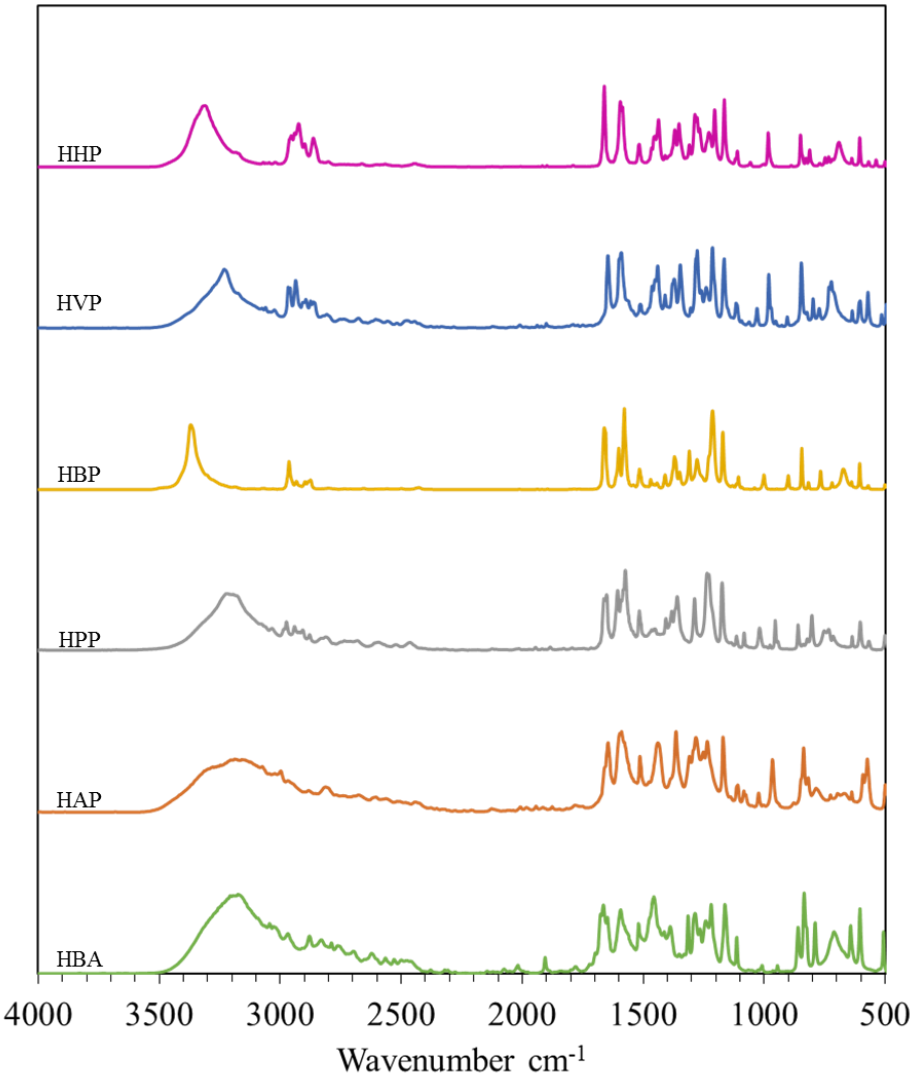

Figure SA.7. Diffuse reflectance Infrared Fourier transform spectra obtained for all the compounds after purification.

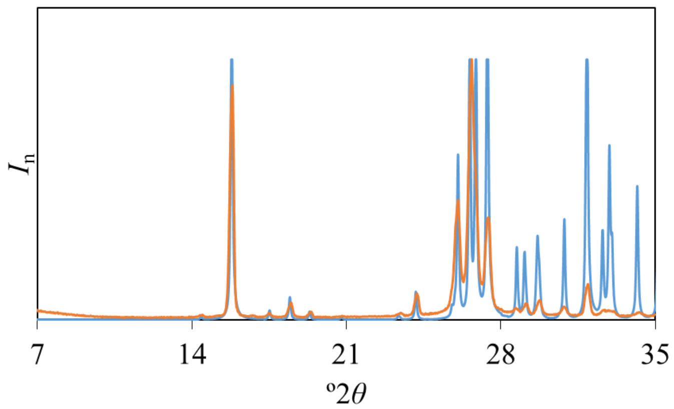

Figure SA.8. Comparison of the X-ray powder diffraction patterns obtained for 4-HBA sample after sublimation (orange pattern) and that found using the single crystal X-ray data for HBA form I, [32] and the program Mercury 3.7 (blue pattern).[40] The intensities were normalized (I_n) relative to the most intense peak observed in each diffractogram**.**

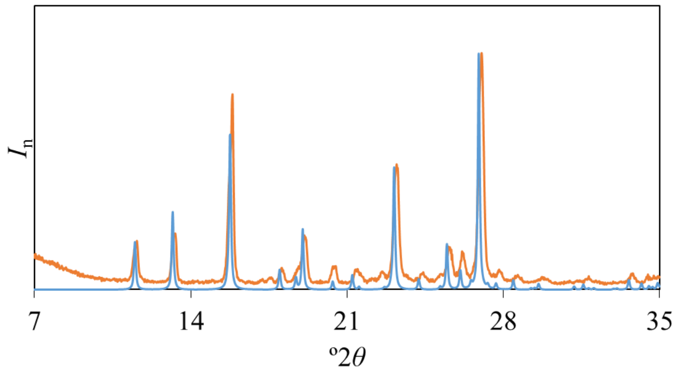

Figure SA.9. Comparison of the X-ray powder diffraction patterns obtained for HAP sample after sublimation (orange pattern) and that found using the single crystal X-ray data for HAP form I,[29] and the program Mercury 3.7 (blue pattern).[40] The intensities were normalized (I_n) relative to the most intense peak observed in each diffractogram.

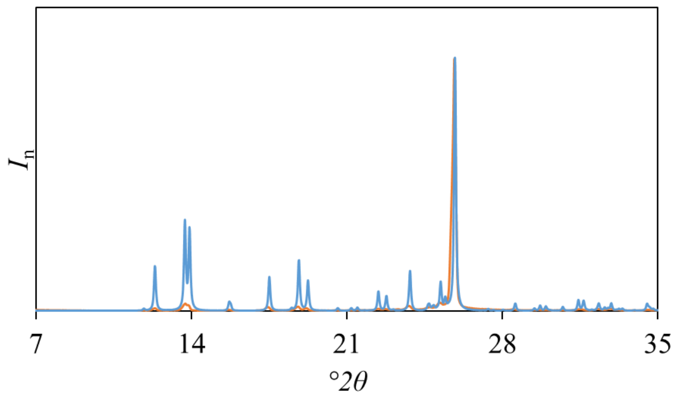

Figure SA.10. Comparison of the X-ray powder diffraction patterns obtained for HPP sample after sublimation (orange pattern) and that found using the single crystal X-ray data for HPP and the program Mercury 3.7 (blue pattern).[40] The intensities were normalized (I_n) relative to the most intense peak observed in each diffractogram.

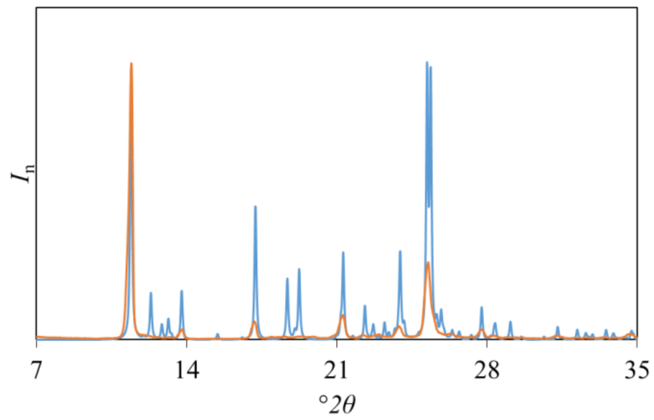

Figure SA.11. Comparison of the X-ray powder diffraction patterns obtained for HBP sample after sublimation (orange pattern) and that found using the single crystal X-ray data for HBP,[33] and the program Mercury 3.7 (blue pattern).[40] The intensities were normalized (I_n) relative to the most intense peak observed in each diffractogram.

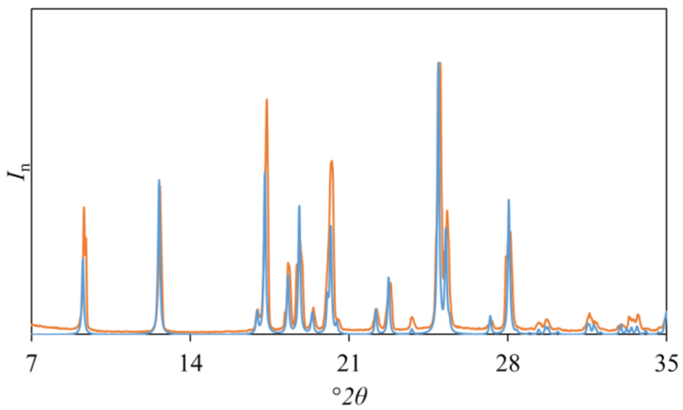

Figure SA.12. Comparison of the X-ray powder diffraction patterns obtained for HVP sample after crystallization with ethanol (orange pattern) and that found using the single crystal X-ray data for HVP,[34] and the program Mercury 3.7 (blue pattern).[40] The intensities were normalized (I_n) relative to the most intense peak observed in each diffractogram**.**

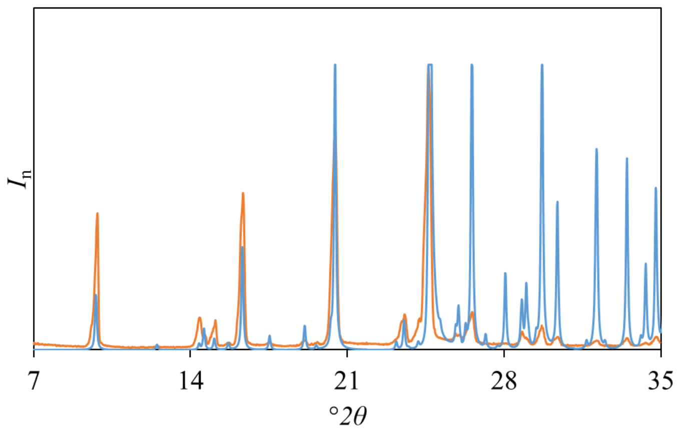

Figure SA.13. Comparison of the X-ray powder diffraction patterns obtained for HHP sample as received (orange pattern) and that found using the single crystal X-ray data for HHP, and the program Mercury 3.7 (blue pattern).[40] The intensities were normalized (I_n) relative to the most intense peak observed in each diffractogram**.**

B) Fusion temperature and enthalpy of fusion

Table SB.1. Temperature and enthalpy of fusion data obtained for 4'-hydroxypropiophenone by differential scanning calorimetry (DSC).

m/mg	T_{on} /K	T_{max} /K	$\Delta_{fus}h^{o}$/J·g^{-1}	$\Delta_{fus}H_m^{o}$/kJ·mol^{-1}
1.314	420.98	422.83	207.5654	31.17
3.398	422.20	423.83	212.9079	31.97
2.299	421.48	423.5	214.4273	32.20
2.262	421.60	422.98	208.8071	31.36
3.658	421.87	423.67	209.9103	31.52

M = 150.177 g·mol^{-1}

$\langle m \rangle \pm u$ = 2.59±0.86 mg

$\langle T_{on} \rangle \pm u$ = 421.6±0.4 K

$\langle T_{max} \rangle \pm u$ = 423.4±0.4 K

$\langle \Delta_{fus}H_m^{o} \rangle \pm u$ = 31.64±0.38 kJ·mol^{-1}

Table SB.2. Temperature and enthalpy of fusion data obtained for 4'-hydroxybutyrophenone by DSC.

m/mg	T_{on} /K	T_{max} /K	$\Delta_{fus}h^{o}$/J·g^{-1}	$\Delta_{fus}H_m^{o}$/kJ·mol^{-1}
1.765	364.80	366.48	146.3952	24.04
1.702	364.74	366.33	146.1204	23.99
1.904	364.79	366.08	145.8661	23.95
1.321	364.43	365.75	146.3230	24.03
1.094	364.52	365.75	145.6703	23.92

M = 164.201 g·mol^{-1}

$\langle m \rangle \pm u$ = 1.56±0.30 mg

$\langle T_{on} \rangle \pm u$ = 364.7±0.2 K

$\langle T_{max} \rangle \pm u$ = 366.1±0.3 K

$\langle \Delta_{fus}H_m^{o} \rangle \pm u$ = 23.99±0.04 kJ·mol^{-1}

Table SB.3. Temperature and enthalpy of fusion data obtained for 4'-hydroxyvalerophenone using DSC 7 from Perkin Elmer.

m/mg	T_{on} /K	T_{max} /K	$\Delta_{fus}h^{o}$/J·g^{-1}	$\Delta_{fus}H_m^{o}$/kJ·mol^{-1}
3.047	334.75	336.58	143.6997	25.61
3.565	334.79	337.00	146.5495	26.12
5.099	334.22	337.17	143.3963	25.56
6.235	333.18	336.90	144.2477	25.71

M = 178.227 g·mol^{-1}

$\langle m \rangle \pm u$ = 5.00±1.52 mg

$\langle T_{on} \rangle \pm u$ = 334.2±0.7 K

$\langle T_{max} \rangle \pm u$ = 336.9±0.2 K

$\langle \Delta_{fus}H_m^{o} \rangle \pm u$ = 25.75±0.26 kJ·mol^{-1}

Table SB.4. Temperature and enthalpy of fusion data obtained for 4'-hydroxyvalerophenone after purification from ethanol using the TA Instruments 2920 MTDSC.

m/mg	T_{on} /K	T_{max} /K	$\Delta_{fus}h^o$/J·g^{-1}	$\Delta_{fus}H_m^o$/kJ·mol^{-1}
5.000	335.65	337.75	149.81	26.70
5.167	335.75	337.85	149.30	26.61
4.617	334.45	337.35	149.51	26.65
15.328	336.72	338.51	149.56	25.65
13.537	335.30	338.21	149.94	26.72

M = 178.227 g·mol^{-1}
$\langle m \rangle \pm u$ = 8.73±4.70 mg
$\langle T_{on} \rangle \pm u$ = 335.6±0.7 K
$\langle T_{max} \rangle \pm u$ = 337.9±0.4 K
$\langle \Delta_{fus}H_m^o \rangle \pm u$ = 26.67±0.04 kJ·mol^{-1}

Table SB.5. Temperature and enthalpy of crystalization data obtained for 4'-hydroxyvalerophenone using the TA Instruments 2920 MTDSC.

m/mg	T_{on} /K	T_{max} /K	$\Delta_{cryst}h^o$/J·g^{-1}	$\Delta_{cryst}H_m^o$/kJ·mol^{-1}
5.000	306.95	300.35	88.15	15.71
5.167	306.85	300.25	89.70	15.99
4.617	310.95	307.05	101.41	18.07
15.328	309.98	305.92	95.42	17.01
13.537	309.15	305.80	93.30	16.63

M = 178.227 g·mol^{-1}
$\langle m \rangle \pm u$ = 8.73±4.70 mg
$\langle T_{on} \rangle \pm u$ = 308.8±1.6 K
$\langle T_{max} \rangle \pm u$ = 303.9±3.0 K
$\langle \Delta_{cryst}H_m^o \rangle \pm u$ = 16.68±0.83 kJ·mol^{-1}

Table SB.6. Temperature and enthalpy of fusion data obtained for 4'-hydroxyvalerophenone after crystallization from melt using the TA Instruments 2920 MTDSC.

m/mg	T_{on} /K	T_{max} /K	$\Delta_{fus}h^o$/J·g^{-1}	$\Delta_{fus}H_m^o$/kJ·mol^{-1}
5.000	324.09	326.87	100.44	17.90
5.167	324.13	326.92	101.00	18.00
4.617	324.53	327.68	102.90	18.34
15.328	324.63	327.95	101.80	18.14
13.537	324.27	328.36	102.90	18.34

M = 178.227 g·mol^{-1}
$\langle m \rangle \pm u$ = 8.73±4.70 mg
$\langle T_{on} \rangle \pm u$ = 324.3±0.2 K
$\langle T_{max} \rangle \pm u$ = 327.6±0.6 K
$\langle \Delta_{fus}H_m^o \rangle \pm u$ = 18.14±0.18 kJ·mol^{-1}

Table SB.7. Temperature and enthalpy of fusion data obtained for 4'-hydroxyheptanophenone by DSC.

m/mg	T_{on} /K	T_{max} /K	$\Delta_{fus}h^o$/J·g^{-1}	$\Delta_{fus}H_m^o$/kJ·mol^{-1}
1.386	364.18	365.58	153.5499	31.67
3.197	364.58	366.33	152.8831	31.54
3.408	364.87	367.17	152.4925	31.46
2.710	364.87	366.67	152.2876	31.41
3.522	364.86	366.92	152.0591	31.37

M = 206.280 g·mol^{-1}

$<m>\pm u$ = 2.84±0.78 mg

$<T_{on}>\pm u$ = 364.7±0.3 K

$<T_{max}>\pm u$ = 366.5±0.6 K

$< \Delta_{fus}H_m^o>\pm u$ = 31.49±0.10 kJ·mol^{-1}

C) Heat Capacities

Table SC.1. Measurements of the standard (p^0 = 1 bar) molar heat capacity on the solid state, $C^{o}_{p,m}$(cr), of 4'-hydroxypropiophenone (HPP) in the temperature range of 288.15 K to 384.15 K . Each run corresponds to an individual experience.

T/K	$C^{o}_{p,m}$ (cr)/J·K^{-1}·mol^{-1}				T/K	$C^{o}_{p,m}$ (cr)/J·K^{-1}·mol^{-1}			
	Run 1	Run 2	Run 3	Run 4		Run 1	Run 2	Run 3	Run 4
288.66	187.49	190.13	190.71	184.54	341.41	214.86	219.78	221.29	217.37
289.98	187.16	190.73	190.54	184.18	342.66	215.62	222.05	221.31	218.01
291.28	188.08	191.22	191.74	185.67	343.91	216.33	223.71	222.32	218.63
292.55	188.65	192.45	192.89	185.50	345.16	217.05	223.63	223.24	218.88
293.82	187.99	193.37	193.22	185.78	346.41	218.33	224.99	224.07	220.59
295.08	189.07	194.84	194.28	187.43	347.66	218.53	224.68	224.48	221.12
296.34	189.92	195.52	194.35	188.77	340.16	214.26	219.13	220.54	215.21
297.60	190.78	195.23	194.88	189.88	341.41	214.86	219.78	221.29	217.37
298.85	190.95	195.01	195.65	190.13	342.66	215.62	222.05	221.31	218.01
300.11	191.01	196.55	196.05	191.00	343.91	216.33	223.71	222.32	218.63
301.36	192.15	197.34	197.21	191.42	345.16	217.05	223.63	223.24	218.88
302.61	192.91	198.61	197.35	192.40	346.41	218.33	224.99	224.07	220.59
303.87	194.57	199.73	199.68	193.64	347.66	218.53	224.68	224.48	221.12
305.13	194.91	200.36	200.25	194.65	348.91	219.21	225.67	224.95	222.39
306.38	196.09	200.64	200.54	195.80	350.15	219.13	226.58	226.20	223.38
307.64	196.15	200.82	200.97	196.04	351.40	220.26	228.06	227.14	224.55
308.89	197.45	201.76	201.53	196.64	352.65	221.52	229.27	227.91	224.83
310.14	196.98	203.11	201.93	197.09	353.90	221.87	229.67	229.04	225.38
311.39	198.07	204.48	203.06	198.37	355.15	222.67	229.08	229.94	226.02
312.64	199.40	205.23	203.07	198.92	356.40	223.87	229.20	229.80	227.15
313.90	200.81	205.70	205.07	199.25	357.65	223.72	229.52	231.09	228.32
315.15	201.15	206.00	205.99	200.86	358.90	224.66	230.91	230.98	229.24
316.40	201.11	207.33	206.52	200.77	360.15	224.49	232.24	231.78	230.07
317.65	202.21	208.16	207.56	201.49	361.40	225.55	234.09	233.37	230.67
318.90	202.15	208.26	207.50	201.74	362.65	226.43	233.96	233.63	231.79
320.15	203.68	209.24	208.39	203.07	363.90	226.67	234.95	234.40	232.67
321.41	204.07	210.32	209.09	204.34	365.15	227.23	235.56	235.21	232.72
322.66	205.21	210.63	209.83	204.91	366.39	227.38	236.76	235.83	233.98
323.91	205.73	211.75	210.25	205.32	367.65	229.57	237.87	236.75	236.18
325.16	206.49	212.70	211.22	206.15	368.90	230.04	238.31	238.07	236.38
326.41	207.58	213.10	211.71	206.99	370.15	231.44	238.49	239.17	237.28
327.66	207.85	213.64	212.35	208.36	371.40	232.03	239.41	239.83	237.71
328.91	208.45	214.75	213.56	209.44	372.65	231.89	240.61	240.42	238.61
330.16	209.16	215.22	214.25	209.36	373.90	232.66	241.75	241.00	239.49
331.41	209.62	215.41	215.38	209.83	375.15	233.37	242.62	241.74	239.56
332.66	211.11	216.15	216.34	210.78	376.40	235.22	244.61	242.08	241.29
333.91	211.50	216.77	216.27	211.76	377.64	235.01	245.08	243.63	241.64
335.16	212.52	217.82	217.13	212.73	378.89	235.84	245.74	244.82	243.32
336.41	212.69	219.74	217.67	214.35	380.14	236.20	247.21	244.81	244.25
337.66	212.98	220.28	218.89	214.37	381.39	236.84	247.56	246.16	244.33
338.91	213.89	220.37	219.68	214.68	382.64	236.23	248.68	246.67	245.80
340.16	214.26	219.13	220.54	215.21	383.89	237.97	250.39	247.89	247.52

Table SC.2. Standard (p^0 = 1 bar) molar heat capacities of the solid state, $C^{o}_{p,\mathrm{m}}$ (cr), for HPP obtained by DSC. These results refer to the mean of four independent determinations and the uncertainties reported correspond to twice the standard deviation of the mean.

T/K	$C^{o}_{p,\mathrm{m}}$(cr) / J·K^{-1}·mol^{-1}	T/K	$C^{o}_{p,\mathrm{m}}$(cr) / J·K^{-1}·mol^{-1}	T / K	$C^{o}_{p,\mathrm{m}}$(cr) / J·K^{-1}·mol^{-1}	T/K	$C^{o}_{p,\mathrm{m}}$(cr) / J·K^{-1}·mol^{-1}
288.66	188.2±1.4	313.90	202.7±1.6	338.91	217.2±1.7	363.90	232.2±1.9
289.98	188.2±1.6	315.15	203.5±1.4	340.16	217.3±1.5	365.15	232.7±1.9
291.28	189.2±1.4	316.40	203.9±1.7	341.41	218.3±1.4	366.39	233.5±2.1
292.55	189.9±1.7	317.65	204.9±1.7	342.66	219.2±1.5	367.65	235.1±1.9
293.82	190.1±1.9	318.90	204.9±1.7	343.91	220.2±1.7	368.90	235.7±1.9
295.08	191.4±1.9	320.15	206.1±1.6	345.16	220.7±1.6	370.15	236.6±1.8
296.34	192.1±1.6	321.41	206.9±1.6	346.41	222.0±1.5	371.40	237.2±1.8
297.60	192.7±1.4	322.66	207.6±1.5	347.66	222.2±1.5	372.65	237.9±2.0
298.85	192.9±1.4	323.91	208.3±1.6	348.91	223.1±1.5	373.90	238.7±2.1
300.11	193.6±1.5	325.16	209.1±1.7	350.15	223.8±1.7	375.15	239.3±2.1
301.36	194.5±1.6	326.41	209.8±1.5	351.40	225.0±1.7	376.40	240.8±2.0
302.61	195.3±1.6	327.66	210.5±1.4	352.65	225.9±1.7	377.64	241.3±2.2
303.87	196.9±1.6	328.91	211.5±1.5	353.90	226.5±1.8	378.89	242.4±2.3
305.13	197.5±1.6	330.16	212.0±1.6	355.15	226.9±1.7	380.14	243.1±2.4
306.38	198.3±1.3	331.41	212.6±1.6	356.40	227.5±1.3	381.39	243.7±2.4
307.64	198.5±1.4	332.66	213.6±1.5	357.65	228.2±1.6	382.64	244.3±2.8
308.89	199.3±1.3	333.91	214.1±1.4	358.90	228.9±1.5	383.89	245.9±2.7
310.14	199.8±1.6	335.16	215.0±1.4	360.15	229.6±1.8		
311.39	201.0±1.6	336.41	216.1±1.6	361.40	230.9±1.9		
312.64	201.7±1.5	337.66	216.6±1.8	362.65	231.4±1.7		

Table SC.3. Standard (p^0 = 1 bar) molar heat capacities, $C^{o}_{p,m}$ (g), of HPP in the gaseous state, obtained with Statistical Mechanics,[51] using harmonic vibration frequencies obtained by B3LYP-D3/cc-pVTZ method and scaled by 0.9889.[55]

T / K	$C^{o}_{p,m}$(g) / J·K^{-1}·mol^{-1}	T / K	$C^{o}_{p,m}$(g) / J·K^{-1}·mol^{-1}	T / K	$C^{o}_{p,m}$(g) / J·K^{-1}·mol^{-1}	T / K	$C^{o}_{p,m}$(g) / J·K^{-1}·mol^{-1}	T / K	$C^{o}_{p,m}$(g) / J·K^{-1}·mol^{-1}
200	122.679	241	143.168	282	163.946	323	184.581	364	204.596
201	123.173	242	143.673	283	164.453	324	185.078	365	205.073
202	123.668	243	144.178	284	164.960	325	185.575	366	205.549
203	124.163	244	144.683	285	165.467	326	186.072	367	206.025
204	124.658	245	145.188	286	165.974	327	186.568	368	206.500
205	125.153	246	145.693	287	166.480	328	187.064	369	206.974
206	125.649	247	146.199	288	166.987	329	187.559	370	207.448
207	126.145	248	146.705	289	167.493	330	188.054	371	207.922
208	126.641	249	147.211	290	167.999	331	188.548	372	208.394
209	127.137	250	147.717	291	168.505	332	189.042	373	208.866
210	127.634	251	148.223	292	169.011	333	189.536	374	209.338
211	128.131	252	148.729	293	169.517	334	190.029	375	209.809
212	128.629	253	149.236	294	170.023	335	190.522	376	210.279
213	129.126	254	149.742	295	170.528	336	191.015	377	210.748
214	129.624	255	150.249	296	171.033	337	191.506	378	211.217
215	130.123	256	150.756	297	171.538	338	191.998	379	211.685
216	130.621	257	151.263	298	172.043	339	192.489	380	212.153
217	131.120	258	151.769	299	172.548	340	192.979	381	212.620
218	131.619	259	152.277	300	173.052	341	193.469	382	213.086
219	132.118	260	152.784	301	173.557	342	193.959	383	213.551
220	132.618	261	153.291	302	174.061	343	194.448	384	214.016
221	133.118	262	153.798	303	174.564	344	194.936	385	214.481
222	133.618	263	154.305	304	175.068	345	195.425	386	214.944
223	134.119	264	154.813	305	175.571	346	195.912	387	215.407
224	134.619	265	155.320	306	176.074	347	196.399	388	215.869
225	135.120	266	155.828	307	176.577	348	196.886	389	216.331
226	135.622	267	156.335	308	177.080	349	197.372	390	216.791
227	136.123	268	156.843	309	177.582	350	197.857	391	217.251
228	136.625	269	157.350	310	178.084	351	198.342	392	217.711
229	137.127	270	157.858	311	178.585	352	198.826	393	218.170
230	137.629	271	158.365	312	179.087	353	199.310	394	218.628
231	138.131	272	158.873	313	179.588	354	199.794	395	219.085
232	138.634	273	159.380	314	180.089	355	200.276	396	219.542
233	139.137	274	159.888	315	180.589	356	200.759	397	219.997
234	139.640	275	160.395	316	181.089	357	201.240	398	220.453
235	140.143	276	160.903	317	181.589	358	201.721	399	220.907
236	140.647	277	161.410	318	182.089	359	202.202	400	221.361
237	141.151	278	161.917	319	182.588	360	202.682		
238	141.655	279	162.425	320	183.087	361	203.161		
239	142.159	280	162.932	321	183.585	362	203.640		
240	142.663	281	163.439	322	184.083	363	204.118		

Table SC.4. Measurements of the standard molar heat capacity on the solid state of 4'-hydroxybutyrophenone (HBP) in the temperature range of 288.15 K to 351.15 K. Each run corresponds to an individual experience.

T/K	$C^{o}_{p,m}$ (cr)/J·K^{-1}·mol^{-1}		
	Run 1	Run 2	Run 3
288.67	227.32	217.71	212.55
289.99	229.79	219.85	214.04
291.29	229.71	219.67	214.61
291.60	230.61	220.35	215.11
292.87	231.93	222.07	216.00
294.14	231.85	223.81	216.80
295.40	232.93	224.64	219.57
296.66	233.94	227.05	221.34
297.92	236.16	227.61	222.17
299.17	236.30	228.22	223.20
300.43	238.02	229.31	225.56
301.68	238.32	230.86	227.82
302.94	239.45	230.99	228.31
304.19	238.72	234.02	231.14
305.45	239.84	233.99	230.77
306.70	242.27	235.59	232.79
307.95	243.61	236.77	235.55
309.21	243.97	237.61	237.43
310.46	244.51	240.54	237.06
311.71	245.78	240.94	239.14
312.96	248.04	241.92	241.28
314.21	248.10	243.41	243.24
315.46	248.88	244.02	244.62
316.71	248.61	245.17	247.08
317.96	250.09	244.77	248.16
319.22	250.67	247.07	249.70
320.47	250.97	248.92	250.68
321.72	253.62	249.11	251.36
322.97	254.62	250.71	253.80
324.23	255.38	251.59	256.63
325.48	256.71	254.31	258.16
326.73	256.78	254.47	259.97
327.98	259.14	255.84	261.64
329.23	258.98	258.00	263.57
330.48	263.27	257.97	265.09
331.73	263.19	260.13	267.54
332.98	265.97	262.61	268.00
334.23	266.09	262.15	269.35
335.48	267.86	264.16	270.73
336.73	271.03	266.83	272.31
337.98	271.40	266.49	273.39
339.23	273.86	267.69	274.48
340.48	277.15	268.59	277.33
341.73	277.96	270.93	279.05
342.98	281.06	271.84	281.71
344.23	282.09	273.83	283.23
345.48	283.24	274.52	285.97
346.73	285.21	276.68	286.65
347.98	287.20	277.49	288.79
349.23	289.41	279.36	292.15
350.48	290.93	282.28	293.88

Table SC.5. Standard (p^0 = 1 bar) molar heat capacities, $C^{o}_{p,\mathrm{m}}$ (cr), of the solid state for HBP obtained by DSC. These results refer to the mean of three independent determinations and the uncertainties reported correspond to twice the standard deviation of the mean.

T/K	$C^{o}_{p,\mathrm{m}}$ (cr)/J·K^{-1}·mol^{-1}	T/K	$C^{o}_{p,\mathrm{m}}$ (cr)/J·K^{-1}·mol^{-1}
288.67	219.2±4.3	320.47	250.2±0.6
289.99	221.2±4.6	321.72	251.4±1.3
291.29	221.3±4.4	322.97	253.0±1.2
291.60	222.0±4.6	324.23	254.5±1.5
292.87	223.3±4.6	325.48	256.4±1.1
294.14	224.2±4.3	326.73	257.1±1.6
295.40	225.7±3.9	327.98	258.9±1.7
296.66	227.4±3.6	329.23	260.2±1.7
297.92	228.6±4.1	330.48	262.1±2.1
299.17	229.2±3.8	331.73	263.6±2.1
300.43	231.0±3.7	332.98	265.5±1.6
301.68	232.3±3.1	334.23	265.9±2.1
302.94	232.9±3.4	335.48	267.6±1.9
304.19	234.6±2.2	336.73	270.1±1.7
305.45	234.9±2.7	337.98	270.4±2.1
306.70	236.9±2.8	339.23	272.0±2.2
307.95	238.6±2.5	340.48	274.4±2.9
309.21	239.7±2.2	341.73	276.0±2.5
310.46	240.7±2.2	342.98	278.2±3.2
311.71	242.0±2.0	344.23	279.7±3.0
312.96	243.7±2.2	345.48	281.2±3.5
314.21	244.9±1.6	346.73	282.8±3.1
315.46	245.8±1.5	347.98	284.5±3.5
316.71	247.0±1.0	349.23	287.0±3.9
317.96	247.7±1.6	350.48	289.0±3.5
319.22	249.1±1.1		

Table SC.6. Standard (p^0 = 1 bar) molar heat capacities, $C^{o}_{p,m}$ (g), of HBP in the gaseous state, obtained with Statistical Mechanics,[51] using harmonic vibration frequencies obtained by B3LYP-D3/cc-pVTZ method and scaled by 0.9889.[55]

T/K	$C^{o}_{p,m}$(g) / J·K^{-1}·mol^{-1}	T/K	$C^{o}_{p,m}$(g) / J·K^{-1}·mol^{-1}	T/K	$C^{o}_{p,m}$(g) / J·K^{-1}·mol^{-1}	T/K	$C^{o}_{p,m}$(g) / J·K^{-1}·mol^{-1}	T/K	$C^{o}_{p,m}$(g) / J·K^{-1}·mol^{-1}
200	137.497	241	160.187	282	183.484	323	206.843	364	229.653
201	138.040	242	160.750	283	184.056	324	207.408	365	230.198
202	138.585	243	161.313	284	184.628	325	207.973	366	230.743
203	139.129	244	161.876	285	185.199	326	208.537	367	231.286
204	139.675	245	162.440	286	185.771	327	209.101	368	231.830
205	140.220	246	163.004	287	186.342	328	209.665	369	232.372
206	140.766	247	163.569	288	186.914	329	210.228	370	232.914
207	141.313	248	164.134	289	187.486	330	210.791	371	233.455
208	141.860	249	164.699	290	188.057	331	211.354	372	233.996
209	142.408	250	165.264	291	188.629	332	211.916	373	234.536
210	142.956	251	165.830	292	189.200	333	212.478	374	235.075
211	143.505	252	166.396	293	189.772	334	213.039	375	235.614
212	144.054	253	166.963	294	190.343	335	213.600	376	236.151
213	144.604	254	167.530	295	190.914	336	214.161	377	236.689
214	145.154	255	168.097	296	191.485	337	214.721	378	237.225
215	145.705	256	168.664	297	192.057	338	215.281	379	237.761
216	146.256	257	169.232	298	192.628	339	215.840	380	238.296
217	146.808	258	169.800	299	193.198	340	216.399	381	238.831
218	147.360	259	170.368	300	193.769	341	216.957	382	239.364
219	147.913	260	170.936	301	194.340	342	217.515	383	239.897
220	148.466	261	171.505	302	194.910	343	218.072	384	240.430
221	149.019	262	172.073	303	195.481	344	218.629	385	240.961
222	149.573	263	172.643	304	196.051	345	219.185	386	241.492
223	150.128	264	173.212	305	196.621	346	219.741	387	242.022
224	150.683	265	173.781	306	197.191	347	220.296	388	242.552
225	151.239	266	174.351	307	197.761	348	220.851	389	243.080
226	151.794	267	174.921	308	198.330	349	221.406	390	243.608
227	152.351	268	175.491	309	198.899	350	221.959	391	244.135
228	152.908	269	176.061	310	199.468	351	222.513	392	244.662
229	153.465	270	176.631	311	200.037	352	223.065	393	245.188
230	154.023	271	177.202	312	200.606	353	223.617	394	245.713
231	154.581	272	177.772	313	201.174	354	224.169	395	246.237
232	155.140	273	178.343	314	201.742	355	224.720	396	246.760
233	155.699	274	178.914	315	202.310	356	225.270	397	247.283
234	156.259	275	179.485	316	202.878	357	225.820	398	247.805
235	156.818	276	180.056	317	203.445	358	226.370	399	248.326
236	157.379	277	180.627	318	204.012	359	226.918	400	248.846
237	157.940	278	181.199	319	204.579	360	227.467		
238	158.501	279	181.770	320	205.145	361	228.014		
239	159.062	280	182.341	321	205.711	362	228.561		
240	159.624	281	182.913	322	206.277	363	229.107		

Table SC.7. Measurements of the standard (p^0 = 1 bar) molar heat capacity of 4'-hydroxyvalerophenone (HVP) by DSC. These results correspond to the solid state, fusion transition and liquid zone, in the temperature range of 288.15 K to 352.15 K. Each run corresponds to an individual experience.

T/K	$C^{o}_{p,m}$ /J·K^{-1}·mol^{-1}							
	Run 1	Run 2	Run 3	Run 4	Run 5	Run 6	Run 7	Run 8
288.67	232.4	222.9	225.7	241.8	244.9	243.7	234.3	234.0
288.92	233.5	222.1	228.3	242.8	242.4	245.4	236.4	236.1
289.17	232.0	222.6	228.4	242.1	241.5	242.1	236.5	236.4
289.42	234.3	225.4	228.0	242.0	244.6	244.1	236.6	236.1
289.67	233.8	223.3	226.4	244.0	246.2	243.7	236.7	233.6
289.92	233.8	222.8	224.8	241.7	244.6	243.3	236.1	235.8
290.17	234.1	224.7	225.1	244.0	244.3	245.5	237.4	237.5
290.42	232.3	223.1	228.4	242.7	243.6	246.8	235.9	237.7
290.68	230.6	224.0	225.3	243.4	245.0	248.2	235.0	235.6
290.93	231.7	225.9	229.2	244.7	240.4	248.2	234.9	235.7
291.18	233.5	228.4	226.2	247.6	239.2	249.8	233.4	235.9
291.43	235.6	226.3	227.9	247.1	243.0	253.0	235.8	235.0
291.68	234.0	226.5	228.6	246.9	246.7	250.7	235.5	233.8
291.93	235.4	226.6	224.8	243.8	243.5	249.5	234.9	235.2
292.18	233.3	227.1	228.1	245.8	245.7	248.2	235.0	235.9
292.43	235.5	226.7	231.0	247.1	246.6	249.9	235.0	236.0
292.68	233.3	227.1	230.2	251.8	247.2	251.7	235.9	235.1
292.93	233.9	227.2	236.6	249.5	248.7	248.1	235.1	237.6
293.18	236.3	228.4	232.7	247.2	246.9	252.3	233.7	239.4
293.43	236.1	228.5	230.8	248.4	247.7	251.7	236.1	240.7
293.68	237.5	227.0	234.8	250.8	247.8	249.4	235.3	240.3
293.93	235.4	225.8	232.1	250.5	249.5	249.5	234.9	240.9
294.18	234.6	226.7	232.5	248.8	247.9	249.3	234.2	239.0
294.44	233.6	228.5	230.1	250.7	247.5	251.1	234.0	237.5
294.69	236.3	229.9	232.9	252.5	246.7	254.6	234.3	238.9
294.94	235.0	229.2	232.7	252.6	246.1	253.2	234.8	239.3
295.19	235.3	229.8	232.6	250.4	247.8	250.8	232.9	239.0
295.44	235.3	231.8	235.5	249.4	246.3	252.0	235.4	238.2
295.69	238.1	231.5	237.2	250.4	246.4	254.9	235.0	239.4
295.94	240.0	229.9	235.8	250.0	247.4	253.3	235.4	237.3
296.19	236.4	229.8	235.2	250.1	248.4	253.8	234.2	238.3
296.44	237.1	231.4	235.3	253.1	251.6	252.9	235.0	240.4
296.69	237.9	231.1	236.5	252.9	249.5	251.4	234.1	240.5
296.94	237.0	229.2	233.1	252.5	251.2	251.9	233.1	241.7
297.19	237.6	228.4	233.8	252.5	250.4	252.2	234.1	242.8
297.44	239.2	230.7	233.6	249.9	252.5	256.4	234.3	241.3
297.69	241.1	231.4	233.3	249.4	249.3	253.8	233.2	241.3
297.94	241.1	231.2	234.9	249.6	250.9	255.9	233.7	242.6
298.19	242.1	232.8	232.1	249.9	250.9	257.5	235.0	241.7
298.44	238.9	235.2	234.1	253.0	249.5	255.6	235.3	241.0
298.69	238.9	233.6	232.8	251.1	247.4	255.7	234.1	241.3
298.94	239.7	233.8	233.7	248.0	247.9	257.3	235.8	241.9
299.19	240.2	234.5	235.8	248.5	247.1	255.1	236.2	240.7
299.44	239.1	232.9	232.9	250.2	249.4	256.9	235.2	241.4
299.69	238.7	234.8	232.7	251.4	252.5	257.4	234.7	241.4
299.94	238.0	233.4	236.6	254.0	253.4	259.2	236.8	241.5

Continued…

T/K	$C^{o}_{p,m}$ /J·K^{-1}·mol^{-1}							
	Run 1	Run 2	Run 3	Run 4	Run 5	Run 6	Run 7	Run 8
300.19	240.5	233.0	237.1	252.9	254.9	258.8	236.6	245.3
300.44	242.1	233.9	234.4	250.0	251.9	259.8	237.0	245.5
300.69	239.8	233.8	234.9	250.6	254.0	258.4	238.2	245.1
300.94	240.4	234.2	234.5	254.4	253.3	259.3	236.5	245.0
301.19	241.7	234.6	234.6	253.7	251.8	258.9	236.0	244.8
301.44	240.5	234.4	234.2	251.5	250.0	259.8	234.9	242.0
301.69	242.5	235.6	235.9	253.2	250.3	259.3	235.5	241.1
301.94	244.5	235.8	237.1	251.8	253.4	259.7	236.0	241.2
302.19	243.6	235.9	236.8	254.2	253.8	259.8	236.9	241.0
302.44	240.7	237.8	235.8	254.5	255.3	259.2	237.1	240.3
302.69	241.0	236.1	234.8	252.7	253.9	260.7	236.6	242.2
302.94	243.0	234.7	236.0	257.0	253.1	259.5	236.8	244.9
303.19	242.8	233.4	239.0	258.0	255.1	260.4	236.5	245.5
303.44	245.1	235.5	239.0	255.3	253.7	260.8	238.4	244.2
303.69	243.7	237.3	238.8	255.3	255.9	261.4	239.7	244.0
303.94	245.6	238.3	237.4	257.6	255.3	262.8	238.5	243.7
304.19	246.1	237.3	237.7	257.7	254.1	264.5	236.5	244.6
304.44	244.4	237.0	239.0	256.8	258.3	262.3	237.7	244.2
304.69	245.4	237.2	237.7	255.0	258.1	260.6	236.1	244.2
304.94	245.8	237.1	237.5	255.2	256.8	262.6	236.5	242.9
305.19	245.7	238.5	237.4	255.0	255.2	267.4	236.5	240.7
305.44	246.1	239.0	239.8	256.0	257.8	267.7	234.8	243.2
305.69	245.4	238.3	238.3	257.7	256.9	264.4	235.1	246.1
305.94	244.1	238.8	239.3	259.2	256.5	262.6	235.9	244.0
306.19	246.1	239.4	238.4	257.1	258.4	264.5	234.0	244.0
306.44	247.8	240.1	239.2	258.2	260.5	265.4	236.1	244.0
306.69	247.4	239.6	235.7	257.0	259.2	269.4	234.9	246.8
306.94	246.9	240.4	240.1	256.2	259.8	270.4	237.5	245.4
307.19	247.6	239.8	246.2	256.4	259.8	270.6	239.6	242.9
307.44	249.0	240.9	240.8	257.6	259.4	269.6	239.4	244.3
307.69	250.3	242.8	240.1	258.0	258.0	268.8	238.3	244.2
307.94	248.4	240.9	240.1	260.0	258.5	267.1	237.0	243.4
308.19	248.3	241.8	238.6	259.9	258.0	267.3	237.6	246.5
308.44	247.1	242.0	238.6	260.1	259.8	268.4	238.4	246.7
308.69	245.4	242.7	238.2	258.4	257.8	268.7	238.7	247.5
308.94	244.9	243.3	238.3	260.3	259.9	269.0	238.5	248.5
309.19	246.4	244.0	241.4	262.2	259.4	268.7	237.1	247.3
309.44	247.6	242.0	242.6	262.0	262.1	272.0	238.8	246.6
309.69	251.4	241.7	244.8	263.5	262.6	274.1	238.5	246.6
309.94	248.9	243.9	243.9	261.8	260.3	271.3	238.9	246.6
310.19	249.4	245.4	244.3	262.4	263.0	273.0	239.7	248.7
310.44	250.0	246.3	244.8	262.1	265.6	271.5	240.6	249.6
310.69	252.5	244.1	245.2	261.2	258.8	271.7	241.2	249.7
310.94	251.3	244.2	244.9	260.7	260.9	270.4	243.1	249.9
311.19	249.2	244.0	241.8	261.0	263.2	271.2	242.2	248.3
311.44	249.5	245.1	241.3	263.3	263.0	269.3	240.1	247.8
311.69	251.2	243.3	243.6	264.1	263.1	271.4	239.2	249.1
311.94	252.2	245.3	244.4	260.3	260.2	270.4	237.1	247.5

Continued…

T/K	$C^{o}_{p,m}$ /J·K^{-1}·mol^{-1}							
	Run 1	Run 2	Run 3	Run 4	Run 5	Run 6	Run 7	Run 8
312.19	251.2	247.6	244.6	260.8	258.9	271.5	240.0	248.1
312.44	250.7	247.1	243.4	260.0	258.6	273.5	237.9	248.2
312.69	250.1	247.2	244.9	261.1	260.0	273.7	242.0	250.2
312.94	250.6	246.9	242.1	262.0	264.8	274.1	241.7	250.0
313.19	251.6	247.6	242.1	261.0	262.1	270.6	239.6	251.8
313.44	252.8	245.2	247.3	260.8	264.2	274.1	240.4	252.0
313.69	252.3	246.9	247.8	263.3	263.6	276.4	239.4	252.0
313.94	253.7	247.0	244.3	263.0	264.7	275.3	240.1	252.2
314.19	254.7	246.0	247.0	261.3	266.7	275.8	239.9	251.9
314.44	254.8	249.7	245.3	264.2	266.6	277.6	240.1	253.4
314.69	253.7	250.2	247.7	263.7	266.9	278.0	241.3	253.8
314.94	253.2	249.9	244.5	264.7	264.8	279.1	240.6	252.1
315.19	252.2	250.9	246.5	264.0	264.3	277.9	240.7	251.8
315.44	252.5	250.6	247.0	264.1	264.6	273.6	241.1	253.1
315.69	252.1	249.3	244.9	264.2	265.2	274.8	241.8	254.4
315.94	253.3	247.9	243.6	264.0	266.4	277.3	241.1	254.6
316.19	254.6	247.1	248.2	264.4	267.2	276.4	239.9	253.6
316.44	252.5	247.5	246.2	265.9	265.9	277.5	241.7	254.0
316.69	254.2	248.3	247.8	264.5	265.9	280.4	241.0	255.3
316.94	255.4	250.6	248.0	266.6	267.4	281.1	241.1	254.0
317.19	253.5	249.9	247.0	265.7	268.3	278.8	240.3	254.5
317.44	255.0	249.4	245.3	266.7	270.2	278.7	240.0	255.5
317.69	254.7	250.5	246.9	267.3	267.0	279.7	241.8	254.8
317.94	254.4	250.7	245.2	265.6	268.8	279.8	240.2	254.3
318.19	254.4	249.9	244.9	263.7	267.9	279.7	242.2	253.3
318.44	254.3	251.7	246.5	265.1	270.1	280.3	243.5	254.5
318.69	253.6	253.7	247.3	266.5	270.2	281.5	243.5	255.1
318.94	255.8	254.4	245.3	266.6	269.0	282.0	242.8	256.9
319.19	259.0	253.4	250.4	267.6	265.3	285.2	242.8	257.0
319.44	258.7	252.7	246.5	269.3	268.7	283.2	240.3	255.6
319.69	258.6	254.6	246.1	268.9	272.1	283.4	242.0	255.4
319.94	258.9	252.4	245.8	268.2	271.4	282.5	241.3	256.8
320.19	257.9	250.6	247.9	271.3	270.8	282.6	239.4	257.5
320.44	258.7	252.8	249.8	267.6	271.0	283.6	240.5	258.7
320.69	257.8	252.5	247.8	268.5	273.1	284.8	242.3	258.1
320.94	258.5	252.1	248.4	271.6	271.9	286.7	242.7	257.4
321.19	259.3	253.3	248.1	274.2	270.3	286.3	241.7	258.0
321.44	259.1	255.2	245.7	271.3	269.9	285.3	241.1	258.3
321.69	259.2	254.4	247.4	271.1	270.8	285.0	242.2	257.4
321.94	259.1	254.1	243.8	267.7	272.3	286.5	244.5	258.9
322.19	259.2	256.9	247.8	266.8	271.1	287.5	242.0	260.3
322.44	257.2	258.6	248.6	268.7	272.8	289.5	243.1	258.4
322.69	259.2	256.0	249.2	270.8	273.2	290.7	243.9	258.6
322.94	260.6	257.6	246.8	271.3	272.9	291.3	242.4	258.3
323.19	261.2	256.1	250.6	272.7	273.2	289.2	243.5	259.4
323.44	259.4	257.0	251.6	273.2	273.0	288.6	243.7	260.0
323.69	262.9	257.0	249.6	270.9	273.8	287.4	242.1	259.0
323.94	264.7	257.1	248.3	270.3	273.6	287.4	243.5	259.2

Continued…

T/K	$C^{o}_{p,m}$ /J·K^{-1}·mol^{-1}							
	Run 1	Run 2	Run 3	Run 4	Run 5	Run 6	Run 7	Run 8
324.19	264.2	256.5	250.1	272.6	275.1	290.9	243.8	259.4
324.44	261.7	256.8	250.7	272.8	274.4	292.2	244.8	260.2
324.69	263.3	256.4	253.8	274.3	275.7	289.3	244.5	257.4
324.94	264.5	257.6	252.2	272.4	277.4	291.6	245.4	259.4
325.19	265.0	259.0	252.6	271.6	276.4	291.4	247.7	257.9
325.44	263.4	261.7	250.7	273.0	274.7	291.5	246.2	259.4
325.69	265.6	261.8	248.2	274.9	275.6	292.1	246.4	261.6
325.94	264.3	263.0	250.7	272.3	277.3	292.2	246.0	262.8
326.19	265.2	261.9	249.6	273.3	279.2	290.6	246.6	262.3
326.44	266.4	263.9	254.2	276.8	277.7	294.7	246.5	260.4
326.69	266.8	261.3	252.3	275.1	278.8	298.5	247.4	261.9
326.94	267.9	260.9	253.4	275.5	277.9	297.3	246.1	260.9
327.19	268.0	259.9	253.9	275.6	280.0	294.5	245.5	260.7
327.44	269.4	262.2	255.3	278.3	277.2	293.7	245.8	259.8
327.69	268.2	263.8	255.8	273.9	280.9	297.6	246.6	259.6
327.94	268.4	262.7	253.8	276.3	285.4	294.9	244.5	261.0
328.19	268.9	264.0	257.7	276.5	283.6	297.1	244.4	259.5
328.44	270.9	265.9	259.9	276.2	279.0	300.3	247.2	258.9
328.69	270.4	265.1	258.4	280.1	282.3	297.8	244.9	259.1
328.94	269.4	264.2	259.5	278.7	283.5	299.3	246.5	261.3
329.19	268.2	265.7	257.0	279.8	282.4	298.5	248.2	262.8
329.44	270.7	266.3	260.1	280.7	284.0	300.8	250.4	263.3
329.69	272.9	265.7	262.0	281.1	285.4	304.0	251.0	263.2
329.94	271.4	264.6	261.6	279.5	285.2	305.2	250.9	264.1
330.19	275.2	265.9	259.6	282.5	286.4	304.2	250.0	265.0
330.44	275.7	266.7	261.8	281.1	283.6	301.4	249.2	265.8
330.69	279.0	270.3	266.7	283.8	284.2	304.0	251.9	265.7
330.94	279.6	271.4	261.9	283.9	288.7	303.1	250.4	266.6
331.19	281.4	272.2	268.6	284.2	291.5	306.1	250.5	266.1
331.44	282.6	270.7	268.1	286.8	292.4	305.8	250.4	266.5
331.69	284.2	271.4	268.0	287.2	292.7	307.8	250.7	266.9
331.94	286.1	273.8	270.3	290.3	295.1	307.7	252.7	267.5
332.19	288.6	276.7	267.7	292.1	297.1	310.4	252.9	268.9
332.44	290.1	278.0	271.3	292.3	300.0	314.8	253.7	270.1
332.69	294.3	275.6	272.9	298.9	300.4	311.6	256.9	273.3
332.94	298.4	279.4	275.1	297.0	303.7	314.6	259.5	273.3
333.19	304.2	282.2	278.5	303.8	308.3	320.2	260.7	275.9
333.44	308.2	289.2	282.6	307.7	312.6	324.7	261.2	279.8
333.69	310.9	294.5	285.5	310.2	323.5	330.9	266.2	281.6
333.94	319.5	300.4	292.7	321.9	329.4	339.7	268.8	286.5
334.19	330.0	308.2	301.1	335.1	343.3	348.4	274.0	294.3
334.44	344.9	319.4	310.4	350.6	359.8	364.0	284.0	302.8
334.69	364.6	332.6	323.8	378.7	389.2	391.1	295.4	315.1
334.94	388.2	354.8	360.2	424.9	429.2	424.4	317.7	338.3
335.19	435.7	386.7	404.8	508.8	509.2	492.9	358.8	374.9
335.44	504.1	447.7	498.0	678.6	676.0	636.2	437.0	452.2
335.69	626.4	547.3	727.6	1078.9	1056.8	936.6	597.1	594.2

Continued…

T/K	$C^{o}_{p,m}$ /J·K^{-1}·mol^{-1}							
	Run 1	Run 2	Run 3	Run 4	Run 5	Run 6	Run 7	Run 8
335.94	843.4	762.9	1411.0	1994.0	1938.4	1628.4	946.4	881.1
336.19	1226.3	1182.3	3306.4	3674.7	3717.8	2926.8	1575.1	1372.3
336.44	1860.5	1857.4	6558.8	6158.5	6225.7	4892.0	2494.0	2117.5
336.69	2709.9	2752.5	10361.4	9057.0	9224.2	7389.4	3600.5	3037.8
336.93	3680.6	3712.5	14472.0	12179.2	12351.1	10021.3	4837.4	4079.7
337.18	4684.1	4685.4	18322.7	15274.4	15330.6	12662.3	6059.5	5143.2
337.43	5682.4	5693.2	21487.6	17674.4	17861.8	15049.3	7378.5	6274.6
337.68	6722.9	6626.0	23267.4	19972.1	19518.1	16797.0	8771.4	7412.4
337.93	7747.1	7663.3	14849.9	19976.0	20534.3	17949.4	10068.4	8554.3
338.18	8701.1	8720.2	1708.6	4640.2	13467.1	15096.1	11186.4	9676.6
338.43	9648.6	9639.6	475.1	769.9	1963.0	2805.6	11993.0	10604.3
338.69	10600.1	10220.2	374.2	415.1	531.3	677.6	12459.6	11499.8
338.94	11268.3	10788.7	366.8	381.2	406.1	423.7	12576.1	12050.1
339.19	11431.7	11113.3	361.0	377.0	385.5	393.1	10946.3	12313.6
339.44	10906.5	11106.4	364.8	378.7	383.5	389.9	3914.1	11872.9
339.69	8753.3	9925.7	365.9	379.2	384.6	389.4	926.4	8745.8
339.94	4076.2	6455.4	367.1	380.4	384.1	387.9	465.8	3691.4
340.19	1286.7	2100.9	366.8	380.8	383.4	389.9	354.4	1237.8
340.44	589.3	773.5	364.5	381.9	379.9	388.6	337.2	588.1
340.69	418.4	454.6	365.2	381.9	384.6	387.9	333.4	419.4
340.94	373.4	381.1	366.4	382.8	386.2	389.4	335.6	376.5
341.19	361.2	358.6	368.2	385.1	383.5	390.6	335.3	362.8
341.44	358.4	356.2	365.7	382.6	381.0	388.4	337.0	358.3
341.69	358.8	355.8	365.4	384.0	385.7	389.2	339.0	358.5
341.94	360.1	352.9	368.6	384.5	385.6	387.3	336.4	361.6
342.19	362.6	351.1	366.1	382.1	381.7	389.0	335.9	360.1
342.44	361.6	352.1	367.4	382.6	384.1	388.0	335.4	360.4
342.69	361.9	356.2	368.7	385.7	386.6	389.7	337.9	361.2
342.94	-	355.1	368.9	385.6	385.5	387.9	337.9	362.7
343.19	-	357.4	369.3	387.7	389.0	390.8	337.6	361.3
343.44	357.2	358.6	371.5	388.5	386.6	389.7	337.5	360.5
343.69	323.1	358.2	370.5	386.6	385.7	389.6	339.4	360.8
343.94	322.9	356.0	372.2	388.6	386.0	390.5	338.0	360.5
344.19	326.1	358.0	368.2	386.1	386.7	393.9	337.4	358.4
344.44	328.5	357.7	369.2	385.7	384.9	395.2	339.5	359.4
344.69	338.7	355.7	374.9	385.3	384.3	394.5	338.6	362.3
344.94	347.0	357.7	374.4	383.2	390.9	396.0	339.0	360.4
345.19	349.0	357.7	376.1	383.6	392.8	398.7	338.5	359.7
345.44	352.7	356.1	376.6	386.0	389.0	394.5	340.7	359.7
345.69	359.3	359.4	375.8	389.2	387.9	392.2	341.7	360.3
345.94	362.7	357.4	376.1	388.4	387.0	394.1	340.2	362.1
346.19	363.0	358.4	374.2	390.1	388.1	393.9	340.5	359.4
346.44	362.8	360.2	374.1	388.8	387.4	393.5	341.2	358.1
346.69	361.8	358.7	378.5	388.2	383.9	395.9	341.6	359.4

Continued…

T/K	$C^{o}_{p,m}$ /J·K^{-1}·mol^{-1}							
	Run 1	Run 2	Run 3	Run 4	Run 5	Run 6	Run 7	Run 8
346.94	365.8	361.4	376.5	390.5	386.9	396.4	341.5	360.3
347.19	365.1	364.5	379.8	387.8	389.3	395.7	340.8	362.1
347.44	366.0	361.4	377.0	386.9	389.0	396.7	342.7	362.9
347.69	365.2	361.0	375.1	393.0	392.7	398.5	340.7	363.6
347.94	367.5	358.1	380.6	390.5	389.5	399.9	340.7	364.9
348.19	368.0	356.4	382.0	390.1	388.6	396.8	340.2	363.2
348.44	365.9	359.2	380.9	391.3	385.7	399.4	340.4	360.6
348.69	364.7	358.1	380.5	391.3	382.1	399.3	337.8	361.0
348.94	365.0	353.9	382.1	388.9	385.9	397.9	339.7	362.6
349.19	366.2	358.8	383.1	391.0	385.6	399.2	339.4	360.9
349.44	368.9	362.2	382.7	391.1	388.5	400.2	339.7	362.1
349.69	367.3	361.4	381.1	392.5	392.5	401.3	339.9	362.5
349.94	367.1	358.8	382.5	390.1	389.8	401.7	339.5	362.6
350.19	367.3	357.8	384.2	395.1	387.8	400.6	340.2	360.0
350.44	368.3	360.9	384.1	394.2	391.8	399.6	342.0	361.9
350.69	367.0	358.9	383.1	394.6	389.4	402.1	341.0	363.0
350.94	364.8	359.0	384.4	392.6	388.5	399.8	338.3	363.9
351.19	365.4	359.9	384.3	393.1	390.9	401.1	340.9	364.7
351.44	366.0	358.9	385.1	396.4	395.1	403.7	344.5	363.1
351.68	366.2	360.0	384.0	395.3	392.0	402.3	342.9	361.9
351.93	367.4	361.1	387.7	396.6	393.9	401.7	341.0	361.0

Table SC.8. Standard (p^0 = 1 bar) molar heat capacities, $C^{o}_{p,\mathrm{m}}$ (cr), of the solid state for HVP obtained by DSC. These results refer to the mean of eight independent determinations and the uncertainties reported correspond to twice the standard deviation of the mean.

T/K	$C^{o}_{p,\mathrm{m}}$ / J·K^{-1}·mol^{-1}	T/K	$C^{o}_{p,\mathrm{m}}$ / J·K^{-1}·mol^{-1}	T/K	$C^{o}_{p,\mathrm{m}}$ / J·K^{-1}·mol^{-1}	T/K	$C^{o}_{p,\mathrm{m}}$ / J·K^{-1}·mol^{-1}
288.67	235.0±2.9	299.94	244.1±3.5	311.19	252.6±3.9	322.44	262.1±5.2
288.92	235.9±2.8	300.19	244.9±3.4	311.44	252.4±4.0	322.69	262.7±5.3
289.17	235.2±2.5	300.44	244.3±3.3	311.69	253.1±4.1	322.94	262.6±5.5
289.42	236.4±2.5	300.69	244.4±3.2	311.94	252.2±3.8	323.19	263.3±5.1
289.67	236.0±3.0	300.94	244.7±3.5	312.19	252.8±3.6	323.44	263.3±5.0
289.92	235.3±2.9	301.19	244.5±3.3	312.44	252.4±4.0	323.69	262.8±5.1
290.17	236.5±2.9	301.44	243.4±3.3	312.69	253.6±3.7	323.94	263.0±5.0
290.42	236.3±2.9	301.69	244.2±3.2	312.94	254.0±4.1	324.19	264.1±5.3
290.68	238.0±3.2	301.94	244.9±3.2	313.19	253.3±3.7	324.44	264.2±5.3
290.93	236.4±2.7	302.19	245.3±3.3	313.44	254.6±3.9	324.69	264.3±5.1
291.18	236.8±3.0	302.44	245.1±3.4	313.69	255.2±4.2	324.94	265.1±5.3
291.43	238.0±3.2	302.69	244.8±3.4	313.94	255.0±4.2	325.19	265.2±5.0
291.68	237.8±3.2	302.94	245.6±3.5	314.19	255.4±4.2	325.44	265.1±5.1
291.93	236.7±3.0	303.19	246.4±3.6	314.44	256.5±4.3	325.69	265.8±5.3
292.18	237.4±2.9	303.44	246.5±3.2	314.69	256.9±4.2	325.94	266.1±5.2
292.43	238.5±3.0	303.69	247.0±3.2	314.94	256.1±4.5	326.19	266.1±5.2
292.68	239.0±3.5	303.94	247.4±3.5	315.19	256.0±4.2	326.44	267.6±5.4
292.93	239.6±2.9	304.19	247.3±3.7	315.44	255.8±3.8	326.69	267.8±5.7
293.18	239.6±3.0	304.44	247.5±3.6	315.69	255.8±4.0	326.94	267.5±5.7
293.43	240.0±3.0	304.69	246.8±3.5	315.94	256.0±4.4	327.19	267.3±5.5
293.68	240.4±3.5	304.94	246.8±3.6	316.19	256.4±4.3	327.44	267.7±5.4
293.93	239.8±3.3	305.19	247.1±3.9	316.44	256.4±4.3	327.69	268.3±5.6
294.18	239.1±3.0	305.44	248.1±4.0	316.69	257.2±4.5	327.94	268.4±5.9
294.44	239.1±3.3	305.69	247.8±3.8	316.94	258.0±4.5	328.19	268.9±5.8
294.69	240.8±3.3	305.94	247.5±3.7	317.19	257.2±4.5	328.44	269.8±5.7
294.94	240.4±3.3	306.19	247.7±3.9	317.44	257.6±4.7	328.69	269.8±5.9
295.19	239.8±3.0	306.44	248.9±3.9	317.69	257.8±4.4	328.94	270.3±5.8
295.44	240.5±2.7	306.69	248.8±4.3	317.94	257.4±4.6	329.19	270.3±5.6
295.69	241.6±2.9	306.94	249.6±4.1	318.19	257.0±4.5	329.44	272.0±5.6
295.94	241.1±2.9	307.19	250.4±3.9	318.44	258.3±4.4	329.69	273.2±5.9
296.19	240.8±3.1	307.44	250.1±3.9	318.69	258.9±4.5	329.94	272.8±6.0
296.44	242,1±3.2	307.69	250.1±3.8	318.94	259.1±4.6	330.19	273.6±6.1
296.69	241.7±3.0	307.94	249.4±3.9	319.19	260.1±4.6	330.44	273.2±5.6
296.94	241,2±3.4	308.19	249.7±3.8	319.44	259.4±4.9	330.69	275.7±5.6
297.19	241.5±3.3	308.44	250.1±4.0	319.69	260.1±4.9	330.94	275.7±5.9
297.44	242.2±3.4	308.69	249.7±3.8	319.94	259.7±4.9	331.19	277.6±6.0
297.69	241.6±3.0	308.94	250.3±4.0	320.19	259.7±5.0	331.44	277.9±6.2
297.94	242.5±3.2	309.19	250.8±4.0	320.44	260.3±4.8	331.69	278.6±6.3
298.19	242.7±3.3	309.44	251.7±4.3	320.69	260.6±5.0	331.94	280.4±6.2
298.44	242.8±3.0	309.69	252.9±4.4	320.94	261.2±5.1	332.19	281.8±6.6
298.69	241.8±3.1	309.94	251.9±4.0	321.19	261.4±5.2	332.44	283.8±6.8
298.94	242.3±2.9	310.19	253.2±4.1	321.44	260.7±5.1	332.69	285.5±6.5
299.19	242.3±2.6	310.44	253.8±3.9	321.69	260.9±5.0	332.94	287.6±6.6
299.44	242.2±3.2	310.69	253.1±3.6	321.94	260.9±5.1	333.19	291.7±7.2
299.69	242.9±3.4	310.94	253.2±3.5	322.19	261.4±5.0	333.44	295.7±7.4

Continued…

T/K	$C^{o}_{p,m}$ / J·K^{-1}·mol^{-1}	T/K	$C^{o}_{p,m}$ / J·K^{-1}·mol^{-1}	T/K	$C^{o}_{p,m}$ / J·K^{-1}·mol^{-1}	T/K	$C^{o}_{p,m}$ / J·K^{-1}·mol^{-1}
333.69	300.4±7.8	338.43	8579.0±1732.3	343.19	386.0±7.5	347.69	373.7±7.0
333.94	379.7±15.3	338.69	6732.0±2034.7	343.44	368.7±6.6	347.94	374.0±7.0
334.19	316.8±9.3	338.94	5605.0±2139.0	343.69	364.2±8.5	348.19	373.1±6.9
334.44	329.5±10.4	339.19	4118.7±2097.2	343.94	364.3±8.8	348.44	372.9±7.0
334.69	348.8±13.0	339.44	3262.4±1917.7	344.19	364.4±8.6	348.69	371.8±7.1
334.94	379.7±15.3	339.69	2584.1±1589.8	344.44	365.0±8.3	348.94	372.0±7.0
335.19	434.0±21.9	339.94	1753.0±843.8	344.69	366.8±7.6	349.19	373.0±7.1
335.44	541.2±37.0	340.19	989.8±232.4	344.94	368.6±7.3	349.44	374.4±7.0
335.69	770.6±77.7	340.44	475.4±55.3	345.19	369.5±7.6	349.69	374.8±7.3
335.94	1300.7±179.6	340.69	393.2±13.1	345.44	369.4±7.0	349.94	374.0±7.3
336.19	2372.7±402.0	340.94	373.9±6.1	345.69	370.7±6.5	350.19	374.1±7.4
336.44	4020.6±775.1	341.19	368.2±6.4	345.94	371.0±6.5	350.44	375.3±7.1
336.69	6016.6±1169.5	341.44	365.9±6.1	346.19	371.0±6.7	350.69	374.9±7.3
336.93	8166.7±1606.7	341.69	367.0±6.2	346.44	370.7±6.5	350.94	373.9±7.3
337.18	10270.3±2016.1	341.94	367.1±6.4	346.69	371.0±6.5	351.19	375.0±7.2
337.43	12137.7±2312.8	342.19	366.1±6.3	346.94	372.4±6.5	351.44	376.6±7.5
337.68	13635.9±2452.5	342.44	366.4±6.4	347.19	373.1±6.5	351.68	375.6±7.4
337.93	13542.0±1965.7	342.69	368.5±6.3	347.44	372.8±6.3	351.93	376.3±7.7

Table SC.9. Standard (p^0 = 1 bar) molar heat capacities, $C^{o}_{p,m}$ (g), of HVP in the gaseous state, obtained with Statistical Mechanics,[51] using harmonic vibration frequencies obtained by B3LYP-D3/cc-pVTZ method and scaled by 0.9889.[55]

T/K	$C^{o}_{p,m}$(g) / J·K^{-1}·mol^{-1}	T/K	$C^{o}_{p,m}$(g) / J·K^{-1}·mol^{-1}	T/K	$C^{o}_{p,m}$(g) / J·K^{-1}·mol^{-1}	T/K	$C^{o}_{p,m}$(g) / J·K^{-1}·mol^{-1}	T/K	$C^{o}_{p,m}$(g) / J·K^{-1}·mol^{-1}
200	152.457	241	177.246	282	202.958	323	228.948	364	254.480
201	153.048	242	177.864	283	203.592	324	229.579	365	255.092
202	153.639	243	178.483	284	204.226	325	230.209	366	255.703
203	154.232	244	179.102	285	204.860	326	230.840	367	256.313
204	154.825	245	179.722	286	205.494	327	231.470	368	256.923
205	155.418	246	180.342	287	206.128	328	232.099	369	257.532
206	156.012	247	180.963	288	206.762	329	232.729	370	258.140
207	156.607	248	181.584	289	207.397	330	233.358	371	258.748
208	157.203	249	182.206	290	208.031	331	233.987	372	259.355
209	157.800	250	182.829	291	208.666	332	234.615	373	259.962
210	158.397	251	183.452	292	209.301	333	235.243	374	260.567
211	158.995	252	184.075	293	209.935	334	235.871	375	261.172
212	159.593	253	184.699	294	210.570	335	236.498	376	261.777
213	160.192	254	185.324	295	211.205	336	237.125	377	262.380
214	160.792	255	185.949	296	211.840	337	237.751	378	262.983
215	161.393	256	186.574	297	212.475	338	238.377	379	263.585
216	161.994	257	187.200	298	213.109	339	239.003	380	264.187
217	162.596	258	187.826	299	213.744	340	239.628	381	264.787
218	163.199	259	188.452	300	214.379	341	240.253	382	265.387
219	163.802	260	189.080	301	215.014	342	240.877	383	265.986
220	164.407	261	189.707	302	215.649	343	241.501	384	266.585
221	165.011	262	190.335	303	216.283	344	242.124	385	267.183
222	165.617	263	190.963	304	216.918	345	242.747	386	267.780
223	166.223	264	191.592	305	217.552	346	243.369	387	268.376
224	166.830	265	192.221	306	218.187	347	243.991	388	268.971
225	167.437	266	192.850	307	218.821	348	244.613	389	269.566
226	168.046	267	193.480	308	219.455	349	245.233	390	270.160
227	168.655	268	194.110	309	220.089	350	245.854	391	270.753
228	169.264	269	194.740	310	220.723	351	246.474	392	271.345
229	169.874	270	195.371	311	221.357	352	247.093	393	271.937
230	170.485	271	196.001	312	221.991	353	247.712	394	272.527
231	171.097	272	196.633	313	222.624	354	248.330	395	273.117
232	171.709	273	197.264	314	223.258	355	248.948	396	273.706
233	172.321	274	197.896	315	223.891	356	249.565	397	274.295
234	172.935	275	198.528	316	224.524	357	250.181	398	274.882
235	173.549	276	199.160	317	225.156	358	250.797	399	275.469
236	174.163	277	199.793	318	225.789	359	251.412	400	276.055
237	174.779	278	200.425	319	226.421	360	252.027		
238	175.395	279	201.058	320	227.053	361	252.641		
239	176.011	280	201.692	321	227.685	362	253.255		
240	176.628	281	202.325	322	228.316	363	253.868		

Table SC.10. Measurements of the standard (p^0 = 1 bar) molar heat capacity of 4'-hydroxyheptanophenone (HHP) done by DSC. These results correspond to the solid state, fusion transition and liquid zone, in the temperature range of 288.15 K to 387.15 K.

T/K	$C^{o}_{p,m}$/J·K^{-1}·mol^{-1}			T/K	$C^{o}_{p,m}$/J·K^{-1}·mol^{-1}		
	Run 1	Run 2	Run 3		Run 1	Run 2	Run 3
288.67	288.67	289.2	284.1	313.20	313.20	321.5	316.8
289.17	289.17	290.1	282.0	313.70	313.70	325.0	317.7
289.67	289.67	289.9	280.7	314.20	289.2	318.5	321.2
290.17	290.17	290.6	280.2	314.70	290.1	319.2	319.7
290.68	290.68	289.4	285.0	315.20	289.9	317.0	319.9
291.18	291.18	292.0	288.2	315.70	290.6	321.6	322.1
291.68	291.68	295.3	288.1	316.20	289.4	323.5	320.4
292.18	292.18	295.4	286.9	316.70	292.0	319.4	323.6
292.69	292.69	296.4	286.8	317.20	295.3	323.4	320.6
293.19	293.19	295.3	290.1	317.70	295.4	320.8	323.6
293.69	293.69	295.2	289.4	318.20	296.4	322.7	325.4
294.19	294.19	298.0	290.8	318.70	295.3	321.1	323.6
294.69	294.69	294.9	289.9	319.20	295.2	322.5	327.9
295.19	295.19	296.8	287.0	319.70	298.0	324.5	322.7
295.69	295.69	300.8	294.9	320.20	294.9	323.0	320.6
296.19	296.19	300.6	293.3	320.70	296.8	325.2	326.3
296.70	296.70	299.5	294.2	321.20	300.8	325.8	330.1
297.20	297.20	301.8	294.4	321.70	300.6	326.3	328.9
297.70	297.70	301.9	293.7	322.20	299.5	330.1	326.0
298.20	298.20	300.2	295.0	322.70	301.8	324.7	327.6
298.70	298.70	305.1	295.6	323.20	301.9	331.9	325.9
299.20	299.20	305.6	292.9	323.70	300.2	328.0	332.8
299.70	299.70	307.1	296.1	324.20	305.1	330.8	328.3
300.20	300.20	303.9	305.3	324.70	305.6	331.5	330.1
300.70	300.70	304.6	302.3	325.20	307.1	331.7	331.8
301.20	301.20	308.3	297.7	325.70	303.9	332.8	331.3
301.70	301.70	308.2	301.9	326.20	304.6	333.1	329.6
302.20	302.20	311.7	297.8	326.70	308.3	331.0	332.8
302.70	302.70	307.7	303.7	327.20	308.2	333.6	334.5
303.20	303.20	309.6	302.4	327.70	311.7	331.8	330.4
303.70	303.70	307.7	301.4	328.20	307.7	331.6	334.0
304.20	304.20	311.9	301.2	328.70	309.6	333.7	335.4
304.70	304.70	311.5	307.3	329.20	307.7	332.7	337.3
305.20	305.20	311.3	307.2	329.70	311.9	337.1	336.3
305.70	305.70	310.6	308.1	330.20	311.5	334.7	337.3
306.20	306.20	314.6	302.6	330.70	311.3	335.9	335.8
306.70	306.70	314.4	309.2	331.20	310.6	335.6	337.8
307.20	307.20	310.6	305.1	331.70	314.6	338.6	336.3
307.70	307.70	310.3	307.6	332.20	314.4	338.3	336.9
308.20	308.20	310.4	307.0	332.70	310.6	344.0	337.4
308.70	308.70	313.3	309.6	333.20	310.3	338.1	337.8
309.20	309.20	314.4	312.8	333.70	310.4	340.9	340.6
309.70	309.70	318.2	308.9	334.20	313.3	342.6	337.9
310.20	310.20	318.4	312.8	334.70	314.4	343.2	337.8
310.70	310.70	318.8	311.7	335.20	318.2	344.3	337.8
311.20	311.20	319.8	312.4	335.70	318.4	346.6	342.4
311.70	311.70	319.5	315.5	336.20	318.8	342.7	340.2
312.20	312.20	321.3	312.9	336.70	319.8	344.5	343.0
312.70	312.70	320.2	314.3	337.20	319.5	344.9	342.2

Continued…

T/K	$C^{o}_{p,m}$ /J·K^{-1}·mol^{-1}			T/K	$C^{o}_{p,m}$ /J·K^{-1}·mol^{-1}		
	Run 1	Run 2	Run 3		Run 1	Run 2	Run 3
337.70	321.3	345.0	341.4	362.69	432.2	426.2	414.8
338.20	320.2	346.2	348.5	363.19	452.0	448.8	439.2
338.70	321.5	346.5	344.3	363.69	483.9	484.8	464.3
339.19	325.0	345.3	343.1	364.19	544.1	562.2	529.1
339.69	359.4	344.2	342.5	364.69	702.4	760.4	714.8
340.20	355.2	346.6	349.5	365.19	1145.7	1409.0	1455.4
340.70	358.7	350.1	348.8	365.69	2410.7	3822.8	4696.2
341.20	355.7	348.1	348.2	366.18	4675.2	8040.6	10343.0
341.70	358.9	347.5	345.8	366.68	7181.5	12514.7	16357.4
342.20	360.0	348.0	346.2	367.18	9813.2	16911.7	20397.8
342.70	360.4	348.5	346.2	367.68	12357.5	20121.7	4788.4
343.19	359.7	350.9	349.7	368.19	13822.3	10032.7	496.0
343.69	357.8	351.2	350.2	368.69	11680.0	704.5	449.2
344.19	362.2	349.4	348.5	369.19	2125.9	474.6	453.3
344.69	363.3	352.8	354.3	369.70	538.4	467.2	451.0
345.19	363.0	353.7	354.4	370.20	455.9	468.8	451.1
345.69	362.0	354.2	349.4	370.70	454.1	470.5	455.7
346.19	363.8	356.7	351.3	371.19	457.5	470.8	456.0
346.69	365.0	354.7	352.0	371.69	453.8	474.4	456.2
347.19	364.5	355.1	355.3	372.19	456.9	475.9	457.3
347.69	365.8	356.1	355.6	372.69	455.6	475.3	455.3
348.19	366.2	360.3	354.4	373.19	456.9	476.0	459.5
348.69	371.3	356.7	356.8	373.69	457.4	481.9	457.9
349.19	371.1	361.5	354.7	374.19	456.4	481.8	458.2
349.69	367.7	361.3	353.6	374.69	459.9	478.6	463.5
350.19	371.9	359.2	354.4	375.19	455.7	474.1	463.2
350.69	371.3	360.3	358.2	375.69	457.8	481.5	460.3
351.19	372.0	359.5	361.3	376.19	456.3	479.9	463.3
351.69	370.5	360.2	361.0	376.69	463.3	476.2	460.3
352.19	371.1	359.7	359.4	377.19	463.6	477.9	460.9
352.69	370.3	363.4	364.3	377.69	464.1	476.5	463.8
353.19	373.5	362.5	360.2	378.19	468.8	480.0	462.8
353.69	373.7	367.4	363.5	378.69	462.1	483.2	464.2
354.19	377.4	366.7	363.9	379.19	463.0	480.5	461.2
354.69	377.8	367.6	364.6	379.69	465.2	485.2	463.3
355.19	379.5	370.3	367.4	380.19	465.7	480.9	463.4
355.69	380.8	375.1	369.8	380.69	468.6	488.4	464.9
356.19	380.2	371.2	369.4	381.19	464.1	490.6	465.1
356.69	384.7	369.1	369.6	381.69	463.6	490.9	467.4
357.19	383.6	374.1	366.6	382.19	462.8	484.5	464.2
357.69	384.8	381.9	373.2	382.69	464.5	487.7	467.9
358.19	385.5	379.7	375.1	383.19	467.0	484.9	465.8
358.69	387.5	380.4	376.4	383.69	469.0	486.4	465.6
359.19	387.8	379.8	379.3	384.19	468.6	488.6	467.4
359.69	391.7	383.7	385.6	384.69	473.6	490.7	467.9
360.19	396.3	390.5	387.2	385.19	472.7	499.3	468.0
360.69	399.9	391.9	389.9	385.69	475.2	495.7	472.5
361.19	408.0	393.4	392.1	386.19	478.6	497.1	470.7
361.69	412.5	403.8	394.2	386.69	477.4	494.3	465.2
362.19	420.9	413.9	404.5				

Table SC.11. Standard (p^0 = 1 bar) molar heat capacities of the solid and liquid state for HHP obtained by DSC. These results refer to the mean of three independent determinations and the uncertainties reported correspond to twice the standard deviation of the mean.

T/K	$\frac{C^{o}_{p,m}}{J \cdot K^{-1} \cdot mol^{-1}}$	T/K	$\frac{C^{o}_{p,m}}{J \cdot K^{-1} \cdot mol^{-1}}$	T/K	$\frac{C^{o}_{p,m}}{J \cdot K^{-1} \cdot mol^{-1}}$	T/K	$\frac{C^{o}_{p,m}}{J \cdot K^{-1} \cdot mol^{-1}}$
288.67	291.0±4.6	310.70	314.9±2.1	332.70	342.3±2.5	354.69	370.0±4.0
289.17	292.2±6.6	311.20	316.7±2.2	333.20	341.3±3.3	355.19	372.4±3.7
289.67	289.9±5.3	311.70	318.0±1.3	333.70	342.1±1.4	355.69	375.2±3.2
290.17	290.9±6.3	312.20	317.3±2.4	334.20	343.3±3.3	356.19	373.6±3.3
290.68	292.7±5.6	312.70	318.1±1.9	334.70	343.6±3.5	356.69	374.5±5.1
291.18	295.0±5.1	313.20	319.2±1.3	335.20	343.9±3.4	357.19	374.8±4.9
291.68	296.8±5.5	313.70	320.9±2.2	335.70	346.5±2.4	357.69	380.0±3.5
292.18	295.6±5.1	314.20	320.5±1.0	336.20	344.9±3.5	358.19	380.1±3.0
292.69	295.3±4.7	314.70	319.8±0.4	336.70	346.6±2.9	358.69	381.4±3.2
293.19	296.8±4.4	315.20	319.7±1.5	337.20	346.4±2.9	359.19	382.3±2.8
293.69	295.0±3.2	315.70	323.3±1.4	337.70	346.9±3.8	359.69	387.0±2.4
294.19	297.4±3.6	316.20	322.8±1.2	338.20	349.4±2.2	360.19	391.3±2.7
294.69	297.4±5.2	316.70	323.2±2.1	338.70	347.8±2.5	360.69	393.9±3.1
295.19	296.8±5.7	317.20	324.0±2.1	339.19	348.2±4.1	361.19	397.9±5.1
295.69	301.0±3.6	317.70	323.8±1.8	339.69	348.7±5.4	361.69	403.5±5.3
296.19	302.3±5.7	318.20	325.7±1.8	340.20	350.4±2.5	362.19	413.1±4.8
296.70	300.1±3.6	318.70	324.1±1.9	340.70	352.5±3.1	362.69	424.4±5.1
297.20	300.6±3.2	319.20	327.1±2.5	341.20	350.7±2.5	363.19	446.7±3.8
297.70	300.7±3.8	319.70	327.1±3.5	341.70	350.7±4.1	363.69	477.7±6.7
298.20	300.2±3.0	320.20	324.7±3.0	342.20	351.4±4.3	364.19	545.1±9.6
298.70	303.0±3.8	320.70	327.1±1.4	342.70	351.7±4.4	364.69	725.9±17.6
299.20	302.5±4.9	321.20	328.9±1.6	343.19	353.4±3.2	365.19	1336.7±96.4
299.70	304.8±4.6	321.70	328.9±1.4	343.69	353.1±2.4	365.69	3643.2±665.8
300.20	307.5±2.9	322.20	330.3±2.6	344.19	353.4±4.4	366.18	7686.3±1645.7
300.70	306.2±2.9	322.70	329.6±3.6	344.69	356.8±3.3	366.68	12017.9±2660.5
301.20	305.9±4.2	323.20	331.2±2.9	345.19	357.0±3.0	367.18	15707.6±3114.3
301.70	306.8±2.5	323.70	332.0±2.2	345.69	355.2±3.7	367.68	12422.5±4426.5
302.20	306.5±4.4	324.20	330.5±1.2	346.19	357.3±3.6	368.19	8117.0±3964.4
302.70	307.3±2.0	324.70	331.9±1.2	346.69	357.3±3.9	368.69	4277.9±3701.8
303.20	308.7±3.4	325.20	333.5±1.8	347.19	358.3±3.1	369.19	1017.9±554.0
303.70	307.9±3.8	325.70	333.6±1.7	347.69	359.2±3.3	369.70	485.5±26.8
304.20	309.2±4.1	326.20	334.4±3.2	348.19	360.3±3.4	370.20	458.6±5.3
304.70	311.7±2.6	326.70	335.0±3.1	348.69	361.6±4.8	370.70	460.1±5.2
305.20	310.0±1.4	327.20	335.2±1.2	349.19	362.4±4.7	371.19	461.4±4.7
305.70	309.6±0.8	327.70	334.1±2.9	349.69	360.9±4.1	371.69	461.5±6.5
306.20	311.9±4.8	328.20	335.0±2.3	350.19	361.8±5.2	372.19	463.4±6.3
306.70	312.9±1.9	328.70	337.4±2.8	350.69	363.3±4.1	372.69	462.1±6.6
307.20	311.4±3.9	329.20	336.3±1.8	351.19	364.3±3.9	373.19	464.1±6.0
307.70	311.2±2.4	329.70	338.1±1.5	351.69	363.9±3.3	373.69	465.7±8.1
308.20	310.6±2.1	330.20	338.7±2.8	352.19	363.4±3.8	374.19	465.5±8.2
308.70	313.4±2.2	330.70	337.8±2.0	352.69	366.0±2.2	374.69	467.4±5.7
309.20	314.0±0.6	331.20	338.5±1.9	353.19	365.4±4.1	375.19	464.3±5.3
309.70	314.4±2.8	331.70	339.5±2.2	353.69	368.2±3.0	375.69	466.6±7.5
310.20	315.8±1.6	332.20	340.3±2.8	354.19	369.3±4.1	376.19	466.5±7.0

Continued…

T/K	$C^{o}_{p,m}$ / J·K^{-1}·mol^{-1}	T/K	$C^{o}_{p,m}$ / J·K^{-1}·mol^{-1}	T/K	$C^{o}_{p,m}$ / J·K^{-1}·mol^{-1}	T/K	$C^{o}_{p,m}$ / J·K^{-1}·mol^{-1}
376.69	466.6±4.9	379.69	471.2±7.0	382.69	473.3±7.2	385.69	481.1±7.3
377.19	467.5±5.3	380.19	470.0±5.5	383.19	472.6±6.2	386.19	482.1±7.8
377.69	468.1±4.2	380.69	474.0±7.3	383.69	473.7±6.4	386.69	479.0±8.5
378.19	470.5±5.0	381.19	473.3±8.7	384.19	474.9±6.9		
378.69	469.8±6.7	381.69	474.0±8.5	384.69	477.4±6.8		
379.19	468.2±6.2	382.19	470.5±7.0	385.19	480.0±9.8		

Table SC.12. Standard (p^0 = 1 bar) molar heat capacities, $C^{o}_{p,m}$ (g), of HHP in the gaseous state, obtained with Statistical Mechanics,[51] using harmonic vibration frequencies obtained by B3LYP-D3/cc-pVTZ method and scaled by 0.9889.[55]

T/K	$C^{o}_{p,m}$(g) / J·K^{-1}·mol^{-1}	T/K	$C^{o}_{p,m}$(g) / J·K^{-1}·mol^{-1}	T/K	$C^{o}_{p,m}$(g) / J·K^{-1}·mol^{-1}	T/K	$C^{o}_{p,m}$(g) / J·K^{-1}·mol^{-1}	T/K	$C^{o}_{p,m}$(g) / J·K^{-1}·mol^{-1}
200	182.274	241	211.337	282	241.950	323	273.265	364	304.295
201	182.962	242	212.068	283	242.709	324	274.029	365	305.041
202	183.650	243	212.800	284	243.469	325	274.792	366	305.787
203	184.339	244	213.532	285	244.229	326	275.556	367	306.531
204	185.029	245	214.266	286	244.990	327	276.319	368	307.275
205	185.721	246	215.000	287	245.751	328	277.083	369	308.019
206	186.413	247	215.736	288	246.512	329	277.845	370	308.761
207	187.107	248	216.472	289	247.274	330	278.608	371	309.503
208	187.802	249	217.209	290	248.036	331	279.370	372	310.244
209	188.498	250	217.947	291	248.799	332	280.133	373	310.984
210	189.194	251	218.686	292	249.561	333	280.894	374	311.724
211	189.892	252	219.426	293	250.324	334	281.656	375	312.463
212	190.592	253	220.166	294	251.087	335	282.417	376	313.201
213	191.292	254	220.908	295	251.851	336	283.178	377	313.938
214	191.993	255	221.650	296	252.615	337	283.938	378	314.675
215	192.696	256	222.393	297	253.378	338	284.698	379	315.411
216	193.399	257	223.137	298	254.142	339	285.458	380	316.146
217	194.104	258	223.881	299	254.907	340	286.217	381	316.880
218	194.810	259	224.627	300	255.671	341	286.976	382	317.614
219	195.517	260	225.373	301	256.436	342	287.735	383	318.346
220	196.225	261	226.120	302	257.200	343	288.493	384	319.078
221	196.934	262	226.867	303	257.965	344	289.251	385	319.809
222	197.644	263	227.616	304	258.730	345	290.008	386	320.539
223	198.355	264	228.365	305	259.495	346	290.765	387	321.268
224	199.067	265	229.114	306	260.260	347	291.521	388	321.997
225	199.781	266	229.865	307	261.025	348	292.277	389	322.724
226	200.495	267	230.616	308	261.791	349	293.032	390	323.451
227	201.211	268	231.367	309	262.556	350	293.787	391	324.177
228	201.927	269	232.120	310	263.321	351	294.541	392	324.902
229	202.645	270	232.872	311	264.086	352	295.295	393	325.626
230	203.364	271	233.626	312	264.852	353	296.048	394	326.349
231	204.084	272	234.380	313	265.617	354	296.801	395	327.071
232	204.804	273	235.135	314	266.382	355	297.553	396	327.793
233	205.526	274	235.890	315	267.147	356	298.305	397	328.513
234	206.249	275	236.645	316	267.912	357	299.056	398	329.233
235	206.973	276	237.402	317	268.677	358	299.806	399	329.952
236	207.698	277	238.159	318	269.442	359	300.556	400	330.669
237	208.424	278	238.916	319	270.207	360	301.305		
238	209.151	279	239.674	320	270.972	361	302.054		
239	209.878	280	240.432	321	271.736	362	302.801		
240	210.607	281	241.190	322	272.500	363	303.549		

D) Enthalpy of sublimation and vaporization

Table SD.1. Results of the standard enthalpy of sublimation measurements on 4'-hydropropiophenone by Calvet microcalorimetry (p^o = 1 bar).[a]

m/g	A-A_b/mV·s	T_i /K	T_f /K	$\Delta_{sub}h$ /(J·g^{-1})
7.1671	342.573	298.11	381.10	750.208
3.1857	153.357	297.80	381.12	755.563
7.3071	347.016	298.20	381.12	745.378
2.6423	124.800	297.84	381.13	741.318
2.9337	140.724	297.85	381.10	752.878
5.9300	281.077	298.19	381.11	743.948
6.9114	331.096	298.31	381.14	751.900

[a] $u(m)$ = ±0.00005 mg; $u(A$-$A_b)$ = ±0.0005 mV·s; $u(T)$= ±0.01 K

M = 150.177 g·mol^{-1}

$<T_i> \pm u$ = 298.04±0.16 K

$<T_f> \pm u$ = 381.12±0.01 K

$<\varepsilon> \pm u$ = 63.713±0.067 mV·J^{-1}·s

$<\Delta_{sub}h> \pm u$ = 748.74±1.98 J·g^{-1}

Overall uncertainty U_c = 2.13 J·g^{-1}

$\Delta_{sub}H^o_m \pm U_c$ = 112.44±0.64 kJ·mol^{-1}

Table SD.2. Results of the standard enthalpy of sublimation measurements on 4'-hydroxybutyrophenone by Calvet microcalorimetry (p^o = 1 bar).[a]

m/g	A-A_b/mV·s	T_i /K	T_f /K	$\Delta_{sub}h$ /(J·g^{-1})
4.1562	182.385	298.05	351.21	684.479
2.8283	127.995	297.79	351.21	705.887
1.3264	58.697	297.76	351.21	690.254
1.7562	79.304	297.99	351.22	704.350
2.1810	95.960	298.04	351.22	686.281
5.8347	261.496	298.21	351.23	699.059

[a] $u(m)$ = ±0.00005 mg; $u(A$-$A_b)$ = ±0.0005 mV·s; $u(T)$= ±0.01 K

M = 164.204 g·mol^{-1}

$<T_i> \pm u$ = 297.97±0.14 K

$<T_f> \pm u$ = 351.22±0.01 K

$<\varepsilon> \pm u$ = 64.111±0.037 mV·J^{-1}·s

$<\Delta_{sub}h> \pm u$ = 695.05±3.79 J·g^{-1}

Overall uncertainty U_c = 3.81 J·g^{-1}

$\Delta_{sub}H^o_m \pm U_c$ = 114.13±1.25 kJ·mol^{-1}

Table SD.3. Results of the standard enthalpy of vaporization measurements on 4'-hydroxyvalerophenone by Calvet microcalorimetry (p^o = 1 bar).[a]

m/g	A-A_b/mV·s	T_i /K	T_f /K	$\Delta_{vap}h$ /(J·g^{-1})
1.9959	68.352	297.96	341.74	535.691
1.8092	62.384	298.16	341.74	539.372
2.2560	77.486	298.00	341.73	537.262
2.6190	89.832	297.97	341.73	536.535
3.5176	121.616	298.08	341.72	540.812
1.5853	55.197	298.13	341.74	544.636

[a] $u(m)$ = ±0.00005 mg; $u(A\text{-}A_b)$ = ±0.0005 mV s; $u(T)$= ±0.01 K

M = 178.231 g·mol^{-1}

$<T_i>\pm u$ = 298.05±0.07 K

$<T_f>\pm u$ = 341.73±0.01 K

$<\varepsilon>\pm u$ = 63.929±0.103 mV·J^{-1}·s

$<\Delta_{vap}h>\pm u$ = 539.05±1.36 J·g^{-1}

Overall uncertainty U_c = 1.61 J·g^{-1}

$\Delta_{vap}H_m^o \pm U_c$ = 96.08±0.57 kJ·mol^{-1}

Table SD.4. Results of the standard enthalpy of vaporization measurements on 4'-hydroxyheptanophenone by Calvet microcalorimetry (p^o = 1 bar).[a]

m/g	A-A_b/mV·s	T_i /K	T_f /K	$\Delta_{vap}h$ /(J·g^{-1})
3.4373	105.873	298.27	381.13	483.437
3.5718	111.661	298.04	381.11	490.666
1.1779	37.737	298.31	381.11	502.841
10.8593	340.417	298.08	381.12	492.018
7.9279	245.476	298.11	381.12	485.985

[a] $u(m)$ = ±0.00005 mg; $u(A\text{-}A_b)$ = ±0.0005 mV s; $u(T)$= ±0.01 K

M = 206.285 g·mol^{-1}

$<T_i>\pm u$ = 298.16±0.11 K

$<T_f>\pm u$ = 381.12±0.01 K

$<\varepsilon>\pm u$ = 63.713±0.067 mV·J^{-1}·s

$<\Delta_{vap}h>\pm u$ = 490.99±3.34 J·g^{-1}

Overall uncertainty U_c = 3.38 J·g^{-1}

$\Delta_{vap}H_m^o \pm U_c$ = 101.28±1.39 kJ·mol^{-1}